


5-2011

Risk of Second Malignant Neoplasms Following Proton Arc Therapy and Volumetric Modulated Arc Therapy for Prostate Cancer

Laura A. Rechner

Follow this and additional works at: http://digitalcommons.library.tmc.edu/utgsbs_dissertations

 Part of the [Medical Biophysics Commons](#), [Oncology Commons](#), and the [Plasma and Beam Physics Commons](#)

Recommended Citation

Rechner, Laura A., "Risk of Second Malignant Neoplasms Following Proton Arc Therapy and Volumetric Modulated Arc Therapy for Prostate Cancer" (2011). *UT GSBS Dissertations and Theses (Open Access)*. Paper 115.

This Thesis (MS) is brought to you for free and open access by the Graduate School of Biomedical Sciences at DigitalCommons@The Texas Medical Center. It has been accepted for inclusion in UT GSBS Dissertations and Theses (Open Access) by an authorized administrator of DigitalCommons@The Texas Medical Center. For more information, please contact laurel.sanders@library.tmc.edu.

**Risk of Second Malignant Neoplasms Following Proton Arc Therapy
and Volumetric Modulated Arc Therapy for Prostate Cancer**

By

Laura Ann Rechner, B.S.

APPROVED:

Wayne D. Newhauser, Ph.D.
Supervisory Professor

Rebecca Howell, Ph.D.

Rajat Kudchadker, Ph.D.

Lei Dong, Ph.D.

Dragan Mirkovic, Ph.D.

Carol Etzel, Ph.D.

APPROVED:

Dean, The University of Texas
Health Science Center at Houston
Graduate School of Biomedical Sciences

**Risk of Second Malignant Neoplasms Following Proton Arc Therapy and
Volumetric Modulated Arc Therapy for Prostate Cancer**

A

THESIS

Presented to the Faculty of
The University of Texas
Health Science Center at Houston
and
The University of Texas
M. D. Anderson Cancer Center
Graduate School of Biomedical Sciences
In Partial Fulfillment

Of the Requirements

For the Degree of

MASTER OF SCIENCE

By

Laura A Rechner, B.S.
Houston, Texas

May, 2011

Dedication

To my parents

For encouraging me in everything I do

To my husband

For always being my buddy

Acknowledgements

I would like to thank my advisor, Dr. Wayne Newhauser, for his guidance and support throughout this project. Being part of this research group has provided educational opportunities above and beyond what I could have imaged. I would also like to thank Dr. Rebecca Howell for her mentorship on my committee and throughout my graduate studies. Also, many thanks to my committee members for their support of this project: Dr. Lei Dong, Dr. Rajat Kudchadker, Dr. Dragan Mirkovic, and Dr. Carol Etzel.

Many other people contributed to this project. I would like to thank the members of my research group, whose help and input were invaluable: Rui Zhang, Annelise Giebeler, Kenny Homann, Dr. Phil Taddei, Dr. Jonas Fontenot, Dr. Angelica Perez-Andujar, Tim Jones, and John Eley. Other students were also an important part of my education: Kelly Kisling, Sarah Scarboro, and Ryan Bosca. Additionally, I would like to thank Jennifer Johnson for taking me under her wing and Scharlene Wilson for taking care of *everything*.

I would also like to thank my family. Their love and support has made me who I am today. Specifically, I would like to thank my husband for the countless hours of listening to my presentations and editing my thesis, putting up with my nerdy conversations about medical physics, picking me up after late nights in the office, and most importantly, moving with me so I could further my education. Thank you.

Risk of Second Malignant Neoplasms Following Proton Arc Therapy and Volumetric Modulated Arc Therapy for Prostate Cancer

Publication No. _____

Laura Ann Rechner, B.S.

Supervisory Professor: Wayne D. Newhauser, Ph.D.

The risk of second malignant neoplasms (SMNs) following prostate radiotherapy is a concern due to the large population of survivors and decreasing age at diagnosis. It is known that parallel-opposed beam proton therapy carries a lower risk than photon IMRT. However, a comparison of SMN risk following proton and photon arc therapies has not previously been reported. The purpose of this study was to predict the ratio of excess relative risk (*RRR*) of SMN incidence following proton arc therapy to that after volumetric modulated arc therapy (VMAT). Additionally, we investigated the impact of margin size and the effect of risk-minimized proton beam weighting on predicted *RRR*. Physician-approved treatment plans were created for both modalities for three patients. Therapeutic dose was obtained with differential dose-volume histograms from the treatment planning system, and stray dose was estimated from the literature or calculated with Monte Carlo simulations. Then, various risk models were applied to the total dose. Additional treatment plans were also investigated with varying margin size and risk-minimized proton beam weighting. The mean *RRR* ranged from 0.74 to 0.99, depending on risk model. The additional treatment plans revealed that the *RRR* remained approximately constant with varying margin size, and that the predicted *RRR* was reduced by 12% using a risk-minimized proton arc therapy planning technique. In conclusion, proton arc therapy was found to provide an advantage over VMAT in regard to predicted risk of SMN

following prostate radiotherapy. This advantage was independent of margin size and was amplified with risk-optimized proton beam weighting.

Table of Contents

Signature Page	i
Title Page	ii
Dedication	iii
Acknowledgements.....	iv
Abstract.....	v
Table of Contents.....	vii
List of Figures.....	x
List of Tables	xiii
Chapter 1 Introduction.....	1
1.1 Prostate Cancer	1
1.2 External Beam Radiation Therapy.....	2
1.2.1 Photon Therapy.....	2
1.2.2 Proton Therapy	6
1.3 Risk of Second Malignant Neoplasms from Radiation Therapy.....	12
1.4 Statement of the Problem.....	16
1.5 Hypothesis and Specific Aimes	17
Chapter 2 Methods and Materials.....	18
2.1 Patient Selection and Contouring	18
2.2 Treatment Planning and Therapeutic Dose Determination	20
2.2.1 Volumetric Modulated Arc Therapy	22
2.2.2 Proton Arc Therapy	23
2.3 Stray Dose Estimation	32
2.3.1 Volumetric Modulated Arc Therapy	32

2.3.2	Proton Arc Therapy	33
2.4	Risk Prediction.....	36
2.4.1	Linear-No-Threshold Model.....	36
2.4.2	Alternate High Dose Risk Models	38
2.4.3	Example Risk Calculations	42
2.4.4	Statistical Analysis.....	44
2.4.5	Uncertainty Analysis	45
2.4.6	Summary of Risk Calculations	49
Chapter 3	Results	50
3.1	Therapeutic Dose Distributions	50
3.1.1	Volumetric Modulated Arc Therapy	50
3.1.2	Proton Arc Therapy	54
3.1.3	Dose-Volume Histogram Comparisons	62
3.2	Stray Dose Determination.....	72
3.2.1	Volumetric Modulated Arc Therapy Stray Dose.....	72
3.2.2	Proton Arc Therapy Stray Dose.....	74
3.3	Risk Prediction.....	74
3.3.1	Statistical Analysis.....	82
3.3.1	Uncertainty Analysis	83
Chapter 4	Discussion and Conclusion	86
4.1	Outcome of the Specific Aims.....	86
4.1.1	Outcome of Specific Aim 1	86
4.1.1	Outcome of Specific Aim 2	87
4.1.1	Outcome of Specific Aim 3	88

4.2	Comparison with Existing Literature.....	88
4.3	Implications and Significance of this Study	91
4.4	Strengths of this Study.....	92
4.5	Limitations of this Study	93
4.6	Future Work.....	95
4.7	Conclusions.....	96
	Bibliography	96
	Vita	118

List of Figures

Figure 1.1: Bragg Curve	6
Figure 1.2: Spread-out Bragg Peak.....	8
Figure 1.3: Stray Neutron Dose.....	11
Figure 1.4: Second Cancer Risk vs. Dose.....	14
Figure 1.5: Second Cancer Risk for Various Risk Models.....	16
Figure 2.1: Margin Sizes Around CTV	21
Figure 2.2: VMAT Arcs	23
Figure 2.3: Proton Margin Definition.....	26
Figure 2.4: Proton Beam Pairs.....	28
Figure 2.5: Varying Proton Margin Definition.....	31
Figure 2.6: Neutron Radiation Weighting Factor	34
Figure 2.7: Bladder Risk Models.....	41
Figure 2.8: Rectum Risk Models	42
Figure 2.9: Example Risk Calculation.....	43
Figure 3.1: Specific Aim 1 Plans, VMAT	51
Figure 3.2: Specific Aim 3 Plans, VMAT	53
Figure 3.3: Dose vs. Margin Size, VMAT.....	54
Figure 3.4: Dose vs. Number of Beams, Proton Arc Therapy.....	55
Figure 3.5: Risk vs. Number of Beams, Proton Arc Therapy.....	55
Figure 3.6: Isodose Lines, Proton Arc Therapy.....	56
Figure 3.7: Specific Aim 1 Plans, Proton Arc Therapy.....	57
Figure 3.8: Specific Aim 2 Plans, Proton Arc Therapy.....	59
Figure 3.9: Specific Aim 2 Plans, Proton Arc Therapy.....	59

Figure 3.10: Specific Aim 3 Plans, Proton Arc Therapy	61
Figure 3.11: Dose vs. Margin Size, Proton Arc Therapy.....	62
Figure 3.12: Bladder and Bladder Wall DVHs.....	63
Figure 3.13: Rectum and Rectal Wall DVHs	63
Figure 3.14: Specific Aim 1 Bladder Wall DVHs	64
Figure 3.15: Specific Aim 1 Rectal Wall DVHs	65
Figure 3.16: Specific Aim 2 Objective 1 DVHs.....	66
Figure 3.17: Specific Aim 2 Objective 2 DVHs.....	67
Figure 3.18: Specific Aim 2 Objective 3 DVHs.....	67
Figure 3.19: Specific Aim 2 Objective 4 DVHs 1.....	68
Figure 3.20: Specific Aim 2 Objective 4 DVHs 2.....	68
Figure 3.21: Specific Aim 3 DVHs, Bladder Wall VMAT	70
Figure 3.22: Specific Aim 3 DVHs, Rectal Wall VMAT.....	70
Figure 3.23: Specific Aim 3 DVHs, Bladder Wall Proton Arc Therapy	71
Figure 3.24: Specific Aim 3 DVHs, Rectal Wall Proton arc Therapy	72
Figure 3.25: Specific Aim 1 <i>ERR</i> Histogram	75
Figure 3.26: Specific Aim 1 <i>RRR</i> Histogram	76
Figure 3.27: Specific Aim 2 <i>ERR</i> vs. Beam Angle.....	78
Figure 3.28: Specific Aim 2 <i>RRR</i> Histogram	79
Figure 3.29: Specific Aim 3 <i>ERR</i> vs. Margin, LNT	81
Figure 3.30: Specific Aim 3 <i>ERR</i> vs. Margin, All Models	81

Figure 3.31: Specific Aim 3 *RRR* vs. Margin, All Models82

Figure 3.32: *RRR* for each Patient with Error Bars85

Figure 3.33: Mean *RRR* for each \bar{w}_R with Error Bars86

List of Tables

Table 2.1: Patient Data	19
Table 2.2: DVH Constraints	20
Table 2.3: Expansion Margins around CTV	22
Table 2.4: Optimization Constraints.....	29
Table 2.5: Specific Aim 2 Objectives.....	30
Table 2.6: Compensator Smearing, Proximal and Distal Margins	32
Table 2.7: Lateral Margins	32
Table 2.8: Neutron Radiation Weighting Factors.....	35
Table 2.9: Risk Model Parameters.....	40
Table 2.10: Summary of Specific Aims	49
Table 2.11: Summary of Neutron Doses	49
Table 3.1: Dose Statistics, Specific Aim 1 VMAT	52
Table 3.2: Dose Statistics, Specific Aim 3 VMAT	53
Table 3.3: Dose Statistics, Specific Aim 1 Proton Arc Therapy	58
Table 3.4: Dose Statistics, Specific Aim 2 Proton Arc Therapy	60
Table 3.5: Dose Statistics, Specific Aim 3 Proton Arc Therapy	61
Table 3.6: DVH Statistics, Specific Aim 1	65
Table 3.7: DVH Statistics, Specific Aim 2.....	69
Table 3.8: DVH Statistics, Specific Aim 3, VMAT	71
Table 3.9: DVH Statistics, Specific Aim 3, Proton Arc Therapy	72
Table 3.10: VMAT Stray Dose.....	73
Table 3.11: Proton Arc Therapy Stray Dose	74
Table 3.12: <i>ERR</i> , Specific Aim 1.....	75

Table 3.13: <i>RRR</i> Specific Aim 1.....	76
Table 3.14: <i>ERR</i> vs. Beam Angle, Specific Aim 2	77
Table 3.15: <i>RRR</i> Specific Aim 2, 1.....	78
Table 3.16: <i>RRR</i> Specific Aim 2, 2.....	79
Table 3.17: Sign Test.....	83
Table 3.18: T-Test	83
Table 3.19: Sensitivity Test for \bar{w}_R	84
Table 3.17: Uncertainties.....	84
Table 4.1: Comparison to Other Work	90

Chapter 1

Introduction

This chapter contains an introduction to prostate cancer (section 1.1) as well as external beam photon (section 1.2.1) and proton (section 1.2.2) radiotherapy techniques. The risk of second malignant neoplasms from radiation therapy (section 1.3) will be briefly reviewed. Finally, the statement of the problem (section 1.4) is followed by the hypothesis and specific aims (section 1.5).

1.1. Prostate Cancer

Prostate cancer is a disease with a large incidence and a high survival rate, which translates into a substantial population of survivors. It is the most common cancer in men, excluding non-melanoma skin cancer, with approximately 217,730 new prostate cancer cases diagnosed in the United States in 2010 (Jemal *et al.*, 2010). Most cases of prostate cancer are curable; the relative 5-year survival rate is nearly 100% and the relative 10-year survival rate is 91% (American Cancer Society, 2011). Consequently, as of 2007, there were approximately 2.3 million prostate cancer survivors in the United States (SEER, 2007).

Another factor contributing to the large population of prostate cancer survivors is that men are being diagnosed with prostate cancer earlier in life and at an earlier stage of disease progression. This is in part due to the development of the prostate-specific antigen (PSA) test, a non-invasive blood test which is widely used in assessing a patient's risk of prostate cancer (American Cancer Society, 2011). The mean age of diagnosis has decreased from 72 years in 1990 (Quinn and Babb, 2002) to approximately 67 years in 2007 (SEER, 2007).

There are multiple effective treatment options for men diagnosed with prostate cancer including surgery, hormone therapy, external beam radiation therapy, and low and high dose

rate brachytherapy. Active surveillance is also an appropriate option for many men who have asymptomatic and slow-growing tumors (American Cancer Society, 2011). The treatment strategy for each specific case is determined by the physician and the patient and takes into account factors like tumor stage, and the patient's age and overall health.

1.2. External Beam Radiation Therapy

External beam radiation therapy (EBRT) is a good treatment option for many patients and is a component of approximately one third of all prostate cancer patients' therapy (Mettlin *et al.*, 1997; Virnig *et al.*, 2002). EBRT is, in part, so prevalent due to its effectiveness. D'Amico *et al.* (1998) reported no statistical difference in biochemical outcomes in patients who were treated with radical prostatectomy vs. EBRT for localized prostate cancer. Additionally, EBRT has the advantage of being non-invasive and safer than radical prostatectomy for patients with lower overall health status by eliminating surgery-specific risks, for example, the risk of infection (Culver *et al.*, 1991).

However, radiation therapy is not free from risk. Patients can experience acute or late effects from radiation due to irradiation of normal tissues. For prostate radiotherapy, acute effects can include urinary urgency or incontinence, bowel irritation, and rectal bleeding (American Cancer Society, 2011), which usually resolve with time. Some patients experience late effects of radiation; for example, patients who survive more than approximately five years have an increased risk of developing secondary solid tumor due to radiation exposure (Brenner *et al.*, 2000).

1.2.1. Photon Therapy

Photons have been used for radiation therapy since the early 1900s after Roentgen discovered the x-ray in 1895. Many technological advances have improved our ability to deliver radiation dose accurately and precisely to tumors and minimize dose to normal tissue. Medical megavoltage linear accelerators (linacs), invented in the 1960's, provided significant

skin sparing compared to lower energy x-ray therapy. Then, in the 1980s, computed tomography (CT) imaging made it possible to visualize the target volume on a three-dimensional (3-D) image. Additionally, it became possible to visualize the dose distribution and anatomy in 3-D with treatment planning systems (TPSs). The standard of care then became 3-D conformal radiation therapy (3DCRT), which refers to radiotherapy that, in addition to being planned in 3-D, is shaped in the beam's eye view around the target volume to reduce dose to normal tissue. These advances facilitated prostate dose escalation from approximately 65 gray (Gy) to doses in the high 70s of Gy (Thompson, 2007). In the 1990s, intensity modulated radiation therapy (IMRT) and image guided radiation therapy (IGRT) became available, which provided additional improvement in accurately delivering conformal dose distributions. In particular for prostate cancer, Zelefsky *et al.* (2000) showed that IMRT improved coverage of the clinical target volume (CTV), decreased bladder and rectal doses, and decreased the incidence of rectal bleeding compared to 3DCRT.

The current standard of care for photon EBRT for prostate cancer at The University of Texas MD Anderson Cancer Center (MDACC) is IMRT. Linac based IMRT creates conformal dose distributions with a multi-leaf collimator (MLC), which modulates the fluence of photons across the two-dimensional cross-section of each beam. There are two ways that the MLC can operate during the delivery of the treatment beam. The first way is dynamically, also known as the sliding window technique, which is achieved by delivering the radiation while the leaves move across the field. The second approach is for the beam to turn off while the leaves move to the next position, only delivering radiation when the leaves are stationary. This second technique is known as step-and-shoot, and is the method implemented at MDACC. Chui *et al.* (2001) and Longobardi *et al.* (2005) compared the two techniques and found comparable dosimetric quality and accuracy between the two (given adequate segments for step-and-shoot, approximately 10 per beam). Chui *et al.* also found that sliding window required approximately

20% more monitor units (MUs), but that the overall treatment time was roughly two times faster than the step-and-shoot method.

The first rotational intensity modulated photon radiotherapy technique, tomotherapy, was proposed by Mackie and colleagues and published in 1993 (Mackie *et al.*, 1993). In this technique, intensity modulation is accomplished by delivering radiation in slices and setting collimating leaves to either fully open or fully closed positions. The first clinical implementation of this “slice therapy” was the PeacockTM system (Nomos Corporation, Sewickley, PA), which used a MIMiCTM MLC mounted on a linac gantry (Carol, 1994; Carol, 1995; Mackie, 2006). Treatment was delivered serially, and the treatment couch was advanced for the delivery of each adjacent slice. Then, TomoTherapy® Incorporated developed a CT scanner type gantry with a linac that rotates and delivers radiation helically while the patient is advanced continuously through the bore (Mackie *et al.*, 1999; Yang *et al.*, 1997; Mackie, 2006). With helical delivery, patient positioning errors were not as critical as with serial delivery, where a 1 mm positioning error could cause dose errors of approximately 10-20% (Carol *et al.*, 1996; Low and Mutic, 1997). The new technique also significantly reduced the treatment time, from the order of 30 minutes for serial delivery (Xia *et al.*, 2000) to a mean treatment time of 10.7 minutes for helical delivery (Sterzing *et al.*, 2008).

A more recently introduced rotational intensity modulated photon radiotherapy technique, which can be administered with a conventional linac, is volumetric modulated arc therapy (VMAT). Unlike tomotherapy, an entire volume, instead of a slice, can be irradiated in single rotation and with a fixed couch position. The specific method was first published by Otto in 2008 (Otto, 2008), which expanded on a method proposed and developed by Yu (1995). Both dose rate and rotation speed are varied during beam delivery, providing additional degrees of freedom in treatment planning. The VMAT optimization algorithm described by Otto was implemented in the Eclipse (Varian Medical Systems, Palo Alto, CA) TPS, which

approximates an arc as multiple static beams, starting with a low resolution and increasing to 177 beams as it optimizes, while constraining both the dose rate and the MLC motion to take into account the mechanical and radiation limitations of the linac and MLC (Otto, 2008). Our institution has treated a small number of patients with VMAT since 2009, including patients with prostate cancer. To date, it appears that the main advantage of this technique is shorter treatment times while preserving plan quality comparable to IMRT (Kjaer-Kristoffersen *et al.*, 2009; Zhang *et al.*, 2009; Palma *et al.*, 2008; Bedford and Warrington, 2009). Otto reported treatment times between about 1.5 to 3 minutes for one arc. Specifically, delivery time for a one-arc nasopharynx VMAT treatment plan was 1.8 minutes, and delivery time for a comparable 7-field nasopharynx IMRT plan was 7.1 minutes (Otto, 2008). The experience at our institution is that two arcs are required for optimal treatment plans, yielding treatment delivery times of approximately three minutes.

An undesirable aspect of *all* EBRT photon radiotherapy techniques is that the patient is also exposed to some stray radiation. The sources of this stray radiation are photon leakage from the treatment head and MLC leaves, photon scatter from the collimator and the patient, and, above approximately 6 MeV, secondary neutrons produced by (γ,n) reactions in the treatment head and, to a lesser degree, the patient (Howell *et al.*, 2009; NCRP, 2005). In or near the treatment field, scatter is the predominant source of stray radiation, whereas far from the treatment field, leakage predominates (Kase *et al.*, 1983; Stovall *et al.*, 1995). Radiation exposures from leakage and scatter photons and photoneutrons (for 10 MV photon beams and above) have been measured and characterized for conventional therapy (Kase *et al.*, 1983; Stovall *et al.*, 2006), IMRT (Kry *et al.*, 2005b; Howell *et al.*, 2006; Wang and Xu, 2008), and tomotherapy (Ramsey *et al.*, 2006). Also, Xu *et al.* (2008) have published a review on the topic. To our knowledge, there have not been any reports on leakage and scatter exposures for VMAT. However, some studies have implicitly made the assumption that the stray radiation dose from VMAT is

equivalent (per MU) to that from IMRT (Palma *et al.*, 2008; Kjaer-Kristoffersen *et al.*, 2009; Wolff *et al.*, 2009; Yoo *et al.*, 2010). To date, VMAT has only been used with 6 MV, thus secondary neutrons are not a concern.

1.2.2. Proton Therapy

Robert Wilson proposed the medical use of protons in the treatment of tumors in 1946 (Wilson, 1946). In his paper, Wilson described the advantageous dosimetric properties of protons, namely, how they deposit a large portion of their dose in the last few millimeters of their range near the peak of the Bragg curve (Figure 1.1). Beyond their range, determined by their initial kinetic energy, the dose falls rapidly to almost zero, thus enabling sparing of the tissue distal to the target.

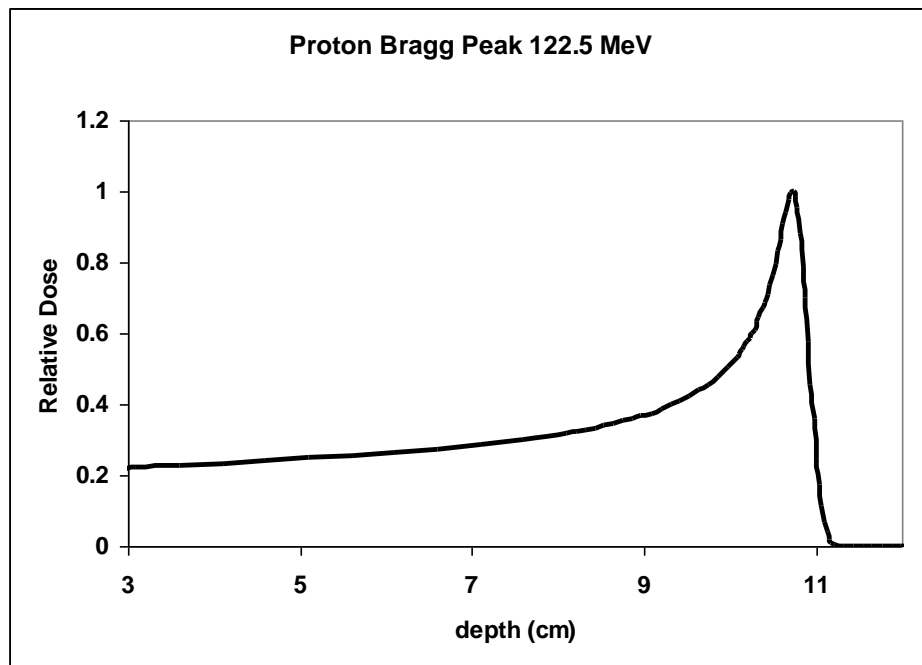


Figure 1.1 – Relative absorbed dose of a simulated Bragg curve from an unmodulated 122.5 MeV proton beam vs. depth in water.

The first therapeutic use of proton therapy in humans was for the pituitary gland in 1954 (Lawrence *et al.*, 1958), then for brain tumors shortly after (Kjellberg *et al.*, 1962; Larsson *et al.*, 1963; Kjellberg and Kliman, 1973; Munzenrider and Liebsch, 1999). Later, proton therapy

was also extensively used in the treatment of ocular tumors, chordomas, and chondrosarcomas (Munzenrider *et al.*, 1980; Suit *et al.*, 1982; Gragoudas, 1986; Munzenrider, 1999).

To date, over 67,000 patients have been treated with proton therapy, and there are approximately 28 centers in operation world-wide (Particle Therapy Co-Operative Group, 2010). Of this large population of proton therapy patients, prostate cancer patients are the majority (Sisterson, 2005), which have resulted in disease-free survival rates comparable to other forms of local therapy and minimal morbidity (Slater *et al.*, 2004; Nihei *et al.*, 2010).

Proton therapy dose is prescribed differently than photon therapy dose. Proton beams are believed by some to have a slightly higher relative biological effectiveness (RBE) compared to photon beams (ICRU, 2007). To attempt to account for these differences, the ICRU recommends a generic RBE value of 1.1 and that the dose be prescribed in units of Gy (RBE), where $D_{RBE}[\text{Gy (RBE)}] = D_{\text{absorbed}}[\text{Gy}] \times \text{RBE}$. This convention is controversial, but is widely used.

There are two main methods to cover the cross-sectional area of a target volume with a proton beam (Chu, 1993). The first method to provide lateral coverage of the target is to spread the pencil beam into a larger field. The second method is to “sweep” the pencil beam across the target using deflecting magnets. These two modes of delivery are referred to as passive scattering and beam scanning (or active scanning), respectively, and passive scattering is far more prevalent around the world (Sisterson, 2005).

Passive scattering is achieved by spreading the pencil beam of protons into a large, uniform field with scattering foils. A double scattering approach was proposed by Koehler *et al.* (1977) and uses a first scatterer to spread the beam, a central beam stop to eliminate the protons in the center of the field, and then a second scatterer to further spread the beam to produce a large and relatively uniform proton field. This approach was subsequently refined by Gottschalk and others and is simple, safe, and versatile (Gottschalk *et al.*, 1991).

It is also necessary to broaden the high dose region over the target volume in depth. A proton's range is determined by its energy, where a higher energy results in a longer range. Therefore, modulating the beam's energy will modulate the beam range. One method is to use a range modulator wheel (RMW), which has steps of varying thickness of absorbing material to modulate the range (Chu, 1993). The RMW rotates quickly through the beam to produce multiple Bragg peaks with varying range. The summation of these modulated pristine peaks produces a spread-out Bragg peak (SOBP) of a desired width (Figure 1.2). This was proposed by Wilson (1946) and implemented by Koehler *et al.* (1975) at the Harvard Cyclotron Laboratory.

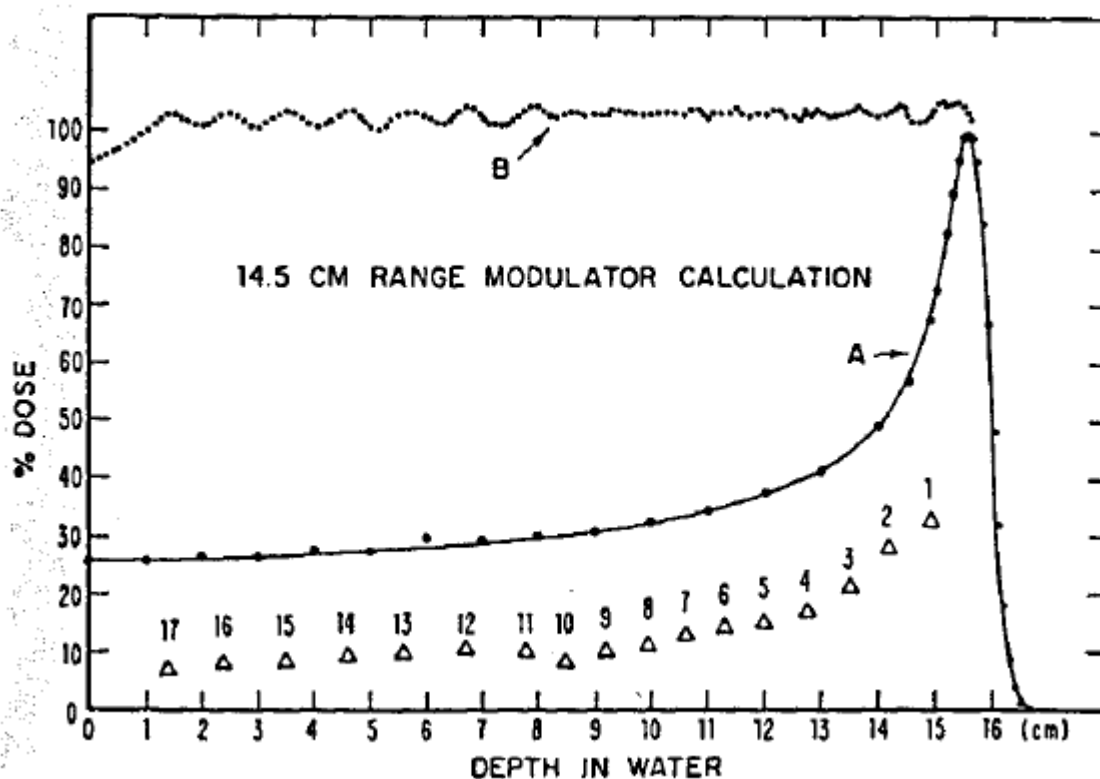


Figure 1.2 – Relative absorbed dose from a spread-out Bragg peak, B, of 14.5 cm width resulting from the sum of the pristine Bragg curves such as A (Koehler *et al.*, 1975). The depths and magnitudes of the shifted Bragg curves relative to A are denoted by the triangles labeled 1-17. Reprinted from Nuclear Instruments and Methods, 131, A.M. Koehler, R.J. Schneider, J.M. Sisterson, Range modulators for protons and heavy ions, 438, 1975, with permission from Elsevier

After a proton beam is spread laterally (cross-field direction) and longitudinally (depth direction), further modifications are required to conform the beam to the target volume. Beam-specific brass apertures are used to collimate the cross-section of the beam to the shape of the target (Wagner, 1982). In addition, to conform the distal end of the SOBP to the target, a beam-specific range compensator is milled to pull the range of the protons back where necessary (Wingate *et al.*, 1977; Goitein, 1978; Wagner, 1982; Urie *et al.*, 1984).

In recent years, interest in rotational delivery of proton beams has increased. To our knowledge, the first appearance of proton arc therapy in the literature was in 1997, when three separate groups published studies on the topic. The first publication was a simulation study for a Ewing sarcoma treatment (Isacsson *et al.*, 1997), the second publication was a phantom study for a chest wall irradiation (Sandison *et al.*, 1997), and the third publication was a patent for a method and apparatus for proton arc therapy (Deasy, 1997). Since proton arc therapy's appearance in the literature, various other papers have been published. Oelfke and Bortfeld (2000) reported a factor of 2 – 3 reduction in integral dose to healthy tissue for inverse planned proton arc therapy when compared to photon IMRT for a simulation of irradiation of a planar circular target. Similarly, Flynn *et al.* (2007) found the integral dose was lowered by a factor of about 2 for proton arc therapy compared to photon IMRT and helical tomotherapy. Sengbusch *et al.* (2009) investigated the energy required to treat patients with proton arc therapy and found that, with an AP arc and a PA arc, each subtending 90 degrees, 90% of the patients in their study could be treated with a proton kinetic energy of 198 MeV or less. One particular design for a compact proton accelerator capable of arc delivery is under commercial development by TomoTherapy Incorporated (Madison, Wisconsin) in partnership with Lawrence Livermore National Laboratory (Mackie *et al.*, 2007; Caporaso *et al.*, 2008; Chen, 2009). This design proposes to use the dielectric wall accelerator technology to achieve a “one room” proton therapy delivery system capable of simultaneous scanned beam delivery and gantry rotation.

One of the reasons for this interest in proton arc therapy is the potential improvement in conformity that arc therapy could provide. Currently, IMRT rivals proton therapy with regard to dose conformity due to the comparatively large number of treatment gantry angles used in IMRT (Bortfeld, 2006; Trofimov *et al.*, 2007). However, it is possible that by increasing the number of beam angles (or a delivering through an arc) proton therapy could provide significantly better conformity than IMRT or VMAT.

Theoretically, one can deliver proton arc therapy with current proton gantries using the passive scattering technique. For example, the SOBPs width can be varied throughout the rotation by altering the gating of the beam through different steps of the range modulator wheel. Then, the range could be varied by using a robotic wedge energy degrader (Chu, 1993; Lu, 2008a, b; Titt *et al.*, 2010; Melancon, 2010), and the shape of the beam could be defined by a proton-appropriate MLC (Brahme *et al.*, 1987; Chu, 1993; Bues *et al.*, 2005; Slopsma and Kooy, 2006; McDonough and Tinnel, 2007). While many technical aspects of proton arc delivery still require research and development, there are no known fundamental obstacles to its implementation.

One poorly understood aspect of proton arc therapy is the exposure of patients to stray radiation. Similar to photon therapy, proton therapy patients are also exposed to stray radiation, which originates from neutrons produced in (p, xn) reactions. These neutrons can be produced externally by reactions in the treatment unit, or internally by reactions in the patient's body. Since the spot scanning technique uses magnetic fields to laterally spread the beam instead of scattering foils, external neutron production is comparatively small (Schneider *et al.*, 2002). However, with optimized design, neutron production in passively scattered proton treatment units can be reduced (Tayama *et al.*, 2006a; Taddei *et al.*, 2008; Brenner and Hall, 2008; Taddei *et al.*, 2009a), diminishing the advantage of scanning delivery. The neutrons produced in the passive scattering technique are dependent on the general construction of the beam

nozzle and increases with increasing proton beam energy, increasing SOBP width, increasing uncollimated proton field size, and decreasing aperture size (Yan *et al.*, 2002; Mesoloras *et al.*, 2006; Zheng *et al.*, 2008a; Taddei *et al.*, 2008). Neutron dose values from the literature vary dramatically between different facilities, suggesting a strong dependence on delivery technique, facility design, and the method of measurement or simulation (a sample of which are plotted in Figure 1.3) (Schneider *et al.*, 2002; Yan *et al.*, 2002; Fontenot *et al.*, 2005b; Polf *et al.*, 2005; Hall, 2006; Mesoloras *et al.*, 2006; Tayama *et al.*, 2006a; Zheng *et al.*, 2007a; Moyers *et al.*, 2008b; Wang *et al.*, 2010; Yonai *et al.*, 2010; Zhang *et al.*, 2010; Clasié *et al.*, 2010). These values range from 0.025 millisieverts per gray (mSv/Gy) (Mesoloras *et al.*, 2006) to 8.92 mSv/Gy (Schneider *et al.*, 2002; Hall, 2006).

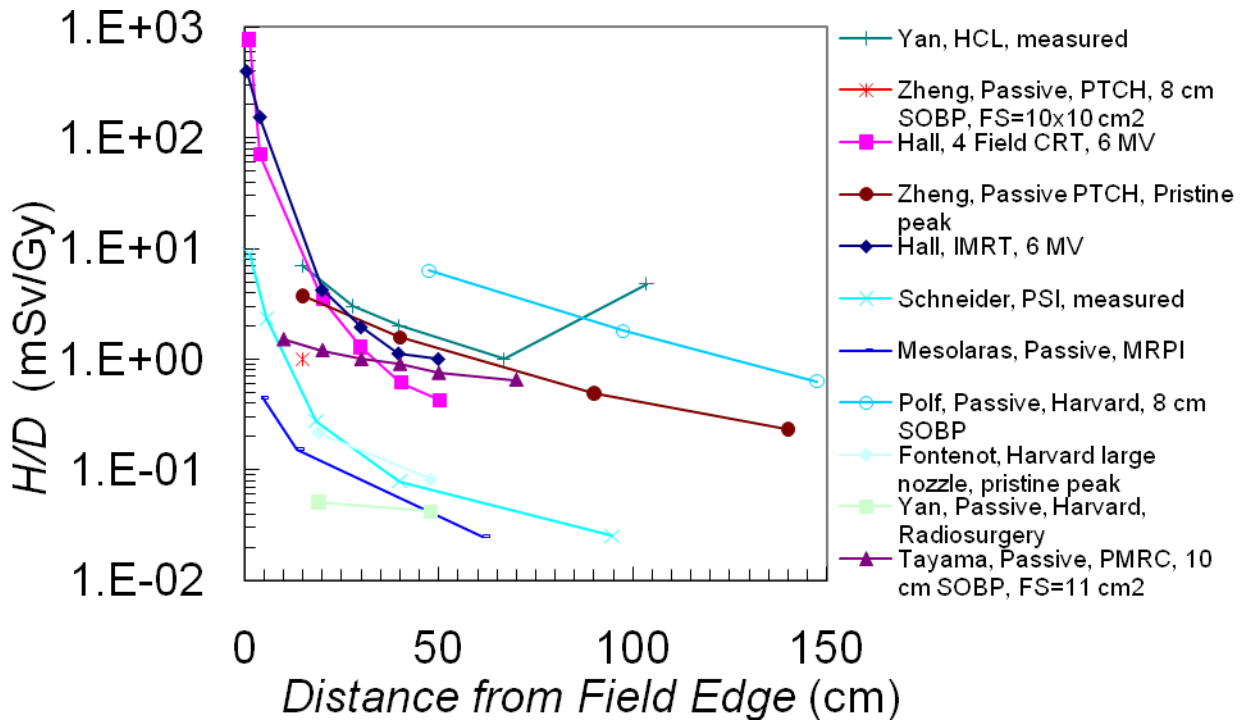


Figure 1.3 – Stray neutron equivalent dose per therapeutic absorbed dose (H/D) for proton beams as a function of distance from proton field edge (Schneider *et al.*, 2002; Yan *et al.*, 2002; Fontenot *et al.*, 2005b; Polf *et al.*, 2005; Hall, 2006; Mesoloras *et al.*, 2006; Tayama *et al.*, 2006a; Zheng *et al.*, 2007a). For comparison, values are also plotted for 6 MV IMRT (navy) and 6 MV 4 field CRT (pink) (Hall, 2006).

There have been some stray equivalent dose measurements and simulations specifically for proton therapy of the prostate (Wroe *et al.*, 2007; Fontenot *et al.*, 2008; Zheng *et al.*, 2008a; Taddei *et al.*, 2008; Wroe *et al.*, 2009; Newhauser *et al.*, 2009b; Yepes *et al.*, 2009). For example, Wroe *et al.* performed measurements at Loma Linda University Medical Center (2007) and Massachusetts General Hospital (2009), which ranged from 0.1 mSv/Gy to 10 mSv/Gy, depending on facility and distance from isocenter. One study from our institution was reported by Zheng *et al.* (2008a), in which the effective dose was found to be 8 mSv/Gy for proton therapy of the prostate. Additionally, Fontenot *et al.* (2008) simulated stray neutron doses resulting from a prostate therapy treatment at our institution and found doses ranging from 1.9 mSv/Gy to 12.3 mSv/Gy, where dose decreased with increasing distance from isocenter. In a similar study, Taddei *et al.* (2008) found equivalent doses ranging from 1.05 mSv/Gy to 19.7 mSv/Gy.

1.3. Risk of Second Malignant Neoplasms from Radiation Therapy

Ionizing radiation damages cells, and when damaged cells are not sterilized, they have the potential to mutate and become carcinogenic (Preston *et al.*, 2007). Therefore, patients receiving radiation therapy are at increased risk for the development of a second primary cancer, or second malignant neoplasm (SMN) (NRC, 2006).

Epidemiological studies on the risk of SMN incidence following prostate radiotherapy are not coherent. Some studies report an increased risk of an SMN, including cancers of the bladder and rectum (Brenner *et al.*, 2000; Moon *et al.*, 2006; Kendal *et al.*, 2007). However, one study reported an increased risk of bladder cancer but not rectal cancer (Curtis *et al.*, 2006). Interestingly, Chrouser *et al.* (2005) only found an increased risk of bladder cancer in those patients who had a prostatectomy prior to radiotherapy, and Pickles and Phillips (2002) found an increased risk of bladder cancer in non-irradiated patients but not in irradiated patients. While much uncertainty remains regarding risk of SMN following prostate radiotherapy, the

absolute risk of incidence of a radiogenic second malignant neoplasm is most likely on the order of a percent or two: 0.3% for all patients, and 1.4% for patients who survive at least 10 years (Brenner *et al.*, 2000).

While epidemiological data would be ideal for assessing risks, large follow-up times are required and the quality and completeness of dosimetric information is often lacking; therefore, it is not feasible to use any single epidemiological study predict patient-specific risk following current radiotherapy techniques. In order to predict patient-specific risk of SMN incidence following a particular radiotherapy treatment or to compare the predicted risk between different treatments, a rigorous, reproducible, and well-understood method is required. First, an accurate and complete knowledge of the dose distribution in the organs of interest is needed. Then, the relationship between radiation dose and the risk of SMN incidence can be applied to the dosimetric information. These methods were previously developed and applied to studies of proton therapy and IMRT for prostate cancer (Kry *et al.*, 2005a; Schneider *et al.*, 2007; Taddei *et al.*, 2008; Fontenot *et al.*, 2009; Bednarz *et al.*, 2010), but not for arc therapies. The current state of knowledge in radiation risk estimation is briefly reviewed below.

It is generally accepted that there is a linear-no-threshold (LNT) relationship between equivalent doses and risk of cancer between 0 Sv and about 2.5 Sv (NCRP, 1993; NRC, 2006); however, the relationship between dose and risk at higher doses is less well understood. At higher doses, cell sterilization increases, and the general relationship between dose and risk for most tissues most likely lies somewhere between a linear and a linear-exponential model (Hall and Wu, 2003; Sachs and Brenner, 2005; Schneider *et al.*, 2007; Schneider *et al.*, 2006; Schneider *et al.*, 2005).

Not surprisingly, different tissues have been shown to exhibit different risk relationships with dose (Boice *et al.*, 1988; Lindsay *et al.*, 2001; Hall and Wu, 2003; Dasu and Toma-Dasu, 2005; Schneider *et al.*, 2005; Sachs and Brenner, 2005) (Figure 1.4). For example, risk of an

SMN in the thyroid has been shown to exhibit a linear-exponential relationship with dose, increasing linearly to an inflection point at approximately 20 - 30 Gy, then decreasing at higher doses (Thompson *et al.*, 1994; Ron *et al.*, 1995; Sigurdson *et al.*, 2005; Ronckers *et al.*, 2006; Bhatti *et al.*, 2010). In stark contrast, the risk of an SMN in the breast has been shown to increase linearly to approximately 40 Gy while showing no evidence of decrease at high doses (Travis *et al.*, 2003; Travis *et al.*, 2005; Inskip *et al.*, 2009).

The dose-risk relationships of the bladder and rectum are of particular interest to this work. For the bladder, some evidence indicates that the risk of an SMN may plateau beyond approximately 10 Gy (Boice *et al.*, 1988; Neugut *et al.*, 1997; Brenner *et al.*, 2000; Ruben *et al.*, 2008). There is less data regarding the rectum, but in a study by Schneider *et al.* (2005), the risk for all organs was assumed to have a linear-exponential relationship to dose, and the organ-specific exponential term was solved for based on epidemiological data from patients who received radiotherapy for Hodgkin's disease. Their model for the colon (which includes the rectum) has an inflection point at approximately 2 Gy.

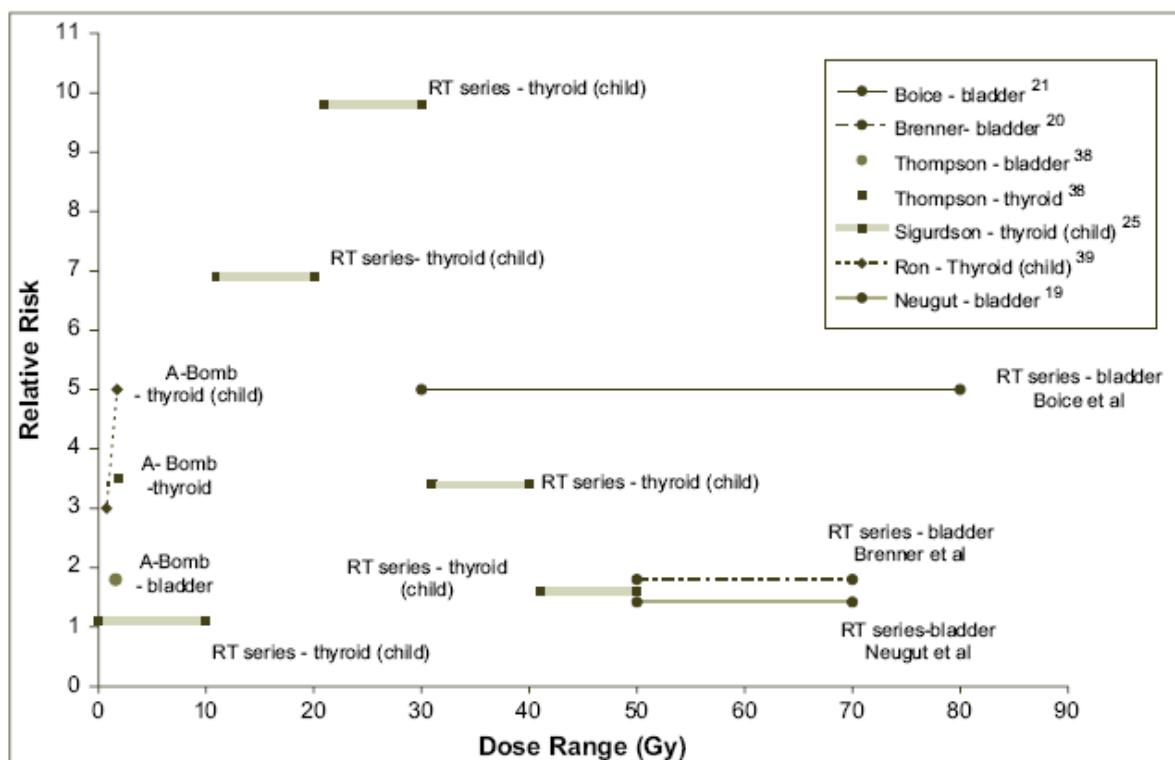


Figure 1.4 - Summary of the data showing the relationship between risk of second cancer and dose from the A-bomb survivors and cancer survivors treated with radiotherapy (Ruben *et al.*, 2008). Reprinted from the International Journal of Radiation Oncology Biology Physics, 70, Jeremy D. Ruben, Sidney Davis, Cherie Evans, Phillip Jones, Frank Gagliardi, Matthew Haynes, Alistair Hunter, Risk of Second Malignant Neoplasms following VMAT and Proton Arc Therapy for Prostate Cancer, 1532, 2008, with permission from Elsevier.

Using the risk models from the literature, Fontenot *et al.* (2009) predicted the risk of SMN incidence (including fatal and non-fatal cancers) following both IMRT and proton therapy for three prostate cancer patients (of small, medium, and large anatomical stature). Specifically, the authors used detailed dosimetric information, including stray dose, and applied risk models to calculate the risk to each organ. In order to cover the range of possible dose-response relationships indicated by the data in the literature, they applied the LNT model (NRC, 2006), the linear-exponential model, and the linear-plateau model. Furthermore, they investigated high-dose (40 Sv) and low-dose (10 Sv) inflection points for the linear-exponential and linear-plateau models, spanning the values reported in the literature. The specific quantities they chose to describe risk were the excess relative risk (*ERR*), where

$$ERR \equiv \frac{\text{Rate in Exposed Population}}{\text{Rate in Unexposed Population}} - 1, \quad (1.1)$$

and the ratio of excess relative risk (*RRR*), where

$$RRR \equiv \frac{ERR_{\text{ProtonTherapy}}}{ERR_{\text{IMRT}}}. \quad (1.2)$$

They found, for all risk models considered, that the *ERR* of an SMN was less for proton therapy than for IMRT (Fontenot *et al.*, 2009) (Figure 1.5) within the uncertainties of the calculation (Fontenot *et al.*, 2010). It was also found that the in-field radiation in the bladder and rectum had the largest impact on the *ERR*. Furthermore, passively scattered (*RRR* = 0.66) and scanned (*RRR* = 0.56) proton therapies both conferred significantly lower predicted risk of SMN incidence than IMRT.

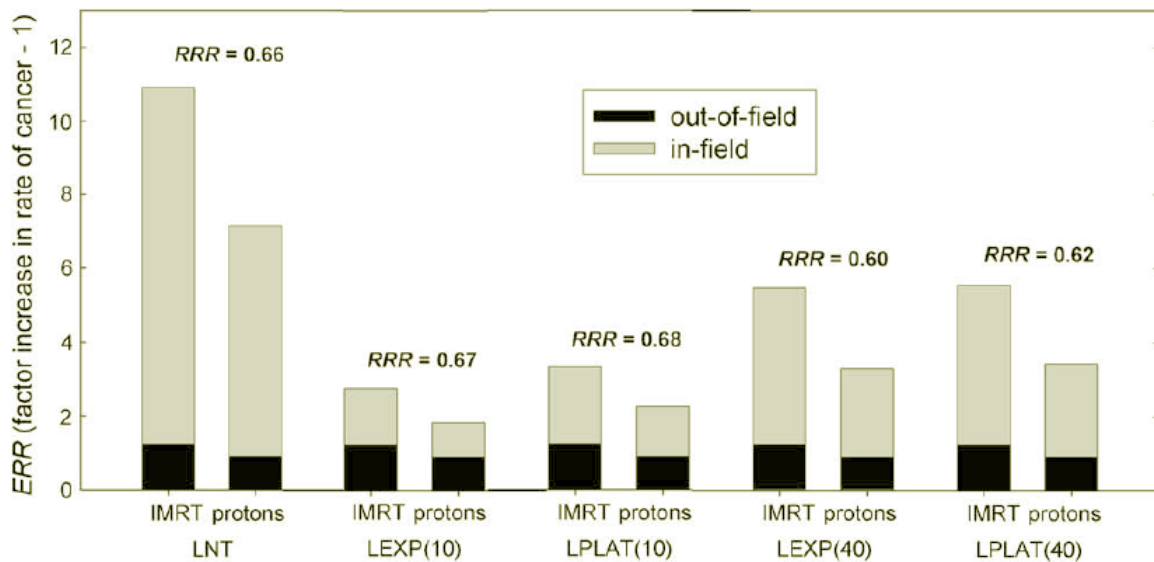


Figure 1.5 – The predicted risk of SMN incidence following IMRT and proton therapy of the prostate from various risk models (Fontenot *et al.*, 2009). It can be seen that the *ERR* of an SMN following IMRT is consistently higher than following proton therapy, and by approximately the same ratio (*RRR*). Reprinted from the International Journal of Radiation Oncology Biology Physics, 74, Jonas D. Fontenot, Andrew K. Lee, Wayne D. Newhauser, Risk of Secondary Malignant Neoplasms from Proton Therapy and Intensity-Modulated X-Ray Therapy for Early-Stage Prostate Cancer, 621, 2009, with permission from Elsevier.

1.4. Statement of the Problem

The risk of SMN incidence following radiotherapy of the prostate is a potentially large public health concern due to the large population of survivors. SMN risk has been estimated for a few case studies following IMRT and proton therapy (Kry *et al.*, 2005a; Schneider *et al.*, 2006; Schneider *et al.*, 2007; Taddei *et al.*, 2008; Fontenot *et al.*, 2009; Bednarz *et al.*, 2010); however, VMAT and proton arc therapy are nascent and proposed modalities, respectively, whose impact on risk of second cancer has not been previously reported. Both are new arc modalities which distribute the therapeutic dose in a different way than their static counterparts. In particular, while arc delivery achieves very conformal distributions in the target region, it spreads lower dose over notably more tissue than static delivery (Kjaer-Kristoffersen *et al.*, 2009; Zhang *et al.*, 2009). Thus, the effect of the differences between static beam and arc delivery on predicted risk is not obvious and requires quantitative investigation.

It is also unknown how the margin size around the clinical target volume (CTV) to create the planning target volume (PTV) affects predicted risk of an SMN for VMAT and proton arc therapy. The required margin size depends on the internal motion, imaging, immobilization, setup uncertainty, and the institution's experience (ICRU, 1999, 2007). With better immobilization and image guided radiotherapy, margin sizes could be reduced. It is expected that the predicted risk of an SMN will decrease with smaller margin sizes.

1.5. Hypothesis and Specific Aims

The hypothesis of this study is that **the predicted *RRR* of SMN incidence in the bladder and rectum 10 years following proton arc therapy relative to that following VMAT will be less than one for prostate cancer for a typical patient exposed at age 60.**

This hypothesis was tested through the following three specific aims:

Specific Aim 1: To predict the *RRR* of SMN incidence following proton arc therapy compared to that following VMAT using calculated dose distributions combined with risk models from the literature.

Specific Aim 2: To investigate the impact of uniform *vs.* variable beam weighting for proton arc therapy based on various host and treatment factors, such as type of second cancer and avoidance of a hip prosthesis, on the predicted *RRR*.

Specific Aim 3: To examine the sensitivity of the predicted *ERR* and *RRR* on the margin size around the clinical target volume following proton arc therapy compared to that following VMAT.

General Methodology

Three patients were selected for this study. For specific aim 1, treatment plans for both VMAT and proton arc therapy were created for each patient, yielding 6 “nominal” treatment plans. Then, the risk of SMN incidence was predicted for each treatment plan using three different risk models: the linear-no-threshold, linear-exponential, and linear-plateau models.

For specific aim 2, variable beam weighting was applied to one of the proton arc plans that was created for specific aim 1, and its impact on risk of SMN incidence examined. Finally, for specific aim 3, the margins around the CTV were varied, and new treatment plans were created for each margin expansion for both VMAT and proton arc therapy. For each new margin plan, the risk of an SMN was predicted to investigate the relationship between risk and margin size.

Chapter 2

Methods and Materials

This chapter describes the methods and materials used in this work, beginning with the patient selection and volume contouring (2.1). Then, the methods for treatment planning and therapeutic dose determination (2.2) is covered, with details pertaining to VMAT (2.2.1) and proton arc therapy (2.2.2). Next, the estimation of stray dose (2.3) is discussed with specifics regarding VMAT (2.3.1) and proton arc therapy (2.3.2). Subsequently, the method used to predict risk of an SMN is discussed (2.4) with specifics regarding the LNT model (2.4.1) and the alternate risk models (2.4.2), followed by an example calculation for each (2.4.3). Finally, the methods section concludes with a review of the methods used for statistical analysis (2.4.4) and uncertainty analysis (2.4.5), and a summary of the risk calculations performed (2.4.6).

2.1. Patient Selection and Contouring

We selected three patients who were previously studied by Fontenot *et al.* (2009) in a comparison of the risk of SMN incidence following IMRT and parallel-opposed beam proton therapy for prostate cancer. For their study, patient information was obtained, in accordance with an institutional review board protocol, from electronic records of patients who were treated at our institution for prostate cancer. A group of 72 patients who were treated in 2007

were analyzed in order to identify patients who represented small, medium, and large patients of the sample based on the range (90% distal dose fall-off) of the lateral proton beam to cover the target volume (prostate, proximal seminal vesicles, and margin). The mean range of the lateral beams was 24.7 cm, with a standard deviation of 1.2 cm. The mean range was determined to be representative of a “medium” patient, and similarly the mean range plus and minus 2σ of the mean range to be representative of a “large” and “small” patient, respectively. A summary of the patients who most closely matched the mean, mean plus 2σ , and mean minus 2σ ranges is presented in Table 2.1.

Table 2.1 - Patient age at exposure, stage of cancer, and range of the proton beam for the selected small, medium and large patients (Fontenot, 2008).

Patient Size	Patient Age at time of Treatment	Adeno-carcinoma stage	Beam Range Formula	Calculated Range (cm)
Small	60 yr	T2a	Mean - 2σ	22.3
Medium	56 yr	T2a	Mean	24.7
Large	46 yr	T1c	Mean + 2σ	27.0

The same organ and structure contours were used for the photon and proton treatment plans for each patient in order to consistently compare the plans. These physician-approved contours included the CTV, PTV, prostate, bladder, rectum, seminal vesicles, and femoral heads. In addition, bladder wall, rectal wall, and various size additional PTV contours were created. The bladder wall and rectal wall thicknesses were defined as 5 mm and 3 mm, respectively (Manieri *et al.*, 1998; Huh *et al.*, 2003), using the automatic margin and Boolean operator tools in the TPS. Slight manual edits were made when the organ wall was clearly visible and the automatically created contour did not match the visible anatomy. The three patients in this study were previously treated with proton therapy, and VMAT and proton arc therapy treatment plans were retrospectively created for the purpose of this study. At the time of simulation,

rectal balloons were used to immobilize the prostate and these immobilization devices were visible on the CT images.

2.2. Treatment Planning and Therapeutic Dose Determination

All treatment plans were created using a commercial treatment planning system (Eclipse, Varian Medical Systems, Palo Alto, CA). The MDACC clinical dose-volume histogram (DVH) constraints (In-house dosimetry guideline, 2009) were used for planning and evaluation of all plans (Table 2.2). Two treatment plans were created for each patient for specific aim 1, one for each modality, and each of the resulting six nominal treatment plans were reviewed, revised as needed, and approved by a board certified radiation oncologist. Additional treatment plans were created for specific aims 2 and 3.

Table 2.2 - Dose volume histogram constraints used for VMAT and proton arc therapy planning. ‘D’ followed by a subscript number corresponds to the percent volume of the organ receiving at least the listed dose constraint, where dose for VMAT is in units of Gy and dose for proton arc therapy is in units of Gy (RBE). For example, $D_{20} \leq 70$ means that 20% of the volume should receive no more than 70 Gy or Gy (RBE).

Organ	DVH Constraints
Bladder	$D_{20} \leq 70$ Gy or Gy (RBE)
Rectum	$D_{60} \leq 40$ Gy or Gy (RBE)
	$D_{50} \leq 45$ Gy or Gy (RBE)
	$D_{40} \leq 60$ Gy or Gy (RBE)
	$D_{20} \leq 70$ Gy or Gy (RBE)
	$D_{15} \leq 76$ Gy or Gy (RBE)
	$D_5 \leq 80$ Gy or Gy (RBE)
Femoral Heads	$D_{15} \leq 45$ Gy or Gy (RBE)

For specific aim 1, the PTV was defined for all patients using margins specified by the current MDACC standard-of-care, which is referred to as the nominal PTV. The CTV was

expanded by 5 mm posteriorly and 7 mm in all other anatomical directions. Then, additional PTVs with smaller and larger margins were created for the medium patient for specific aim 3. All PTVs were created using the “margin for structure” tool to expand the CTV (Figure 2.1).

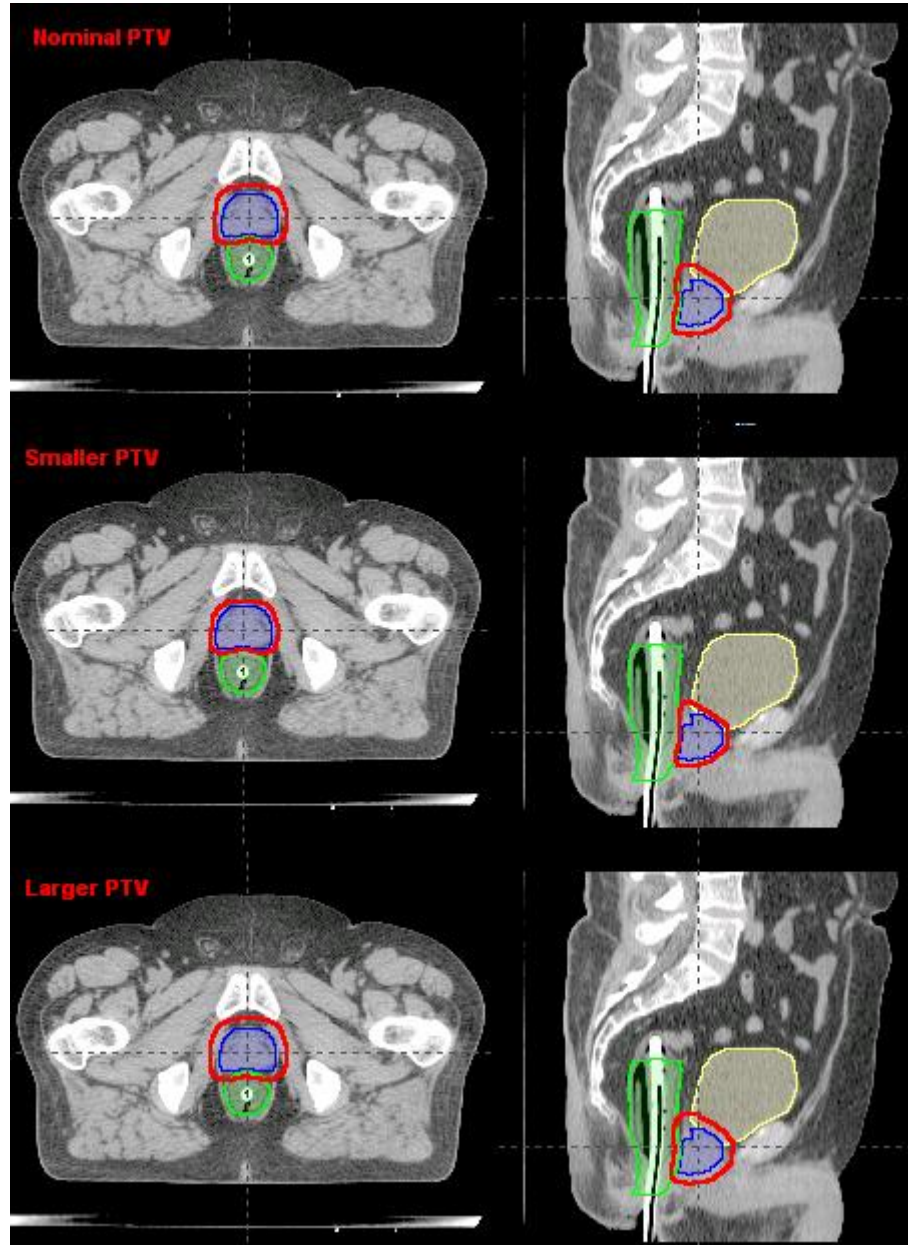


Figure 2.1 - Axial (left) and sagittal (right) CT slices showing the prostate (blue), PTV (red), the rectum and contents (green), and the bladder and contents (yellow) for the nominal PTV (top), a smaller PTV (middle), and a larger PTV (bottom). Notice the decreased amount of normal tissue encompassed within the smaller PTV and the increased amount of normal tissue encompassed within the larger PTV.

In this study the majority of the additional PTVs were smaller than the nominal PTV because it is likely that future improvements in immobilization and imaging technologies will

enable smaller margins, *i.e.* a reduction from our current nominal PTV margins. We used margin expansions ranging from 0 mm (the theoretical limit) to 6 mm posteriorly and 8 mm in all other anatomical directions. A detailed list of all PTV margins used in this study can be found in Table 2.3.

Table 2.3 – Variable CTV expansion margins used to create different PTVs and their differences from the nominal expansions. “Else” refers to all anatomical directions other than posterior.

Plan Index	Posterior Expansion (mm)	Else Expansion (mm)	Posterior Difference from Nominal (mm)	Else Difference from Nominal (mm)	Comment
-	5	7	0	0	Nominal
1	0	0	-5	-7	Smallest
2	0	2	-5	-5	
3	2	4	-3	-3	
4	3	5	-2	-2	
5	4	6	-1	-1	
6	6	8	1	1	Largest

2.2.1. Volumetric Modulated Arc Therapy

The Eclipse TPS (Version 8.6) was used for VMAT planning. Dose was computed with the Anisotropic Analytical Algorithm (AAA) (Van Esch *et al.*, 2006) with heterogeneity corrections and a 2.5 mm calculation grid. The TPS was commissioned for clinical use at our institution (R. M. Howell, pers. comm.). All of the VMAT plans were planned with 6 MV photons to a prescribed mean dose of 76 Gy to the PTV in 38 fractions. Then, in accordance with the standard-of-care, a normalization was applied to provide coverage of the 76 Gy isodose line around the PTV, 96.4% was the largest normalization required, and, in order for the prescription dose to be a control in this study, the normalization of 96.4% was applied to all plans. The photon absorbed dose in gray is equal to the equivalent dose in sieverts due to a radiation weighting factor of 1 for photons (ICRP 1990).

VMAT treatment planning for this study was consistent with the MDACC clinical practice (R. M. Howell, pers. comm.). Each treatment plan had two overlapping 220 degree arcs, each subtending the angle from 110 to 250 degrees (one clockwise and one counter clockwise arc). Two arcs double the possible number of control points and allows a higher degree of modulation, and the 60 degree gap minimizes entrance dose to the rectum (Figure 2.2). The collimator rotation was set to 30 degrees for the first arc and 330 degrees for the second to minimize overlap of inter-leaf leakage from the two arcs. In addition, for beam optimization purposes, avoidance structures were used to further conform the dose. For example, constraints were applied to a rectal avoidance volume that included the posterior portion of the rectum.

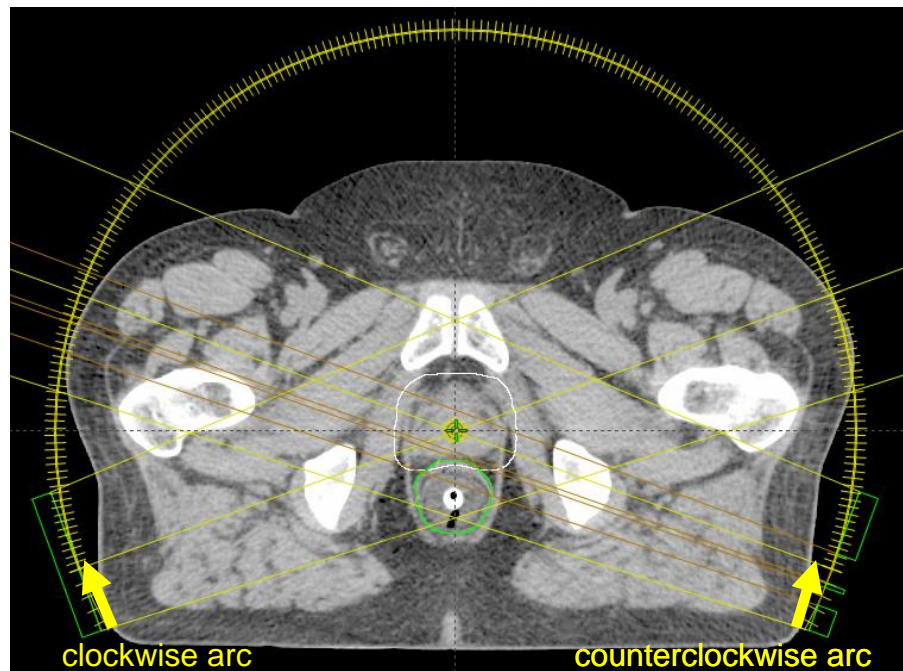


Figure 2.2 – Illustration of the two arcs used for VMAT treatment planning. It can be seen that the angle and modulation (orange lines inside yellow field lines, which are visible on the counterclockwise arc) spare the rectum (green) of entrance dose.

For specific aim 1, treatment plans were optimized for the nominal PTV for the small, medium, and large patients. For specific aim 3, additional treatment plans were optimized for each of the alternate PTVs for the medium patient. The same objectives and constraints were used for both the nominal and alternate PTVs (Table 2.3). Therefore, the main difference between these treatment plans was the volume of the high-dose region.

2.2.2. Proton Arc Therapy

The Eclipse TPS (Version 8.9) was used for proton arc therapy planning. Dose was computed with a proton pencil beam algorithm (Schaffner, 2008) with heterogeneity corrections and a 2.5 mm calculation grid. The TPS was previously configured and tested for proton radiotherapy at our institution (Newhauser *et al.*, 2007b). The prescribed mean dose was 76 Gy (RBE) to the PTV in 38 fractions. Then, similarly to the VMAT plans (section 2.2.1), all plans were normalized to 96.4%, resulting in a mean dose of 78.8 Gy (RBE) to the PTV. Treatment planning techniques for photon arc therapies are approximated with static treatment beams (Mackie *et al.*, 1993; Yu, 1995; Otto, 2008; Bzdusek *et al.*, 2009). In the same way, we approximated proton arc delivery in the TPS with static, discrete treatment beams, each representing an arc segment centered at the beam angle (Flynn *et al.*, 2007).

In order to determine the number of static proton beams required for a reasonable approximation in the treatment planning of arc delivery, treatment plans with 4, 6, 8, 12, 16, 24, and 32 equally spaced gantry angles were investigated. Because the dose distribution in a 4-beam plan with angles of 0, 90, 180 and 270 degrees depended on starting angle for a coarse beam resolution, a second 4-beam treatment plan was created with beam angles of 45, 135, 225, and 315 degrees. The mean doses to the bladder (and contents), bladder wall, rectum (and contents), rectal wall, femoral heads, and normal tissue of the pelvis were plotted vs. the number of beams to test for dosimetric sensitivity to the choice of beam number in approximating arc plans.

Based on the results of the above experiment (results are described more fully in section 3.1.2), we found that sixteen beams were adequate to approximate arc therapy for the purposes this study. The sixteen beams were equally spaced at the angles of 22.5, 45, 67.5, 90, 112.5, 135, 157.5, 180, 202.5, 225, 247.5, 270, 292.5, 315, 337.5, and 360 degrees around the patient, where each static beam approximated 22.5 degrees of arc delivery.

Unlike the procedure used for VMAT treatment planning, the PTV was not explicitly used to design the proton treatment plans. Instead, margins around the CTV were selected to provide conservative coverage, which consequently encompassed the PTV within a high dose region. A generic PTV is not suitable as the primary planning volume for proton therapy because it is a geometrical concept that assumes the “static dose cloud approximation” (Unkelbach *et al.*, 2009). Under this approximation, it is assumed that the location in space and shape of the dose distribution are virtually unaffected by changes in the anatomy, *e.g.* setup errors or tumor motion. This approximation is appropriate for photon therapy, but not for proton therapy where changes in anatomy or positioning could cause range errors (Urie *et al.*, 1984; Zhang *et al.*, 2007; Lomax, 2008; Unkelbach *et al.*, 2009). The ideal margins around the CTV are determined based on factors like beam range, SOBPs width, and uncertainties in delivery such as motion (Moyers *et al.*, 2001; Moyers and Miller, 2003; ICRU, 2007). A diagram of how proton therapy treatment margins are usually defined is shown in Figure 2.3.

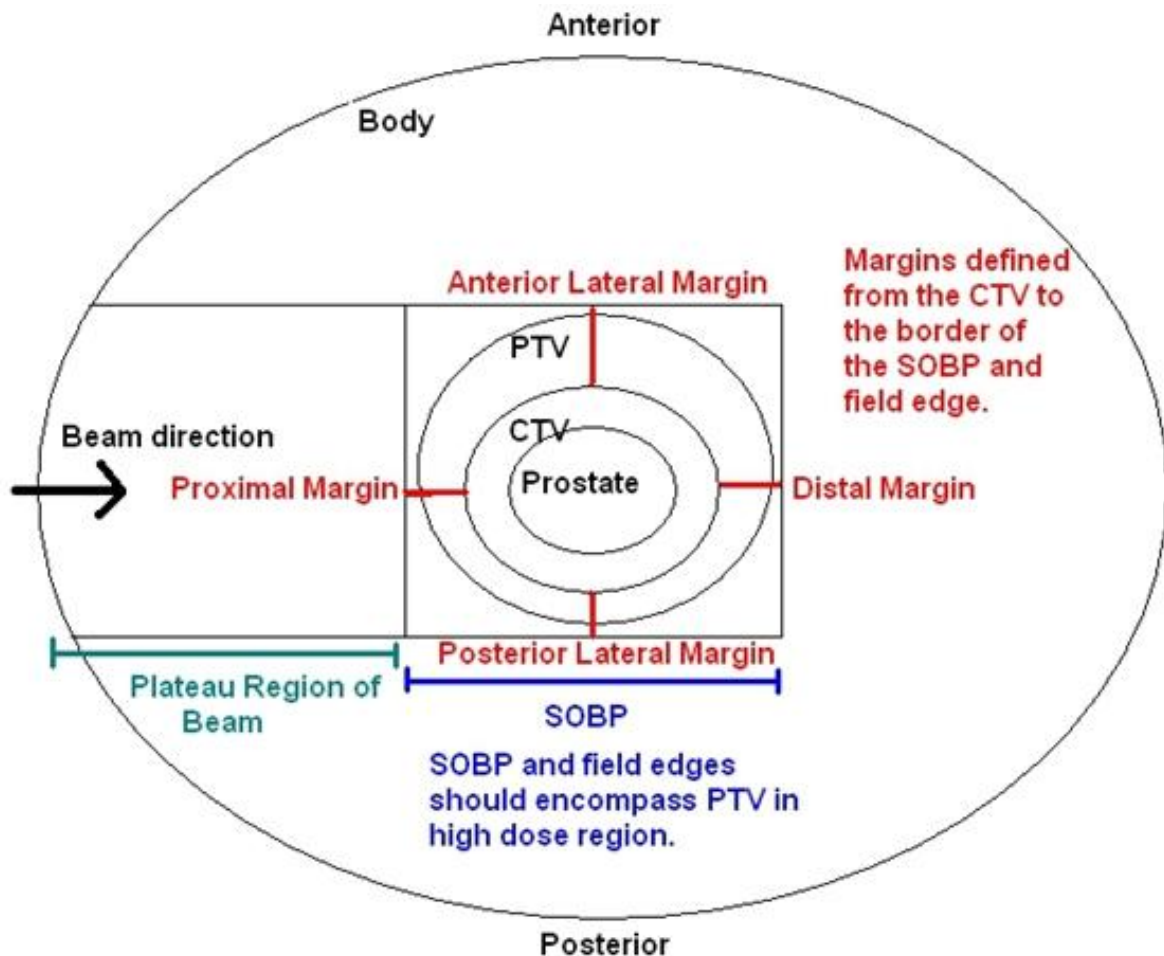


Figure 2.3 - Margins defined in treatment planning for proton therapy of the prostate. Proximal and distal margins are defined as the distance from the CTV to the edge of the SOBP. Lateral margins are defined as the distance from the CTV to the lateral field edge. The labels anterior and posterior could apply to lateral, proximal, or distal margins, depending on beam direction. For example, an anterior-posterior beam would have a posterior distal margin at the end of range of the beam. The box defined by the SOBP and the field edges is the high-dose region, which should *at least* encompass the PTV.

For all gantry angles, the margins, border smoothing, and compensator smearing (Urie *et al.*, 1984; Urie *et al.*, 1986) were determined based on techniques that were the standard-of-care for lateral opposed proton therapy for prostate cancer at MDACC in 2010 (In-house dosimetry guideline, 2009). The lateral margin from the CTV was set to 1.7 cm, and reduced by 0.2 cm posteriorly to 1.5 cm to provide rectal sparing for the 6 lateral-most beams (67.5, 90, 112.5, 247.5, 270, and 292.5 degrees). Then, a “test beam” was applied to each field to cover the CTV with zero margins, and the SOBP and range of each “test beam” were used to calculate the treatment parameters. The distal margins were calculated as 3 mm plus 3.5% of the range, and

the proximal margins were calculated as 3 mm plus 3.5% of the range minus the SOBP width (Moyers *et al.*, 2001). The border smoothing was set to the typically used standard-of-care value of 1 cm. The compensator smearing was found by taking the quadratic sum of 3% of the range and the sum of setup and motion uncertainty. Anterior-posterior (AP) and posterior-anterior (PA) beams are not part of the standard-of-care at our institution. However, it was desired to replicate the rectal sparing provided by the 0.2 cm posterior reduction in the lateral margins in the AP and PA beams. In order to provide this sparing, 0.2 cm was subtracted from the posterior margins of the 6 AP- and PA-most beams (22.5, 157.5, 180, 202.5, 337.5, and 360 degrees). Then, the margins, border smoothing, and compensator smearing were applied in the TPS to calculate the final treatment beams (which resulted in a final range and SOBP for each beam). Following this method, treatment plans with uniform beam weighting were created for the small, medium, and large patient for specific aim 1, and were defined as the nominal proton arc treatment plans for these patients.

Specific aim 2 investigated the dosimetric impact of variable beam weighting for the proton arc therapy plan for the medium patient. The *ERR* of SMN incidence attributed to the therapeutic dose from each individual beam was determined using an LNT risk model (section 2.4) and minimized using a gradient search algorithm (Microsoft Office Excel 2003, Microsoft Corporation, Redmond, WA). Corresponding contralateral beams (Figure 2.4) had nearly identical risk of an SMN due to anatomical symmetry of the pelvis (for example, 45 and 315 degrees). Because of this symmetry, the risks from contralateral beams were averaged then minimized as a pair of right and left beams with equal weights. The objective function to be minimized was based on the risk of an SMN of the bladder, rectum, or a combination of the two. However, because the AP and PA beams were on the sagittal axis, these two beams did not require a contralateral pair.

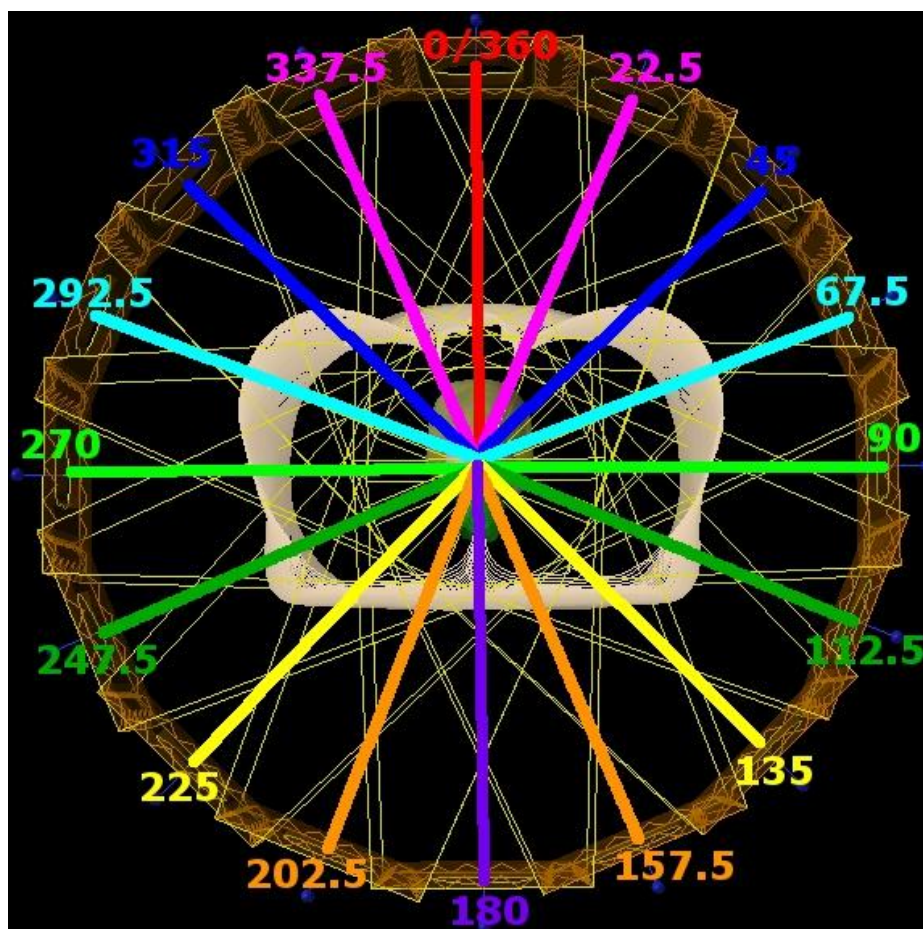


Figure 2.4 – Illustration of beam pairs. Paired beams are denoted by the same color line. Beams were paired because they contributed approximately the same risk of SMN due to the symmetry of the pelvis. Because the AP (0/360 degrees) and PA (180 degrees) beams were on the sagittal axis, they were not paired.

Constraints on the optimization ensured that the maximum and minimum weights of each beam were within the mechanical and radiation limitations of the treatment unit (Table 2.4). The dynamic range of the proton gantry rotation speed was measured to be a factor of 10, ranging from 0.1 rpm to 1 rpm. The dynamic range of the dose rate spanned 0.2 Gy/min to 2 Gy/min. A proton therapy MLC would be required to routinely deliver the proton arc therapy plans described in this work, and the maximum MLC leaf speed was estimated from the literature to be 3 cm/s (Wijesooriya *et al.*, 2005). The maximum leaf speed required for the nominal proton arc treatment plan was determined by measuring the distance from the cranial-caudal axis at isocenter in 0.5 cm intervals for each aperture, finding the maximum difference in distance between consecutive static apertures, then dividing the distance by the minimum

time per beam. It was found that the maximum leaf speed required was 0.75 cm/s (ignoring acceleration requirements, which were deemed of secondary importance compared to the other approximations). Therefore, it was not necessary to explicitly constrain beam weighting based on MLC leaf operating characteristics. The treatment time was constrained at 5 minutes or less for patient comfort, and facility throughput and efficiency. The constraints in this work were estimated for the purpose of theoretically testing the feasibility of proton arc delivery. In general, these limitations are facility- and machine-specific.

Table 2.4 - Constraints placed upon the optimization algorithm to determine beam weighting.

Constraint	Minimum	Maximum	Unit
Gantry Rotation Speed	0.1	1	rpm
Total Treatment Time	1	5	minutes
Dose Rate	0.2	2	Gy/min
MLC speed	0	3	cm/s

Sets of optimal beam weights were separately determined for the following objectives: minimize the total of risk of an SMN in the bladder and the rectum, the bladder only, and the rectum only. The latter two cases are mainly for illustrative purposes, but could have hypothetical clinical implications. For example, in the unusual case that a patient has had a cystectomy or proctectomy, it would be impossible to induce an SMN in an organ that has been removed.

An additional special case was considered for specific aim 3. A treatment plan with a set of non-uniform beam weights optimized to minimize the risk of second cancers in the bladder and rectum was generated for a patient with a prosthetic hip. For this patient, the beams traversing through the prosthesis on the ipsilateral side of the patient (67.5, 90, and 112.5 degrees) were disallowed due to complications with treating through a large, metal implant including range limitations and CT artifacts (Newhauser *et al.*, 2008), then the optimization was performed as

before. Due to the asymmetry of the anatomy and limitations on allowed beam angles, beams were not mirrored during optimization.

A summary of the four optimization objectives for which optimized treatment plans were created for specific aim 2 is provided in Table 2.5.

Table 2.5 – Objectives and constraints for specific aim 2 for which optimal beam weighting was found using gradient search optimization. Then, the beam weights were applied to the medium patient’s nominal treatment plan to create risk-minimized plans for each objective.

Objective Index	Constraints and Objectives Taken into Account		
	Minimize Risk of SMN of Bladder	Minimize Risk of SMN of Rectum	Forbidden Angles [degrees]
1	Constrained	Constrained	-
2	Constrained	-	-
3	-	Constrained	-
4	Constrained	Constrained	67.5, 90, 112.5

Specific aim 3 investigated the impact of margin size on predicted risk. Therefore, proton arc treatment plans were created for the medium patient with varying margins around the CTV, each with a corresponding VMAT treatment plan as described in section 2.2.1. However, as mentioned previously, there are subtleties regarding the comparison of margins from photon and proton plans due to differences in planning procedure (Moyers *et al.*, 2001; Moyers and Miller, 2003; ICRU, 2007). Photon plans were directly planned to the PTV, while proton plans were planned to the CTV with margins that did not exactly correspond to expansions to a PTV (Figure 2.3).

As mentioned above, the proton arc plans were not *explicitly* planned to the PTV. Therefore, in order to create plans for specific aim 3, the differences in PTV size from nominal (last two columns in Table 2.3) were applied to the nominal proximal, distal, and lateral margins around the CTV to produce plans that were appropriate for the different sized PTVs. Figure 2.5 illustrates this method, which corresponds to the middle section of the diagram in Figure 2.3. The resulting treatment margins and compensator smearing for the treatment plans created for specific aim 3 are listed in Tables 2.6 and 2.7.

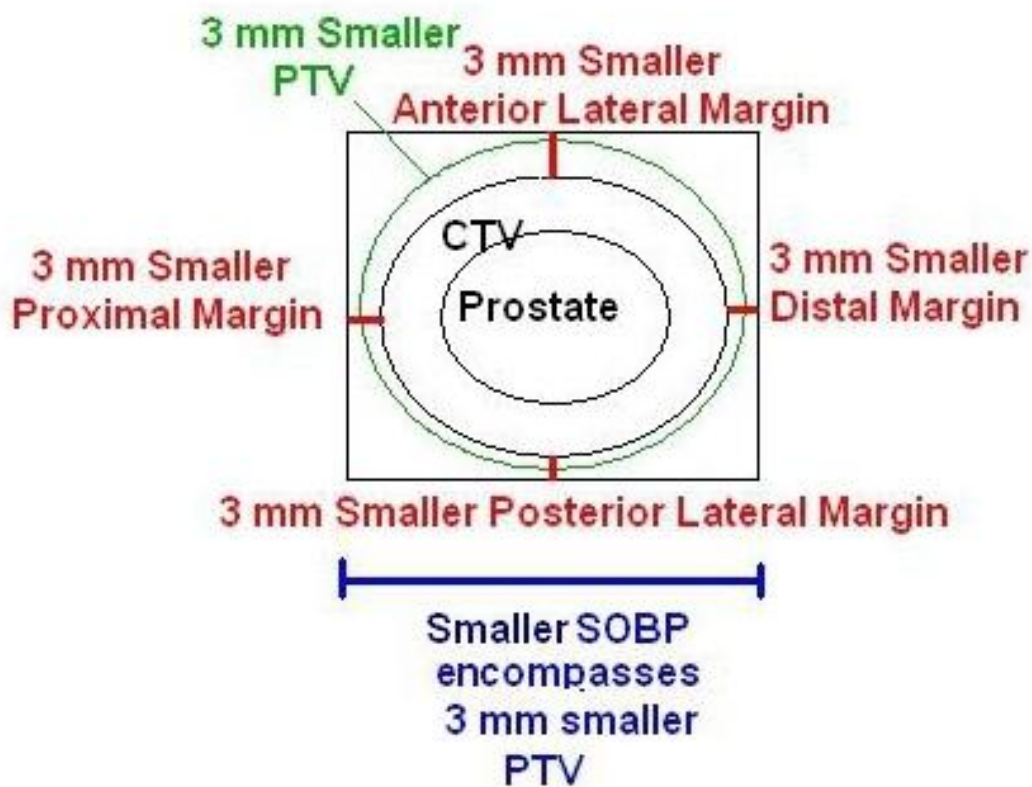
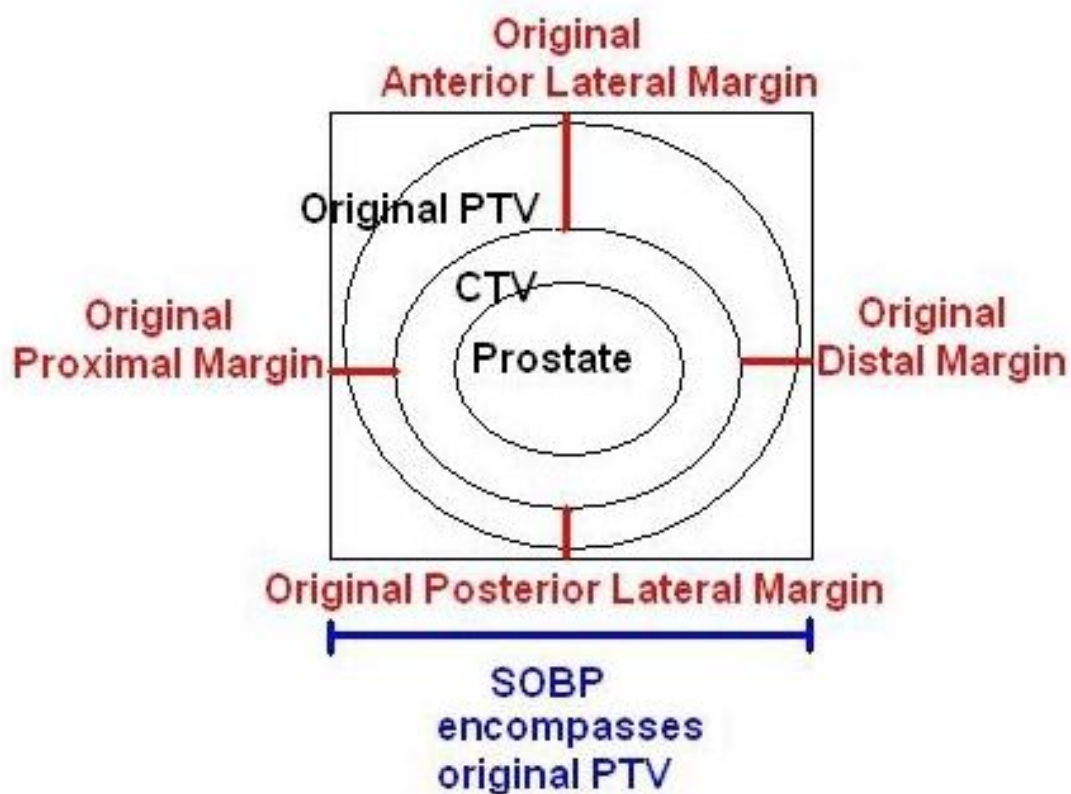


Figure 2.5 - Diagram showing the transformation applied to margins to cover a different sized PTV. Here, the PTV below is 3 mm smaller. Therefore, 3 mm is subtracted from all margins to

provide the appropriate field size and SOBP to at least encompass the smaller PTV (diagram not to scale).

Table 2.6 - Compensator smearing and proximal and distal margins (in cm) from the CTV for the proton arc plans. Plan indices correspond to those of the expansions listed in Table 2.3. The beams angles are in units of degrees.

Beam Angle	Comp smear	Nominal Plan		Plan 1		Plan 2		Plan 3		Plan 4		Plan 5		Plan 6	
		Distal Margin	Prox Margin	Distal Margin	Prox Margin	Distal Margin	Prox Margin	Distal Margin	Prox Margin	Distal Margin	Prox Margin	Distal Margin	Prox Margin	Distal Margin	Prox Margin
360.0	0.7	0.7	0.7	0.2	0.0	0.2	0.2	0.4	0.4	0.5	0.5	0.6	0.6	0.8	0.8
337.5	0.7	0.7	0.7	0.2	0.0	0.2	0.2	0.4	0.4	0.5	0.5	0.6	0.6	0.8	0.8
315.0	0.8	1.0	0.7	0.3	0.0	0.5	0.2	0.7	0.4	0.8	0.5	0.9	0.6	1.1	0.8
292.5	0.9	1.1	0.9	0.4	0.2	0.6	0.4	0.8	0.6	0.9	0.7	1.0	0.8	1.2	1.0
270.0	0.9	1.1	0.9	0.4	0.2	0.6	0.4	0.8	0.6	0.9	0.7	1.0	0.8	1.2	1.0
247.5	0.8	1.1	0.9	0.4	0.2	0.6	0.4	0.8	0.6	0.9	0.7	1.0	0.8	1.2	1.0
225.0	0.7	1.0	0.7	0.3	0.0	0.5	0.2	0.7	0.4	0.8	0.5	0.9	0.6	1.1	0.8
202.5	0.5	0.8	0.4	0.1	0.0	0.3	0.0	0.5	0.1	0.6	0.2	0.7	0.3	0.9	0.5
180.0	0.5	0.8	0.4	0.1	0.0	0.3	0.0	0.5	0.1	0.6	0.2	0.7	0.3	0.9	0.5
157.5	0.5	0.8	0.4	0.1	0.0	0.3	0.0	0.5	0.1	0.6	0.2	0.7	0.3	0.9	0.5
135.0	0.7	1.0	0.7	0.3	0.0	0.5	0.2	0.7	0.4	0.8	0.5	0.9	0.6	1.1	0.8
112.5	0.8	1.1	0.9	0.4	0.2	0.6	0.4	0.8	0.6	0.9	0.7	1.0	0.8	1.2	1.0
90.0	0.8	1.1	0.9	0.4	0.2	0.6	0.4	0.8	0.6	0.9	0.7	1.0	0.8	1.2	1.0
67.5	0.8	1.1	0.9	0.4	0.2	0.6	0.4	0.8	0.6	0.9	0.7	1.0	0.8	1.2	1.0
45.0	0.6	1.0	0.7	0.3	0.0	0.5	0.2	0.7	0.4	0.8	0.5	0.9	0.6	1.1	0.8
22.5	0.6	0.7	0.7	0.2	0.0	0.2	0.2	0.4	0.4	0.5	0.5	0.6	0.6	0.8	0.8

Table 2.7 - Lateral margins (in cm) from the CTV for the proton arc plans. Plan indices correspond to those of the expansion margins listed in Table 2.3. “Rectal Side” refers to the posterior margin, which encroaches on the rectum. The beam angles are in units of degrees.

Beam Orientation	Beam Angle	Nominal Plan		Plan 1		Plan 2		Plan 3		Plan 4		Plan 5		Plan 6	
		Rectal Side	All Other Sides	Rectal Side	All Other Sides	Rectal Side	All Other Sides	Rectal Side	All Other Sides	Rectal Side	All Other Sides	Rectal Side	All Other Sides	Rectal Side	All Other Sides
Lateral-most	67.5, 90, 112.5, 247.5, 270, 292.5	1.5	1.7	1.0	1.0	1.0	1.2	1.2	1.4	1.3	1.5	1.4	1.6	1.6	1.8
Non-lateral	22.5, 45, 135, 157.5, 180, 202.5, 225, 315, 337.5, 360	N/A	1.7	N/A	1.0	N/A	1.2	N/A	1.4	N/A	1.5	N/A	1.6	N/A	1.8

2.3. Stray Dose Estimation

2.3.1. Volumetric Modulated Arc Therapy

Commercial TPSs accurately calculate therapeutic dose (Aspradakis *et al.*, 2003), but underestimate stray radiation (Howell *et al.*, 2010a; Howell *et al.*, 2010b). Howell *et al.* (2010a; 2010b) reported that the TPS used in this study underestimated the stray dose by an average of $40\% \pm 20\%$ for regions where the reported dose was less than 5% of the prescribed dose. In that study, they found that the worst underestimation occurred farthest from the field edge (i.e. very low isodose regions).

Therefore, in this study, to more accurately approximate stray radiation, we increased the doses that were less than 5% of the prescription dose. This was accomplished by multiplying the doses in the differential dose-volume histogram (DVH) ranging from 0% to 5% of the prescription dose by 1.4. This procedure was conservative in that the average distance from the field edge in our study exceeded that reported by Howell *et al.* Then, the risk was calculated using the modified DVH.

2.3.2. Proton Arc Therapy

Because the commercial TPSs for proton therapy do not predict stray neutron dose, an in-house Monte Carlo method was used to predict these values. Monte Carlo methods have been used in the past to estimate stray doses for proton therapy (Agosteo *et al.*, 1998; Schneider *et al.*, 2002; Paganetti *et al.*, 2004; Fontenot *et al.*, 2005a; Polf and Newhauser, 2005; Jiang *et al.*, 2005; Herault *et al.*, 2005; Tayama *et al.*, 2006b; Zheng *et al.*, 2007a; Zheng *et al.*, 2007b; Zheng *et al.*, 2008b; Moyers *et al.*, 2008a; Zacharatou Jarlskog *et al.*, 2008; Taddei *et al.*, 2008; Fontenot *et al.*, 2008; Fontenot *et al.*, 2009; Newhauser *et al.*, 2009a; Taddei *et al.*, 2009b; Bednarz *et al.*, 2009; Fontenot *et al.*, 2010; Zhang *et al.*, 2010; Taddei *et al.*, 2010a; Taddei *et al.*, 2010b; Taddei *et al.*, 2010c). The Monte Carlo code MCNPX (Monte Carlo N Particle eXtended) (Waters *et al.*, 2007; Pelowitz, 2007) has been used extensively by our research group (Newhauser *et al.*, 2007b) and was chosen for this work.

Monte Carlo simulations were completed to estimate the stray neutron dose for the proton arc therapy treatment plan for the medium patient. The process is reviewed here, and further details can be found in the literature (Newhauser *et al.*, 2007b; Fontenot *et al.*, 2008; Zheng *et al.*, 2008a; Fontenot, 2008). We used an in-house code that converts patient CT and other treatment plan information into MCNPX input files, runs MCNPX simulations with version 2.7c of the code, then converts the output into Digital Imaging and Communications in Medicine (DICOM) files that can be re-imported into the TPS for visualization and analysis.

For these simulations, the entire proton nozzle was simulated (Newhauser *et al.*, 2007a), and the patient CT dataset was used as the voxelized phantom on which the dose was calculated using F6 tallies. Once the simulated dose distributions were re-imported in to the TPS, mean neutron doses to the bladder wall and rectal wall were computed and recorded.

Because neutrons have a different RBE for carcinogenesis than photons, a radiation weighting factor must be applied to convert absorbed dose to equivalent dose. The equation describing the relationship between absorbed dose and equivalent dose is

$$H = \bar{w}_R \times D, \quad (2.1)$$

where H is the equivalent dose, \bar{w}_R is the radiation weighting factor for neutrons, and D is the absorbed dose. Publication 92 of the International Commission on Radiological Protection (ICRP) (2003) recommends a continuous function for the weighting factor of neutrons based on neutron energy (Figure 2.6), with a maximum of approximately 20 at 1 MeV.

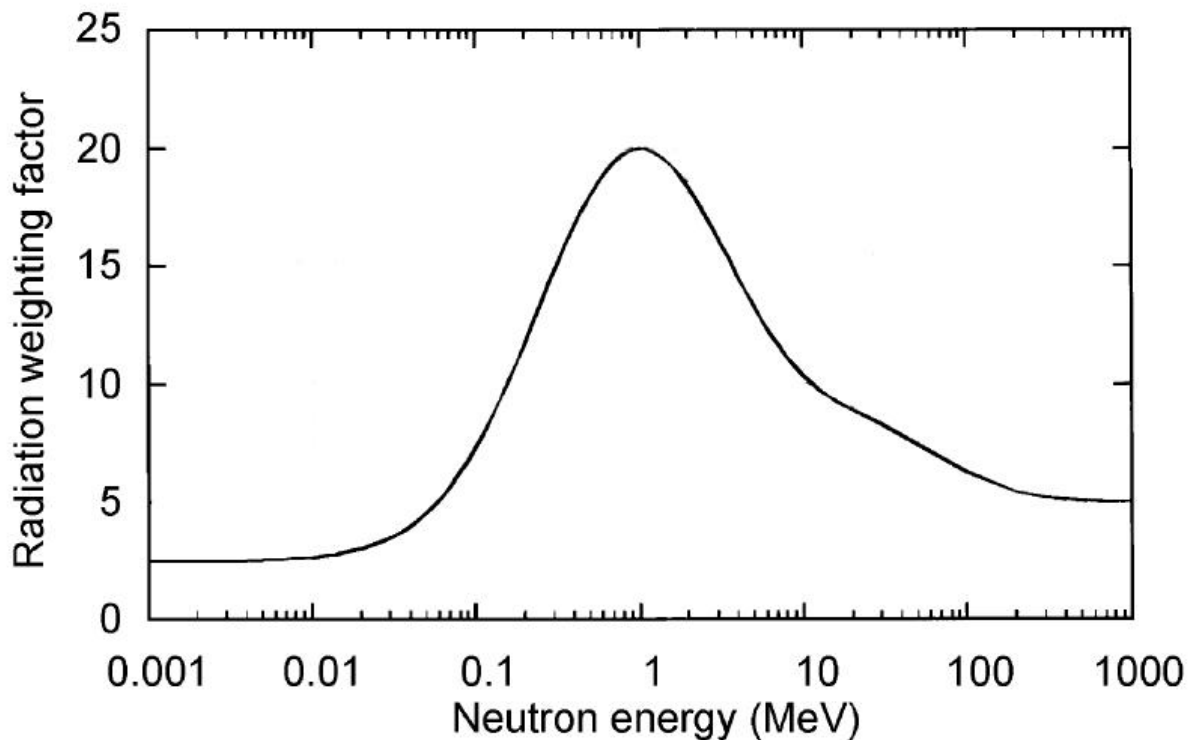


Figure 2.6 - Radiation weighting factor (w_R) for neutrons vs. neutron energy (reprinted with permission) (ICRP, 2003).

Because the neutron spectra incident upon each organ are unique, \bar{w}_R values are also unique to each organ. These were determined by Fontenot *et al.* (2008; 2008; 2009) for a parallel-opposed proton therapy treatment of the prostate (Table 2.8) for the same three patients as studied in this work. In order to be conservative, the largest values of \bar{w}_R of the three patients were used for all three patients in our study. Because of the uncertainty in determining \bar{w}_R values (Kellerer *et al.*, 2006; Hall, 2007; Fontenot, 2008; Fontenot *et al.*, 2010), factors of 0.5, 2, and 5 were applied to the ICRP values for sensitivity analyses (Table 2.8), where a value of 5 corresponds to a maximum neutron radiation weighting factor of approximately 100. The sensitivity of risk predictions to uncertainty in the radiation weighting factor was evaluated using the medium patient’s nominal treatment plan.

Table 2.8 – Mean neutron radiation weighting factors for the bladder and rectum for a parallel-opposed proton therapy treatment of the prostate determined in the work of Fontenot *et al.* (2008; 2008; 2009). For sensitivity analysis, the \bar{w}_R values were modulated by factors of 0.5, 2 and 5.

Organ	\bar{w}_R	0.5* \bar{w}_R	2* \bar{w}_R	5* \bar{w}_R
Bladder	7.36	3.68	14.72	36.80
Rectum	6.94	3.47	13.88	34.70

Then, the total equivalent dose for each dose-bin of the bladder wall and rectal wall from a proton therapy treatment for prostate cancer was found with the equation

$$H_{\text{total}} = 1.1 \times D_{\text{absorbed}} + H_{\text{stray}} \quad (2.2)$$

where H_{total} is equal to the total equivalent dose in sieverts for the dose-bin, 1.1 is the recommended generic RBE value for protons (section 1.2.2) to convert to Gy (RBE), D_{absorbed} is the absorbed therapeutic proton dose in gray, and H_{stray} is the stray equivalent dose (equation 2.1).

The stray doses for the small and large patients in this study were approximated as the stray doses estimated by Fontenot *et al* (2008) using MCNPX. In their study, the stray dose from parallel-opposed beam proton therapy was simulated for the same prostate cancer patients as used in this work. The *total* stray dose from parallel-opposed beam proton therapy of the prostate apparently provides a conservative estimate of the total stray dose from proton arc therapy of the prostate (Sengbusch *et al.*, 2009). Neutron production increases as proton energy increases (Zheng *et al.*, 2008a) and the highest beam energies in a proton arc therapy treatment plan occur at the lateral angles. Therefore, the lower energy protons from other angles produce fewer neutrons and contribute to a lower overall stray dose. However, the beam arrangement is uniformly distributed around the patient for our study, which could produce a different distribution of neutrons throughout the body. Despite the discrepancies in the beam arrangement, this was determined to be a reasonable estimate of neutron dose for this study.

2.4. Risk Prediction

Unlike previous studies (Taddei *et al.*, 2008; Fontenot *et al.*, 2009), the risk to the bladder and rectum were found using organ wall contours instead of the conventional whole organ contour, including contents. The motivation behind our choice is that the contents of those organs will be excreted from the body and therefore do not have carcinogenic capabilities. Consequently, for detailed dosimetric studies predicting carcinogenic risk, it naturally follows to delineate organs as solely the organ tissue and to exclude the contents.

2.4.1. Linear-No-Threshold Risk Model

The BEIR VII report (NRC, 2006) provides a method for predicting risk of radiogenic cancers and assumes an LNT relationship of risk of second cancer and dose. The quantity of excess relative risk (*ERR*) was chosen as the metric to express the risk of *incidence* of an SMN for this work. *ERR* is defined as

$$ERR \equiv \frac{R_{\text{exposed}}}{R_{\text{unexposed}}} - 1, \quad (2.3)$$

where R_{exposed} is the rate of the exposed population, $R_{\text{unexposed}}$ is the rate of the unexposed population. The risk coefficient of $\frac{ERR}{H}$ (Sv^{-1}) is calculated with the following equation:

$$\frac{ERR}{H} = \beta_M e^{\gamma e^*} \left(\frac{a}{60} \right)^\eta, \quad (2.4)$$

where e^* is equal to the age at exposure in years minus 30 when the age at exposure is less than 30 years and equal to zero when the age at exposure is greater than 30 years; a is attained age (years); β_M is the age-specific, and organ-specific instantaneous ERR/Sv value for males; γ accounts for the per-decade increase in age at exposure over the range of zero to 30 years, and η represents the exponent of attained age (NRC, 2006). From the information in BEIR VII and equation 2.4, risk coefficients were derived to be 0.51 ERR/Sv for the colon and 0.40 ERR/Sv for the bladder for the three patients studied (Fontenot, 2008). In addition, to separate the rectum from the colon, relative mass-fractions from Publication 89 of the ICRP (2002) were applied; 0.2 for the rectum and 0.8 for the colon.

Then, the ERR for each dose-bin, i , from the differential DVH was found by applying the risk coefficient to the equivalent dose of each dose-bin,

$$ERR_{T,i} = \frac{m_{\text{subregion}}}{m_T} \times \frac{V_i}{V_T} \times H_i \times \left(\frac{ERR}{H} \right)_T, \quad (2.5)$$

where $\frac{m_{\text{subregion}}}{m_T}$ is the fractional mass of the subregion compared to the total mass of the organ (0.2 for the rectum, 1 for the bladder), V_i is the volume of the dose-bin (cm^3), V_T is total the

volume of the tissue (cm^3), H_i is the total equivalent dose (Sv) of the dose-bin, and $\left(\frac{ERR}{H}\right)_T$ is the tissue-specific risk coefficient derived from the equation 2.4 above (Sv^{-1}).

Next, the $\left(\frac{ERR}{H}\right)_T$ was summed over n dose-bins to find the ERR for a given tissue:

$$ERR_T = \sum_{i=1}^n \left(\frac{ERR}{H}\right)_T \cdot H_i. \quad (2.6)$$

It should also be noted that, for the LNT model, multiplying the risk coefficient by the tissue mean equivalent dose is the same as equation 2.6 because of the linear relationship of risk and dose. This concept is described mathematically in equation 2.7,

$$ERR_T = \sum_{i=1}^n \left(\frac{ERR}{H}\right)_T \cdot H_i = \frac{m_{\text{subregion}}}{m_T} \times H_T \times \left(\frac{ERR}{H}\right)_T, \quad (2.7)$$

where, H_T is the mean equivalent dose of the tissue.

Finally, the total ERR for the patient was obtained from the sum over m tissue ERR s ($m=2$ for our study: bladder and rectum),

$$ERR = \sum_{j=1}^m \left(\frac{ERR}{H}\right)_T \cdot H_{Tj}. \quad (2.8)$$

Once the ERR was determined (regardless of risk model), the ratio of excess relative risk (RRR) was calculated by

$$RRR = \frac{ERR_{\text{ProtonArc}}}{ERR_{\text{VMAT}}}. \quad (2.9)$$

According to this definition, an RRR less than one indicates a lower risk of an SMN following proton arc therapy and an RRR greater than one indicates a lower risk of an SMN following VMAT.

2.4.2. Alternate High Dose Risk Models

The LNT relationship of the BEIR VII report is appropriate to predict radiogenic cancer risk for low doses up to a few sieverts (NCRP, 1993; Hall and Wu, 2003; NRC, 2006), but the relationship between dose and risk is less well understood at higher doses. As discussed in section 1.3 and following the approach of Fontenot *et al.* (2008; 2009), the linear-exponential and linear-plateau models are proposed alternatives to the LNT model that account for cell sterilization. These models decrease or plateau, respectively, beyond a given equivalent dose which ranges from approximately 10 Sv to 40 Sv in the literature. The forms of the alternate risk models were similar to the work by Schneider *et al.* (2005; 2006; 2007) and were generated and applied by Fontenot *et al.* (2008; 2009). Both dose levels for inflection of the risk models were investigated in this work and will be denoted as the name of the risk model with a “-10” or “-40” suffix, *e.g.*, “linear-exponential-10”.

The linear-exponential model of *ERR* for a dose-bin $(ERR_T)_i$ was calculated with the equation,

$$(ERR_T)_i = \frac{m_{\text{subregion}}}{m_T} \times \frac{V_i}{V_T} \times \left(\frac{ERR}{H} \right)_T^0 \times H_i \times e^{-\alpha_T H_i}, \quad (2.10)$$

where $\left(\frac{ERR}{H} \right)_T^0$ is the organ-specific LNT risk model from BEIR-VII, H_i is the tissue-specific equivalent dose for the dose-bin, and α_T is the tissue specific parameter that accounts for cell sterilization. Likewise, the linear-plateau excess relative risk for a dose-bin is given by

$$(ERR_T)_i = \frac{m_{\text{subregion}}}{m_T} \times \frac{V_i}{V_T} \times \frac{\left(\frac{ERR}{H} \right)_T^0}{\alpha_T} \times \left(1 - e^{-\alpha_T H_i} \right), \quad (2.11)$$

where the variables correspond to those in equation 2.10. The values for $\left(\frac{ERR}{H}\right)_T^0$ and α_T for the bladder and rectum were computed by Fontenot *et al.* (2008) and are listed in Table 2.9, below.

Table 2.9 - Risk model parameters for the linear-exponential and linear-plateau models for the bladder and rectum in Sv^{-1} (Fontenot, 2008).

Risk Model	Bladder		Rectum	
	$\left(\frac{ERR}{H}\right)_T^0$	α_T	$\left(\frac{ERR}{H}\right)_T^0$	α_T
Linear-exponential-10	0.49	0.090	0.61	0.090
Linear-exponential-40	0.46	0.025	0.57	0.025
Linear-plateau-10	0.51	0.250	0.65	0.250
Linear-plateau-40	0.47	0.068	0.58	0.068

Then, the *RRRs* for the linear-exponential and linear-plateau models were found using the same method as for the LNT model. First the ERR_{db} was summed over all dose-bins (equation 2.6), then the ERR_T was summed over all tissues (equation 2.8), and finally the *RRR* was found by taking the ratio of the $ERR_{ProtonArc}$ to ERR_{VMAT} (equation 2.9).

To illustrate the behavior of risk as a function of dose, Figures 2.7 and 2.8 plot the predicted risk for incidence of SMN in the bladder and rectum, respectively.

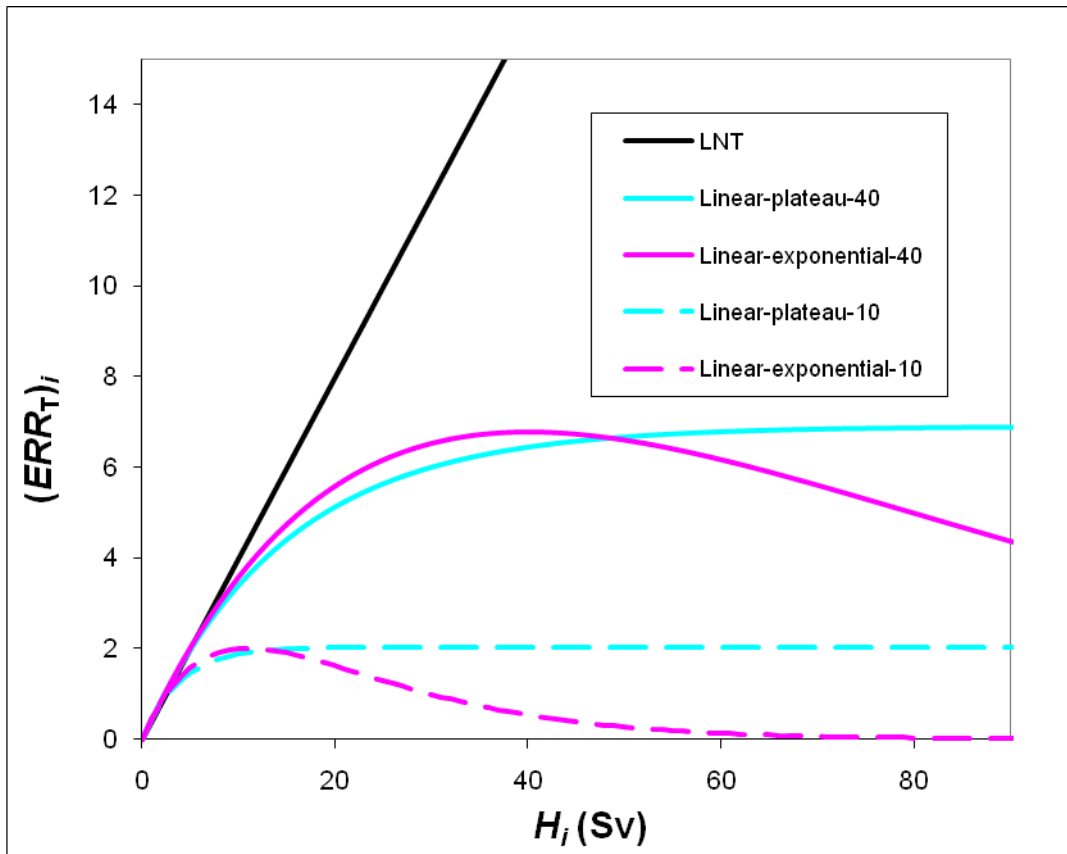


Figure 2.7 - The LNT, linear-exponential, and linear-plateau risk models used to predict ERR of SMN incidence of the bladder (Fontenot *et al.*, 2009). Volume-weighting for the fractional volume of a specific dose-bin, $\frac{V_i}{V_T}$, has been set to 1 for this figure.

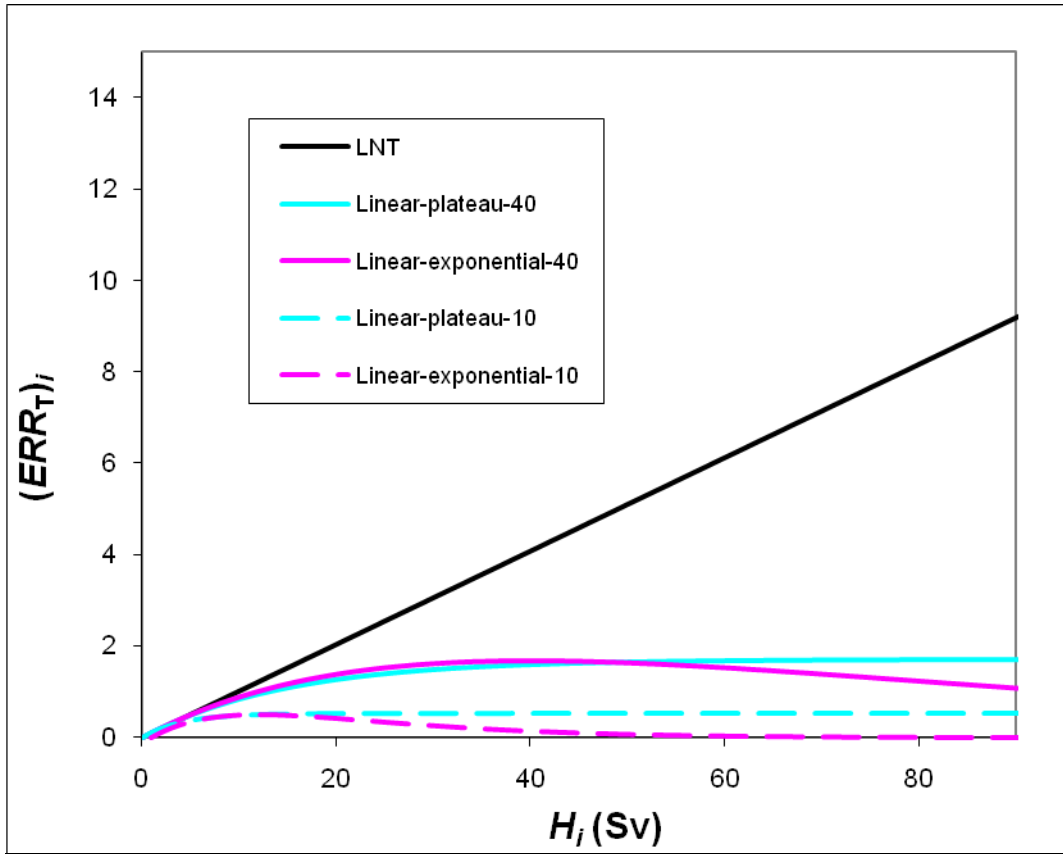


Figure 2.8 - The LNT, linear-exponential, and linear-plateau risk models used to predict ERR of SMN incidence of the rectum (Fontenot *et al.*, 2009). Volume-weighting for the fractional volume of a specific dose-bin, $\frac{V_i}{V_T}$, has been set to 1 for this figure. It can be seen that, partially due to the 0.2 mass-weight for the rectum, the ERR per Sv is less for the rectum than for the bladder.

2.4.3. Example Risk Calculations

To clarify the process of risk calculation, an example for both the LNT and an alternate risk model are provided below. First, the risk of an SMN of the bladder (wall) for the medium patient following VMAT was found using the LNT model. In this case, the mean dose to the bladder wall was 16.8 Sv (see sections 3.1.1 and 3.2.1), and the organ-specific, patient-specific risk coefficient for the bladder was 0.4 Sv^{-1} (section 2.4.1). Therefore, following equation 2.7, the LNT ERR for the bladder was given by

$$16.8 \text{ Sv} \times 0.4 \text{ Sv}^{-1} = 6.7. \quad (2.12)$$

The second example calculation, shown below, describes the prediction of the risk of SMN incidence in the rectum (wall) for the medium patient following proton arc therapy for the linear-exponential-10 risk model. The differential DVH for the tissue of interest was required for this calculation, and was exported from the treatment planning system into a spreadsheet. A graph of the differential DVH for the rectal wall was shown below in dark blue in Figure 2.9. After the differential DVH was obtained, the stray dose was added to every dose-bin. Then, equation 2.10 was applied to each dose-bin to obtain the differential excess relative risk contributed by each dose-bin (Figure 2.9).

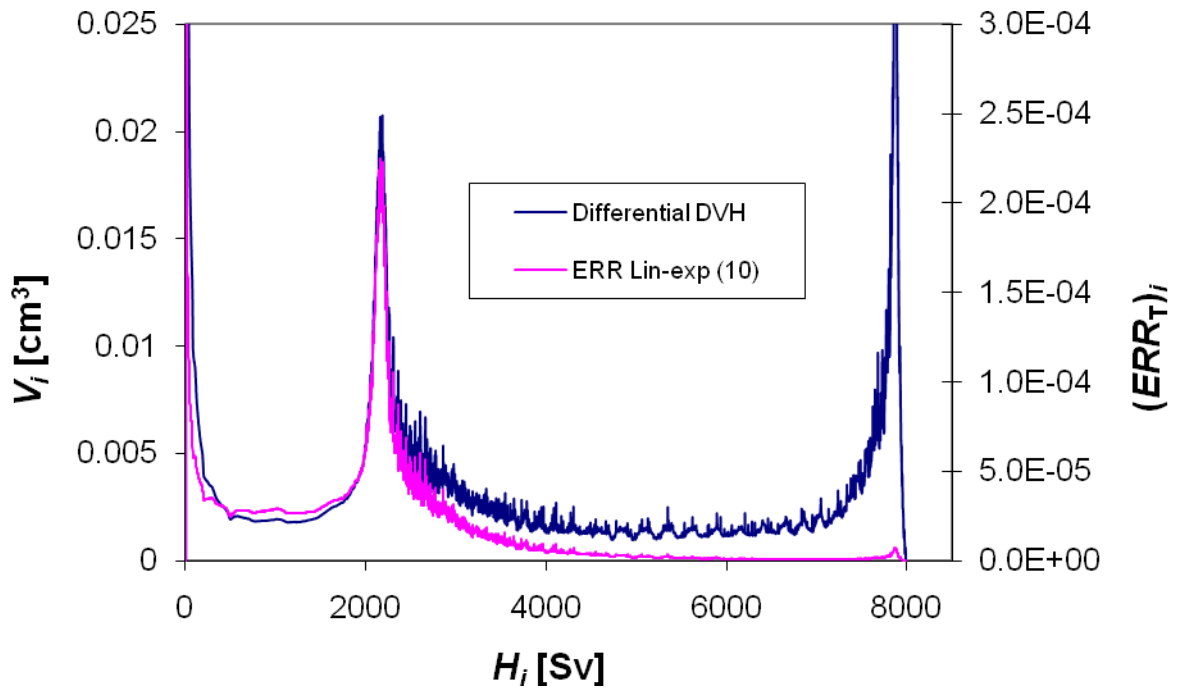


Figure 2.9 - Calculated differential DVH and $(ERR_T)_i$ for the rectum for the nominal proton arc therapy plan for the medium patient.

Finally, the differential risks were summed to yield the total risk for the tissue. Combining equations 2.6 and 2.10, this process can be expressed as

$$\langle ERR_T \rangle = \sum_{i=1}^n 0.2 \times \frac{V_i}{33} \times 0.61 \times H_i \times e^{-0.09 H_i} = 0.19, \quad (2.13)$$

where the sum was over all dose-bins, the 0.2 weighting factor is the $\frac{m_{\text{subregion}}}{m_T}$ for the rectum, V_i is the volume of the dose-bin in cm^3 , 33 is the V_T of the rectal wall in cm^3 , 0.61 is the $\left(\frac{ERR}{H}\right)_T^0$ for the linear-exponential-10 model for the rectum (Sv^{-1}), H_i is the equivalent dose for the dose-bin (Sv), and 0.09 is α_T for the rectum (Sv^{-1}) (Table 2.9).

2.4.4. Statistical Analysis

Due to time constraints on the length of this thesis project, the sample size for this work was limited to three patients. Despite the limited sample size, two statistical tests were chosen to compare the proton arc therapy and VMAT risk estimates: the sign test and the t-test (Rosner, 2006). The objectives of the tests in this work were mainly educational. However, these tests would be appropriate for a larger sample size, *e.g.*, a future work. The software package StatXact® version 7.0 from Cytel Studio (Cambridge, MA) was used for both statistical tests.

The sign test is a nonparametric test that determines whether two samples are from the same distribution but ignores the magnitude of the differences, which makes it insensitive to outliers. Because of the small sample size, the exact sign test was performed. For our purposes, the quantity of interest was RRR and the value of interest was one (meaning equal risk following proton arc therapy and VMAT), and each RRR was defined as “+” if it was greater than one and “-” if it was less than one. The null hypothesis was $H_0: P(+)\geq P(-)$ and the alternate hypothesis was $H_1: P(+)<P(-)$, where $P(\pm)$ is the probability of a + or -, respectively. The test statistic T is found, which is the total number of -’s ($RRR < 1$). Then, n was defined to be the total number of +’s and -’s, excluding ties. Next, t is found using the equation

$$t = \frac{1}{2} \left(n + w_\alpha \Phi \left(\frac{1}{2} \right) \right), \quad (2.14)$$

where w_α is the 95th percentile of the w distribution for a one-sided significance level (α) of 0.05 (α is also the probability of a falsely rejecting the null hypothesis). Finally, H_0 was rejected at the level of α if T is greater than or equal to $n-t$ (Conover, 1980).

The t-test is a parametric test that determines whether the mean of a sample distribution is the same as the population mean. It should be noted that the t-test assumes a t-distribution for the sample mean, which may not be assumable for a sample size of three, given the underlying distribution of ERR . Regardless of the small sample size, it was decided that performing the t-test was of pedagogical value. In this case, to test null hypothesis $H_0: RRR \geq 1$ vs. the alternate hypothesis: $H_1: RRR < 1$, with a one-sided significance level α of 0.05, the test statistic t was computed (Rosner, 2006) according to

$$t = \frac{\bar{x} - \mu_0}{s / \sqrt{n}}, \quad (2.15)$$

where \bar{x} is the sample mean (RRR), μ_0 is the expected or population mean (1), s is the sample standard deviation, and n is the sample size. The null hypothesis was rejected if $t < t_{n-1,1-\alpha}$, where $t_{n-1,1-\alpha}$ is the 5th percentile of the t distribution with $n-1$ degrees of freedom for a one-sided test.

2.4.5. Uncertainty Analysis

In order to estimate the uncertainty associated with the prediction of the mean RRR , error propagation was performed. A derivation of the formula for uncertainty in RRR for a patient was reported by Fontenot *et al.* (2008; 2010) and was adapted for this work. One of the differences in our formula is that the uncertainty in therapeutic and stray dose for VMAT (analogous to IMRT in the work of Fontenot *et al.*) was combined into one factor due the method utilized for stray dose estimation. Another difference is that there is a term for the uncertainty in the \bar{w}_R added in quadrature. Additionally, our error propagation is explicitly for

the mean RRR , in order to incorporate the covariance from the correlations between the modalities. Finally, it was found that the uncertainty in risk model was asymmetric when the LNT model was assumed as the baseline risk model. Therefore, a term for uncertainty in the risk model was added in quadrature, but only to the negative side. This resulted in an asymmetrical overall relative uncertainty in the mean RRR :

$$\begin{aligned}
+\left(\frac{\sigma_{\overline{RRR}}}{\overline{RRR}}\right)^2 &= \sum_{p=1}^3 \left\{ \left(\frac{\sum_{T=1}^2 ERR_1^2 \left(\frac{\sigma_{D_1}}{D_1}\right)^2}{\left(\sum_{T=1}^2 ERR_T\right)^2} \right)_V + \left(\frac{\sum_{T=1}^2 \left(ERR_1^2 \left(\frac{\sigma_{D_1}}{D_1}\right)^2 + ERR_2^2 \left(\frac{\sigma_{D_2}}{D_2}\right)^2 \right)}{\left(\sum_{T=1}^2 ERR_T\right)^2} \right)_P \right\} \\
&+ \left(\frac{\sigma_{\overline{RRR}}}{\overline{RRR}}\right)_{w_R}^2 - 2 \frac{\sigma_{ERR_V ERR_P}}{ERR_V ERR_P} \tag{2.16a}
\end{aligned}$$

and

$$\begin{aligned}
-\left(\frac{\sigma_{\overline{RRR}}}{\overline{RRR}}\right)^2 &= \sum_{p=1}^3 \left\{ \left(\frac{\sum_{T=1}^2 ERR_1^2 \left(\frac{\sigma_{D_1}}{D_1}\right)^2}{\left(\sum_{T=1}^2 ERR_T\right)^2} \right)_V + \left(\frac{\sum_{T=1}^2 \left(ERR_1^2 \left(\frac{\sigma_{D_1}}{D_1}\right)^2 + ERR_2^2 \left(\frac{\sigma_{D_2}}{D_2}\right)^2 \right)}{\left(\sum_{T=1}^2 ERR_T\right)^2} \right)_P \right\} \\
&+ \left(\frac{\sigma_{\overline{RRR}}}{\overline{RRR}}\right)_{w_R}^2 + \left(\frac{\sigma_{\overline{RRR}}}{\overline{RRR}}\right)_{RM}^2 - 2 \frac{\sigma_{ERR_V ERR_P}}{ERR_V ERR_P} . \tag{2.16b}
\end{aligned}$$

In this formula, $\left(\frac{\sigma_{\overline{RRR}}}{\overline{RRR}}\right)$ is the relative uncertainty in the mean RRR , and the quantity σ represents one standard deviation (therefore a 68% confidence interval). The outermost sum is over the 3 patients (p), and the inner sums are over the two tissues (T) - the bladder and the rectum. The subscript V denotes VMAT and the subscript P denotes proton arc therapy. ERR_1

is the excess relative risk from primary radiation, $\left(\frac{\sigma_{D_1}}{D_1}\right)$ is the relative uncertainty in the therapeutic dose from the treatment planning system for proton arc therapy and the total uncertainty in the VMAT dose, ERR_2 is the excess relative risk from the stray radiation, $\left(\frac{\sigma_{D_2}}{D_2}\right)$ is the relative uncertainty in the stray dose, and ERR_T is the total excess relative risk for a given tissue. The $\left(\frac{\sigma_{D_1}}{D_1}\right)$ from the VMAT plan was estimated using the quadratic sum of the relative uncertainty in the therapeutic dose from the treatment planning system and the uncertainty in the stray dose correction method (section 3.2.1). The two terms $\left(\frac{\sigma_{\overline{RRR}}}{\overline{RRR}}\right)_{w_R}$ and $\left(\frac{\sigma_{\overline{RRR}}}{\overline{RRR}}\right)_{RM}$ are the relative uncertainty in the mean RRR contributed from the uncertainty in the $\overline{w_R}$ and risk model, respectively. Both of these quantities were determined with a sensitivity analysis to evaluate their effect on RRR , which is why they are relative to RRR and added in quadrature to the rest of the equation. $\left(\frac{\sigma_{\overline{RRR}}}{\overline{RRR}}\right)_{w_R}$ was estimated by assuming the 95% confidence interval of the $\overline{w_R}$ was $0.5 * \overline{w_R}$ to $5 * \overline{w_R}$ (Table 2.8) for each patient and dividing the range in resulting mean RRR by 2 to find 2σ . Then, 2σ was divided by 2 to obtain the numerator in the uncertainty term. $\left(\frac{\sigma_{\overline{RRR}}}{\overline{RRR}}\right)_{RM}$ only contributed to the negative overall uncertainty term (2.16b). This term was also found with a sensitivity analysis, where the range in mean RRR values from the risk models studied in this work was assumed to be one σ of the distribution of RRR from uncertainty in the risk model. The last term accounts for the

covariance, which, in this case, reduces the relative uncertainty in the mean RRR because correlations in the error of the terms used in the calculation of the mean RRR . The covariance was calculated using the equation:

$$\sigma_{ERR_v, ERR_p} = \frac{1}{n} \sum_{i=1}^n \left(ERR_{V_i} - \overline{ERR}_{V_i} \right) \left(ERR_{P_i} - \overline{ERR}_{P_i} \right), \quad (2.17)$$

where n is the number of patients (3 for this study), and \overline{ERR} denotes the mean value (Taylor, 1982).

In addition to propagating the uncertainty for the mean RRR , the uncertainty was propagated for two specific cases. First, the uncertainty was propagated for each patient individually according to the equations:

$$\left(\frac{\sigma_{RRR}}{RRR} \right)^2 = \left(\frac{\sum_{T=1}^2 ERR_1^2 \left(\frac{\sigma_{D_1}}{D_1} \right)^2}{\left(\sum_{T=1}^2 ERR_T \right)^2} \right)_V + \left(\frac{\sum_{T=1}^2 \left(ERR_1^2 \left(\frac{\sigma_{D_1}}{D_1} \right)^2 + ERR_2^2 \left(\frac{\sigma_{D_2}}{D_2} \right)^2 \right)}{\left(\sum_{T=1}^2 ERR_T \right)^2} \right)_P + \left(\frac{\sigma_{RRR}}{RRR} \right)_{w_R}^2 \quad (2.18a)$$

$$\left(\frac{\sigma_{RRR}}{RRR} \right)^2 = \left(\frac{\sum_{T=1}^2 ERR_1^2 \left(\frac{\sigma_{D_1}}{D_1} \right)^2}{\left(\sum_{T=1}^2 ERR_T \right)^2} \right)_V + \left(\frac{\sum_{T=1}^2 \left(ERR_1^2 \left(\frac{\sigma_{D_1}}{D_1} \right)^2 + ERR_2^2 \left(\frac{\sigma_{D_2}}{D_2} \right)^2 \right)}{\left(\sum_{T=1}^2 ERR_T \right)^2} \right)_P + \left(\frac{\sigma_{RRR}}{RRR} \right)_{w_R}^2 + \left(\frac{\sigma_{RRR}}{RRR} \right)_{RM}^2 \quad (2.18b)$$

where the variables correspond to equations 2.16a and 2.16b, but are for each patient instead of the mean. Second, the uncertainty was propagated for the mean RRR (according to equations

2.16a and 2.16b) without the $\left(\frac{\sigma_{RRR}}{RRR} \right)_{w_R}^2$ and the covariance term.

2.4.6. Summary of Risk Calculations

In order to clarify and summarize the methods for this work, the various combinations of variables studied are organized below in Tables 2.10 and 2.11.

Table 2.10 - Summary of variables and their corresponding specific aim.

Goal	Patient Model	Risk Model	Modality Studied	Proton Arc Beam Weighting	Spec. Aim
Baseline LNT RRR Estimate	Small	Linear-no-threshold	VMAT and Proton Arc	Uniform	1
	Medium	Linear-no-threshold			
	Large	Linear-no-threshold			
Sensitivity of RRR to Risk Model	Small, Med, and Large	Linear-exponential-10	VMAT and Proton Arc	Uniform	1
	Small, Med, and Large	Linear-exponential-40			
	Small, Med, and Large	Linear-plateau-10			
	Small, Med, and Large	Linear-plateau-40			
Sensitivity of RRR to Neutron \bar{w}_R	Medium	Linear-no-threshold	Proton Arc	Uniform	1
Sensitivity of RRR to Beam Weighting	Medium	Linear-no-threshold	Proton Arc	Non-uniform	2
Sensitivity of RRR to Margin Size	Medium	Linear-no-threshold	VMAT and Proton Arc	Uniform	3
		Linear-exponential-10			
		Linear-exponential-40			
		Linear-plateau-10			
		Linear-plateau-40			

Table 2.11 - Summary of the source of stray doses for the proton arc therapy treatment plans.

Patient Model	Specific Aim	Source of Neutron Dose Estimate
Small	1	Fontenot <i>et al.</i> (2008)
Medium	1, 2 and 3	Simulations from this work
Large	1	Fontenot <i>et al.</i> (2008)

Chapter 3

Results

The results from this work are presented in this chapter. First, the treatment plans and therapeutic dose determination will be presented (section 3.1). Specifically, details of the VMAT (section 3.1.1) and proton arc (section 3.1.2) treatment plans are presented, followed by dose-volume histogram comparisons in section 3.1.3. Next, the results of the stray dose determination are presented (section 3.2). Finally, section 3.3 presents the predicted *ERR* values for VMAT and proton arc therapy, the *RRR* of the two modalities, the statistical analysis (section 3.3.1), and the uncertainty analysis (section 3.3.2).

3.1. Therapeutic Dose Distributions

3.1.1. Volumetric Modulated Arc Therapy

The VMAT treatment plans created for specific aim 1 are presented below. Figure 3.1 shows the therapeutic dose using a colorwash scale ranging from 10 Gy (blue) to 80 Gy (red). The prescribed dose for each patient was 76 Gy (normalized to 78.8 Gy to the mean of the PTV; section 2.2.1), and the MUs required for the small, medium and large patients' treatment plans were 669, 962, and 920, respectively. For the small patient, the maximum dose was located in the PTV in the right seminal vesicle and was 107.9%. The maximum dose for the medium patient was located in the left, inferior, posterior portion of the PTV and was 108.8%. For the large patient, the maximum dose was located in the PTV in the left seminal vesicle and was 108.0%. The minimum, mean, and maximum doses to the CTV, PTV, rectum (and contents), rectal wall, bladder (and contents), and bladder wall for these treatment plans are presented in Table 3.1, below. In general, the low dose was distributed over a large amount of healthy tissue, but the high dose was conformed to the PTV. A high dose gradient existed in the rectum, which was desirable to minimize toxicities and satisfy the DVH constraints (Table 2.2).

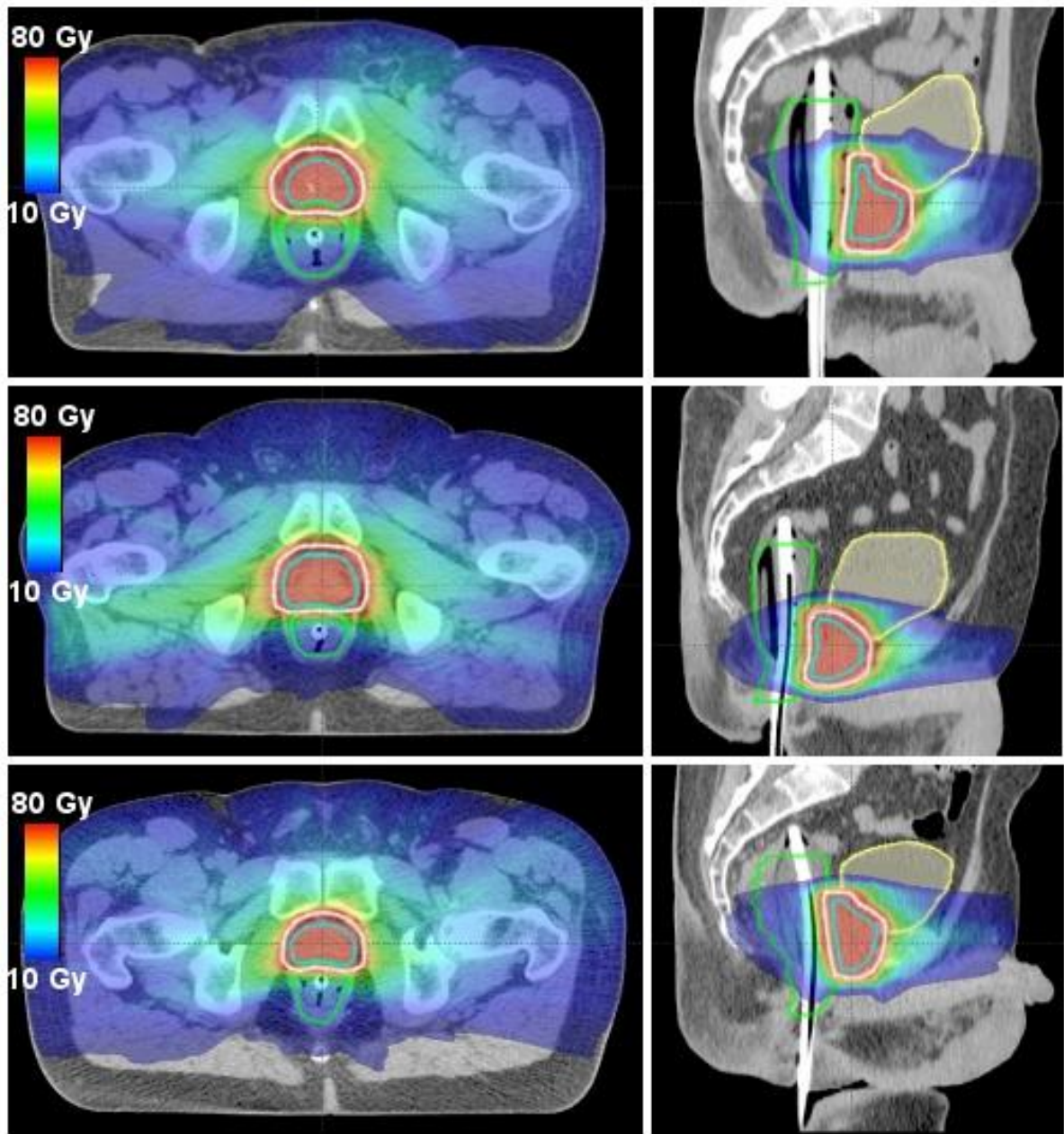


Figure 3.1 - Axial (left) and sagittal (right) CT slices of the small (top), medium (middle), and large (bottom) patients' VMAT treatment plans showing a colorwash of the dose distribution from 10 Gy to 80 Gy. The CTV is shown in cyan, the PTV in white, the bladder in yellow, and the rectum in green. The 30 Gy isodose level is represented by cyan.

Table 3.1 - Minimum, mean, and maximum therapeutic doses for the CTV, PTV, rectum and contents, rectal wall, bladder and contents, and bladder wall for the small, medium, and large patients for the VMAT treatment plans with nominal margins for specific aim 1.

Volume	Statistic	Dose [Gy]		
		Small Patient Plan	Medium Patient Plan	Large Patient Plan
CTV	D _{min}	76.5	76.0	76.3
	D _{mean}	78.4	78.3	78.4
	D _{max}	81.2	80.8	80.6
PTV	D _{min}	73.3	71.9	72.1
	D _{mean}	78.8	78.8	78.8
	D _{max}	82.0	82.7	82.1
Rectum (and contents)	D _{min}	2.2	1.5	2.5
	D _{mean}	26.4	20.5	25.9
	D _{max}	80.6	80.5	80.6
Rectal Wall	D _{min}	2.2	1.5	2.5
	D _{mean}	28.5	23.8	29.8
	D _{max}	80.3	80.4	80.4
Bladder (and contents)	D _{min}	1.1	0.9	1.8
	D _{mean}	19.9	13.1	25.2
	D _{max}	80.9	81.7	81.4
Bladder Wall	D _{min}	1.1	0.9	1.8
	D _{mean}	22.1	16.4	26.9
	D _{max}	80.8	80.8	81.4

The VMAT treatment plans created for specific aim 3 with various size margins around the CTV are shown below in Figure 3.2. It can be seen that as the margins from the CTV increase, the high-dose area (red) increases to cover the larger PTV and the medium dose (30 Gy) (cyan) extends further into the rectum. The effect of margin size on dose to the bladder wall and rectal wall is presented in Table 3.2 and graphed in Figure 3.3 below, where it can be seen that mean doses to the bladder wall and rectal wall increase as margin size increases.

However, maximum and minimum doses remain relatively constant with increasing margin size. This is because the bladder wall and rectal wall are already receiving very close to the maximum dose for the plan. Therefore, as the high dose encroaches further into the organs, the mean dose increases while the maximum dose remains fairly stable. Similarly, the

minimum dose to the organs remains relatively constant because it is determined by the dose far from the target, which is not significantly affected by the size of the high dose region.

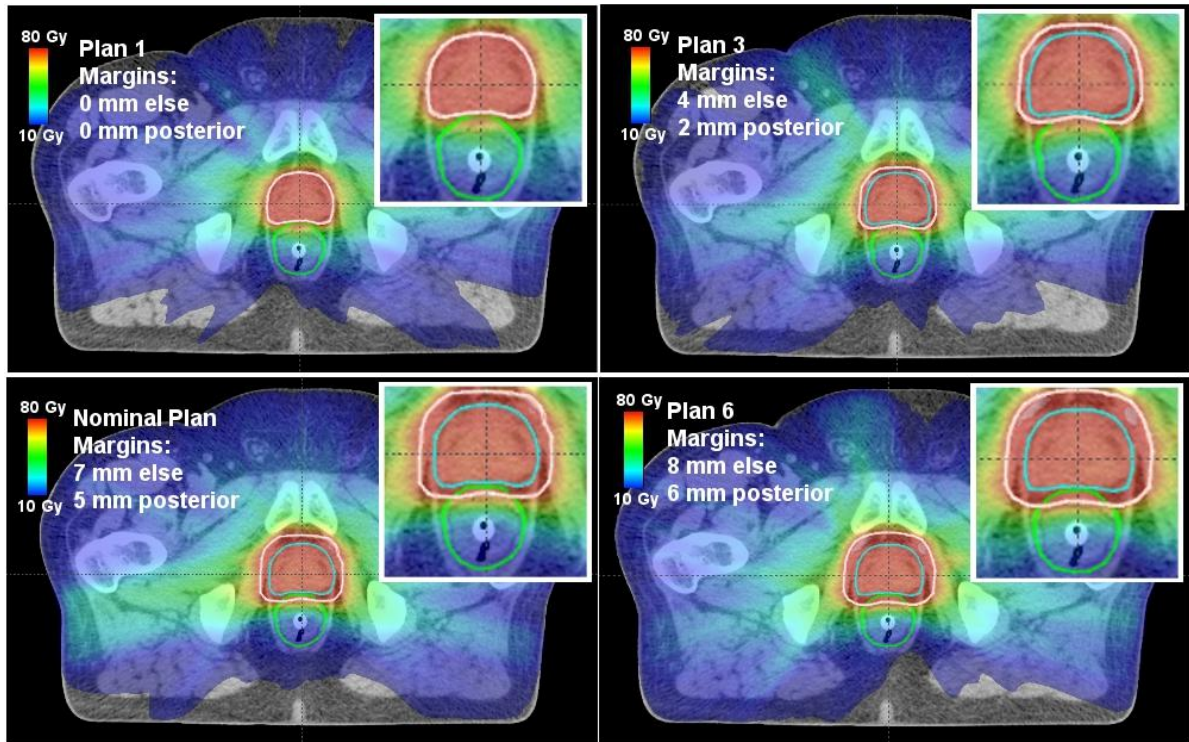


Figure 3.2 – Axial images of a sampling of the VMAT treatment plans with varying margin size around the CTV. Plan indices correspond to those in Table 2.3, where the margins increase as the plan index increases. The CTV is shown in cyan, the PTV in white, and the rectum in green. Close-up views of the central region including the CTV, PTV and rectum are inset.

Table 3.2 - Minimum, mean and maximum doses to the bladder wall and rectal wall for VMAT as a function of margin size around the CTV. Plan indices correspond to Table 2.3, where plan 1 has the smallest expansion and plan 6 has the largest expansion. As expected, mean doses to both the bladder wall and rectal wall increase as margin size increases.

		VMAT Dose [Gy]						
Volume	Statistic	Plan 1 (Smallest)	Plan 2	Plan 3	Plan 4	Plan 5	Nominal Plan	Plan 6 (Largest)
Bladder Wall	D_{min}	0.7	0.7	0.8	0.9	0.9	0.9	1.0
	D_{mean}	11.3	13.3	14.8	14.9	15.2	16.4	17.0
	D_{max}	82.3	81.0	80.8	81.0	81.7	80.8	81.5
Rectal Wall	D_{min}	1.1	1.2	1.3	1.3	1.4	1.5	1.5
	D_{mean}	18.3	20.5	21.9	22.3	22.7	23.8	24.8
	D_{max}	80.0	80.0	80.0	79.9	80.1	80.4	81.4

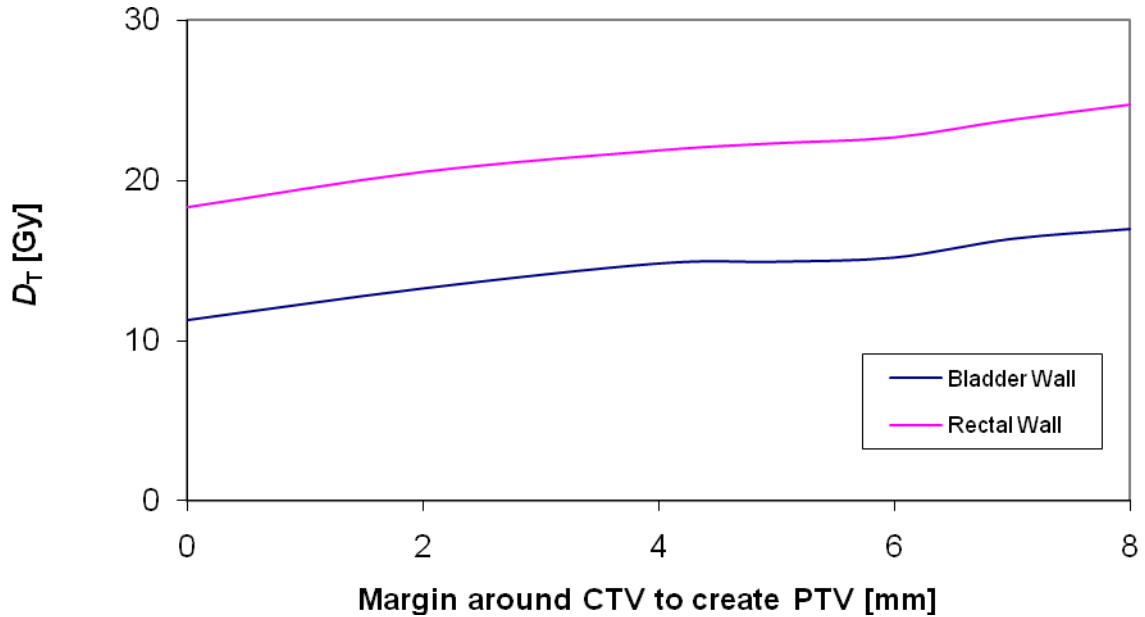


Figure 3.3 – Therapeutic mean absorbed dose to the bladder wall and rectal wall as a function of “else” margin size around the CTV to create the PTV for the VMAT treatment plans for specific aim 3. Posterior margins are 2 mm less than those graphed, except for 0 mm “else” expansion, where the posterior margin is also 0 mm. Margin sizes correspond to Table 2.3. The nominal expansion is 7 mm in the “else” anatomical directions. As expected, mean dose increases with margin size.

3.1.2 Proton Arc Therapy

The proton arc therapy treatment plans with varying number of treatment beams are presented below. The mean doses to the bladder (and contents), bladder wall, rectum (and contents), rectal wall, femoral heads, and normal tissues were plotted *vs.* the number of treatment beams. Figure 3.4 demonstrates the weak dependence of mean dose on number of beams beyond 8 beams. The risk of second cancer of the bladder and rectum was also calculated for these treatment plans (method described in section 2.4), which also shows a weak dependence on number of beams (Figure 3.5). Because of the smooth shape of the isodose lines produced with the 16-field plan (Figure 3.6), we approximated all arc dose distributions using 16 static fields.

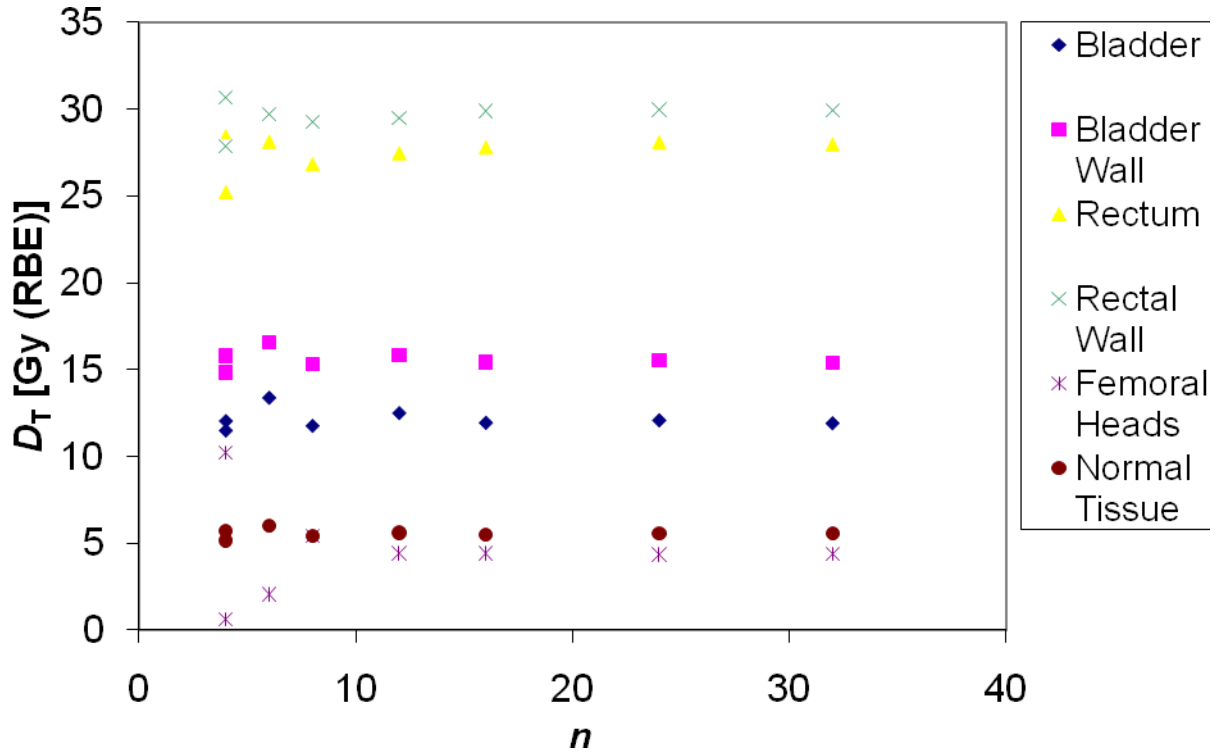


Figure 3.4 – Calculated mean dose (D_T) vs. the number of equally spaced and uniformly weighted treatment beams (n). Little variation is observed beyond 8 beams.

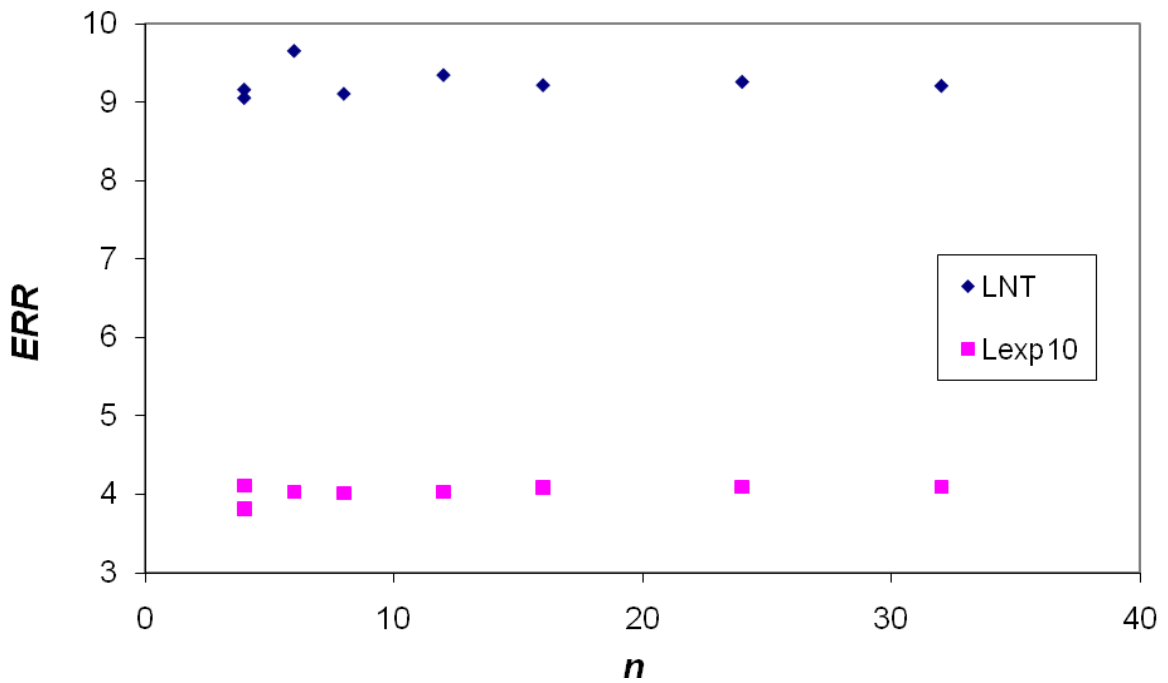


Figure 3.5 – Predicted excess relative risk (ERR) of a second malignant neoplasm in the bladder and rectum vs. number of equally spaced and uniformly weighted beam angles, n , for two different risk models. The linear-no-threshold (LNT) model is the least dependent on the

distribution of dose in a volume, and the linear-exponential-10 (Lexp10) is the most dependent on the distribution of dose. A weak dependence on the number of beams was observed.

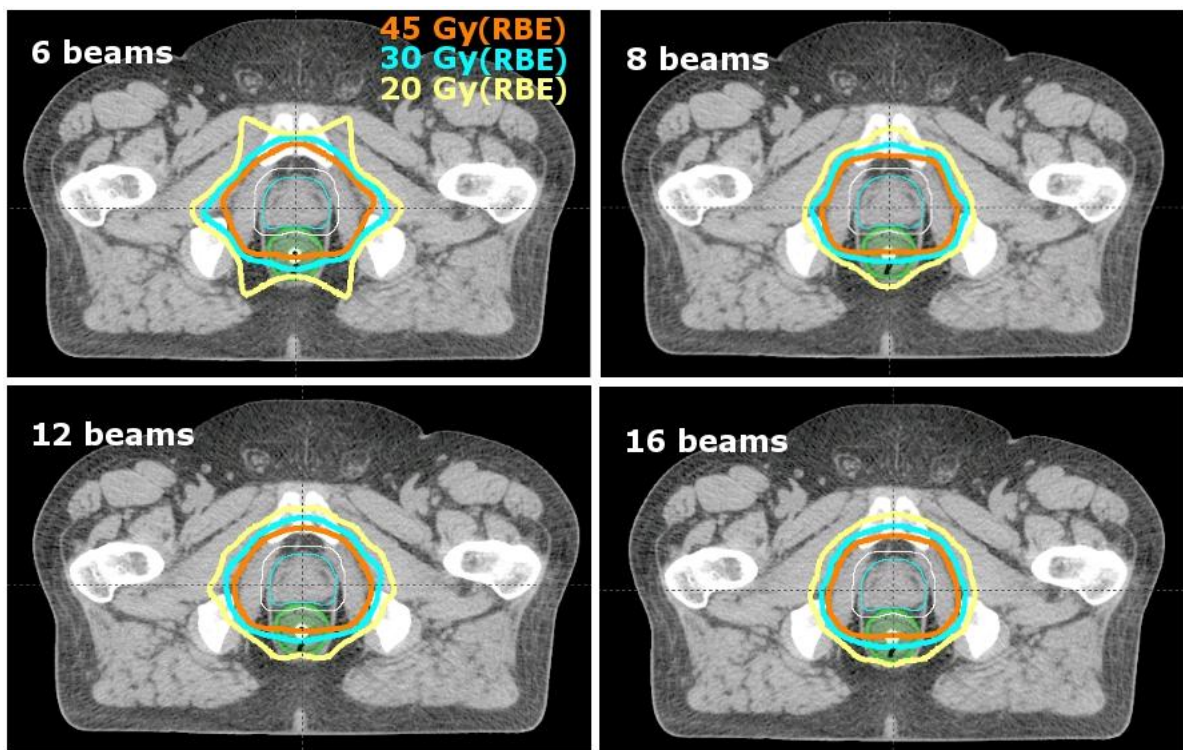


Figure 3.6 - Isodose lines of the 6, 8, 12, and 16-beam treatment plans, showing the 45 Gy (RBE) (orange), 30 Gy (RBE) (cyan), and 20 Gy (RBE) (yellow) isodose lines, revealing a significant smoothing with increasing number of beams. 16 beams produced extremely smooth isodose lines. The CTV is shown in cyan, the PTV in white, and the rectum in green.

The proton arc therapy treatment plans created for specific aim 1 are presented below. Figure 3.7 shows the therapeutic dose using a colorwash scale ranging from 10 Gy (RBE) to 80 Gy (RBE). For the small patient, the maximum dose was located in the PTV in the seminal vesicles and was 106.6%. The maximum dose to the medium patient was in the PTV in the bladder wall and was 105.5%. For the large patient, the maximum dose was within the CTV and was 105.6%. The minimum, mean, and maximum doses to the CTV, PTV, rectum (and contents), rectal wall, bladder (and contents), and bladder wall for these treatment plans are presented in Table 3.3, below. It can be seen that the low dose region encompasses a smaller overall volume than the VMAT plans (Figure 3.1). On average, proton arc therapy reduced the volume of normal tissue exposed to doses between 10 and 30 Gy or Gy (RBE) by 73%. The

high dose region is very conformal, but because proton treatment beams are typically designed with larger margins, the high dose region is slightly larger in the proton arc therapy plans than in the VMAT plans. Specifically, the small, medium, and large patients' irradiated volumes (volume receiving at least 76 Gy or Gy (RBE)) were 106, 156 and 159 cm³, respectively, for proton arc therapy, and 89, 138 and 135 cm³, respectively, for VMAT.

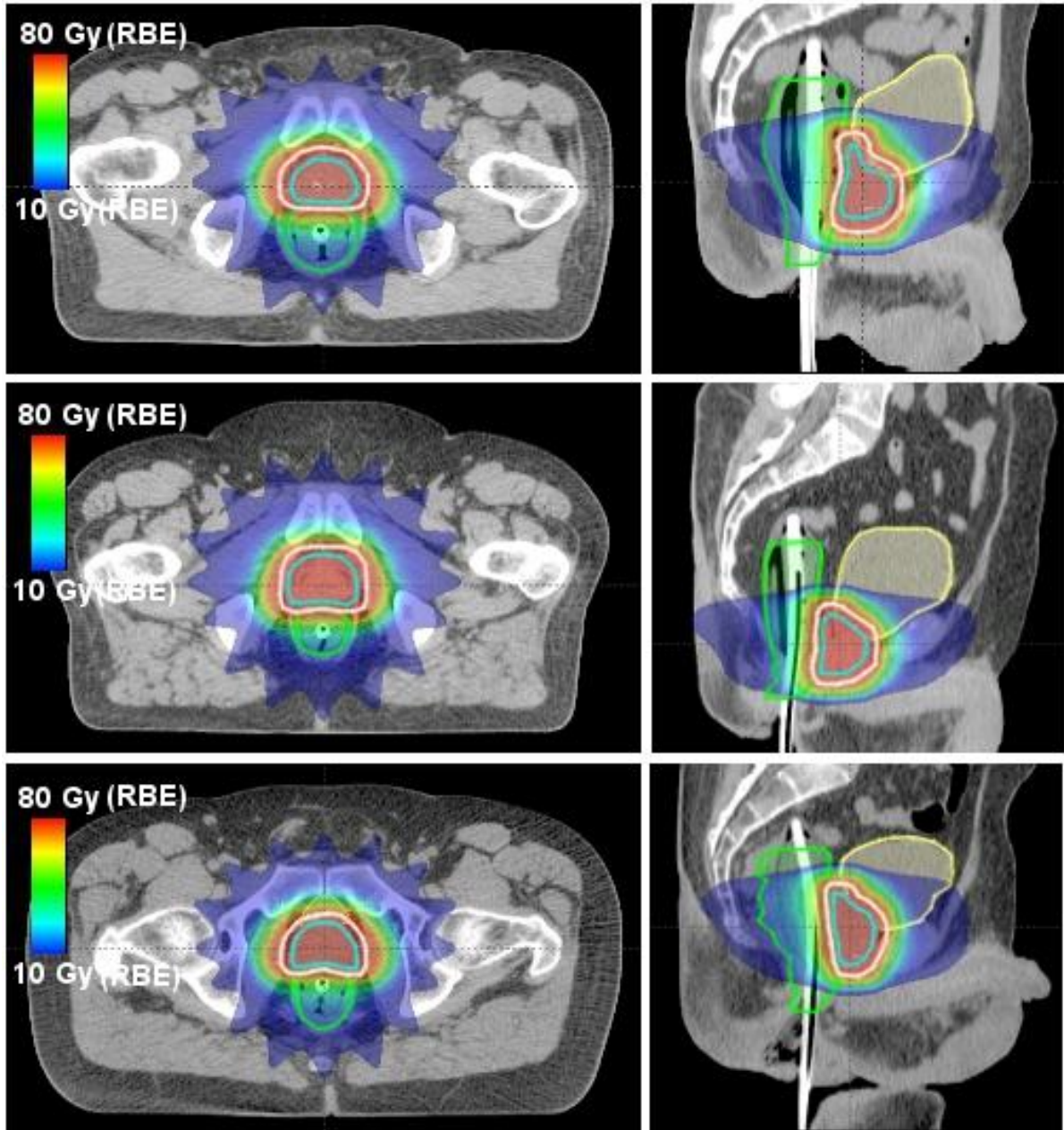


Figure 3.7 - Axial (left) and sagittal (right) CT images of the small (top), medium (middle), and large (bottom) patients' proton arc treatment plans showing a colorwash of the dose distribution from 10 Gy (RBE) to 80 Gy (RBE). The CTV is shown in cyan, the PTV in white,

the bladder in yellow, and the rectum in green. The 30 Gy (RBE) isodose level is represented by cyan.

Table 3.3 - Minimum, mean, and maximum therapeutic doses for the CTV, PTV, rectum and contents, rectal wall, bladder and contents, and bladder wall for the small, medium, and large patient for the proton arc therapy treatment plans with uniform beam weighting and nominal margins for specific aim 1.

Volume	Statistic	Dose [Gy(RBE)]		
		Small Patient Plan	Medium Patient Plan	Large Patient Plan
CTV	D _{min}	77.9	78.3	78.0
	D _{mean}	79.4	79.3	79.3
	D _{max}	81.0	80.2	80.3
PTV	D _{min}	73.1	73.2	74.9
	D _{mean}	78.8	78.8	78.8
	D _{max}	81.0	80.2	80.3
Rectum (and contents)	D _{min}	0.0	0.0	0.0
	D _{mean}	29.5	26.9	31.1
	D _{max}	80.4	79.8	80.0
Rectal Wall	D _{min}	0.0	0.0	0.0
	D _{mean}	30.4	29.1	33.4
	D _{max}	80.4	79.8	79.9
Bladder (and contents)	D _{min}	0.0	0.0	0.0
	D _{mean}	18.1	12.2	23.2
	D _{max}	80.9	80.2	80.2
Bladder Wall	D _{min}	0.0	0.0	0.0
	D _{mean}	20.3	15.6	24.3
	D _{max}	80.9	80.2	80.2

The first set of proton arc therapy treatment plans created using non-uniform beam weights (specific aim 2) is shown below in Figure 3.8 (optimization objectives 1, 2, and 3 from Table 2.5, respectively). The beam angles found through optimization to minimize the combined risk of second cancer of the bladder and rectum were 90 and 270 degrees, a 2-field lateral-opposed treatment with equal beam weighting. The beam angles that minimized the risk of second cancer of the bladder only were posterior oblique beams at 157.5 and 202.5 degrees with equal weighting. The beam angles that minimized the risk of second cancer of the rectum only were

anterior oblique beams at 45 and 315 degrees with equal weighting. The minimum, mean, and maximum doses to the bladder wall and rectal wall from these treatment plans are listed in Table 3.4.

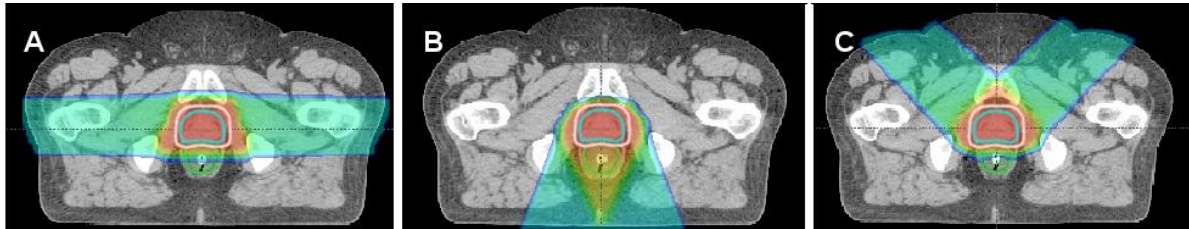


Figure 3.8 - Proton arc therapy treatment plans with SMN risk-minimized beam weighting for combined bladder and rectum (A, 90 and 270 degrees with 1:1 weighting), bladder only (B, 157.5 and 202.5 degrees with 1:1 weighting), and rectum only (C, 45 and 315 degrees with 1:1 weighting).

Another goal of specific aim 2 was to determine the optimal beam weighting for a patient with a prosthetic hip (objective 4 from Table 2.5). The resulting treatment plans are shown in Figure 3.9 below. The plan labeled “prosthetic hip plan 1” utilized 270 and 292.5 degree beams with weighting of 1.94:1, respectively. This plan minimized the risk of SMN incidence in the bladder and rectum, but deposited an unacceptable amount of dose in the healthy femoral head: 15% of the right femoral head received at least 64.8 Gy (RBE). The clinical objective for the femoral heads is that 15% of the structure should receive no more than 45 Gy (RBE). A second treatment plan, “prosthetic hip plan 2”, shown on the right in Figure 3.9) utilized 270 and 157.5 degree beams with weighting of 1.94:1, respectively, and met the clinical DVH constraints for the femoral head, bladder, and rectum. The minimum, mean, and maximum doses to the bladder wall, rectal wall, and femoral head from these treatment plans are listed in Table 3.4.

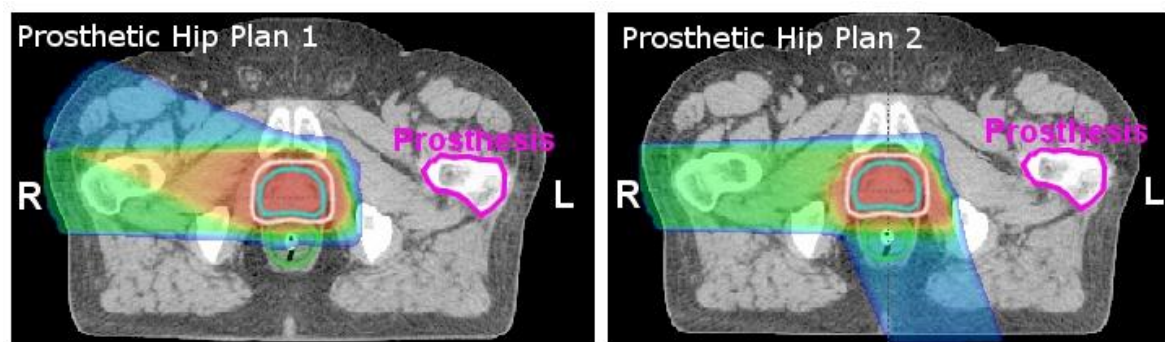


Figure 3.9 - Proton arc therapy treatment plans with SMN risk-minimized beam weighting for combined bladder and rectum with a prosthetic hip. The figure on the left shows “Prosthetic Hip Plan 1”, with the angles of 270 and 292.5 degrees and weights of 1.94:1, respectively. The figure on the right shows “Prosthetic Hip Plan 2”, with angles of 270 and 157.5 degrees and weights of 1.94:1, respectively. Notice the reduction in high dose to the right femoral head in prosthetic hip plan 2.

Table 3.4 - Minimum, mean and maximum doses to the bladder wall and rectal wall from various risk-optimized proton arc therapy treatment plans.

Volume	Statistic	Dose [Gy(RBE)]					
		SA 1 Nominal Plan	Combination Bladder and Rectum Plan	Bladder Only Plan	Rectum Only Plan	Prosthetic Hip Plan 1	Prosthetic Hip Plan 2
Bladder Wall	D _{min}	0.0	0.0	0.0	0.0	0.0	0.0
	D _{mean}	15.6	13.4	10.9	18.3	14.1	12.7
	D _{max}	80.2	80.1	82.2	80.6	79.8	80.8
Rectal Wall	D _{min}	0.0	0.0	0.0	0.0	0.0	0.0
	D _{mean}	29.1	20.0	45.8	18.8	20.7	28.6
	D _{max}	79.8	80.1	81.0	80.2	81.0	80.5
Right Femoral Head	D _{min}	0.0	0.0	0.0	0.0	0.0	0.0
	D _{mean}	4.3	21.0	0.0	1.1	36.1	27.8
	D _{max}	13.8	36.2	0.0	38.8	72.8	48.0

The proton arc therapy treatment plans with varying margins created for specific aim 3 are shown below in Figure 3.10. Similar to the VMAT plans, as the margins from the CTV increase, the red high-dose region increases to cover the larger PTV and the cyan region of medium dose (30 Gy (RBE)) extends further into the rectum. The dose to the bladder wall and rectal wall are presented for each treatment plan in Table 3.5 and graphed in Figure 3.11 below, where it can be seen that doses to the bladder wall and rectal wall increase as margin size increases. Similar to the VMAT plans for specific aim 3, the minimum and maximum doses to the bladder wall and rectal wall are relatively insensitive to margin size (section 3.1.1).

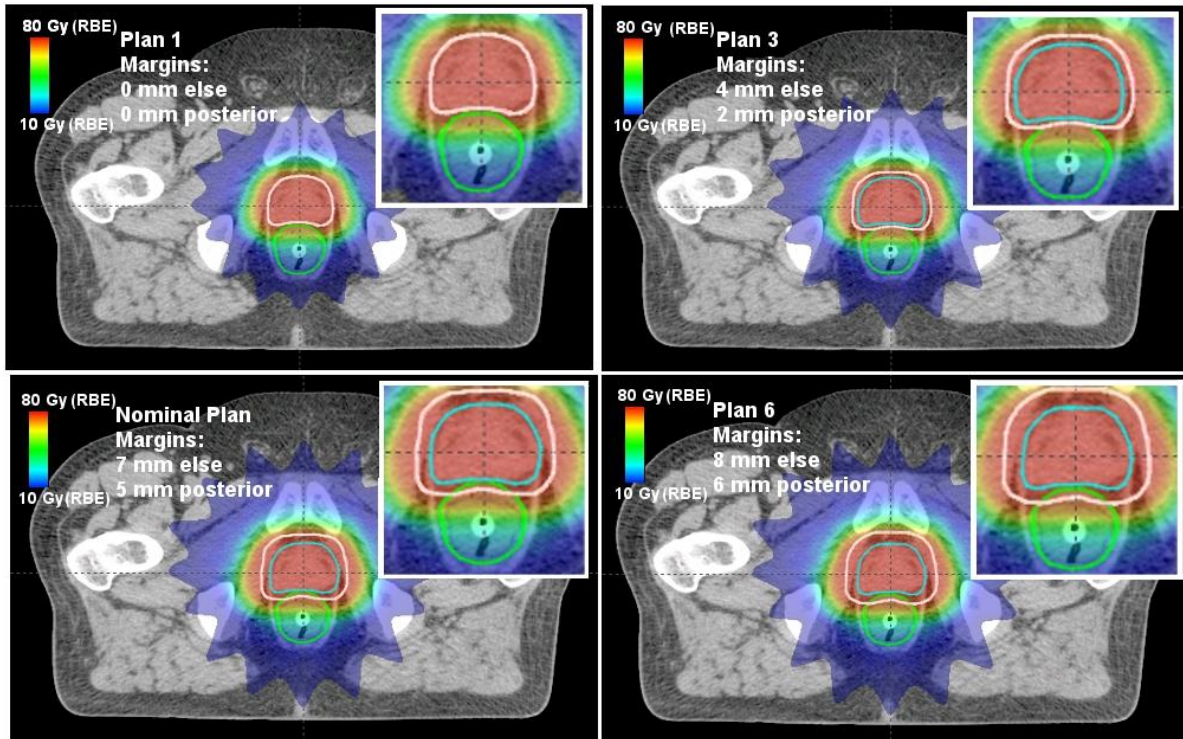


Figure 3.10 – Axial CT images of a sample of the proton arc treatment plans with varying margins from the CTV. Plan indices correspond to Tables 2.6 and 2.7, where the margins increase with plan index. The margins listed on the figure correspond to the margins from the CTV to create the PTV. Lateral, distal and proximal margins around the CTV can be found in Tables 2.6 and 2.7. The CTV is shown in cyan, the PTV in white, and the rectum in green. The colorwash scale is from 10 Gy (RBE) to 80 Gy (RBE). Close-up views of the central region including the CTV, PTV and rectum are inset.

Table 3.5 - Minimum, mean and maximum doses to the bladder wall and rectal wall for proton arc therapy as a function of margin size around the CTV. Plan indices correspond to Tables 2.6 and 2.7, where plan 1 has the smallest margin and plan 6 has the largest margin.

		Proton Arc Therapy Dose [Gy(RBE)]						
Volume	Statistic	Plan 1 (Smallest)	Plan 2	Plan 3	Plan 4	Plan 5	Nominal Plan	Plan 6 (Largest)
Bladder Wall	D_{min}	0.0	0.0	0.0	0.0	0.0	0.0	0.0
	D_{mean}	10.5	11.9	13.4	14.0	14.8	15.6	16.2
	D_{max}	79.4	79.9	80.0	80.0	80.1	80.2	80.3
Rectal Wall	D_{min}	0.0	0.0	0.0	0.0	0.0	0.0	0.0
	D_{mean}	20.8	22.4	25.2	26.6	27.8	29.1	30.3
	D_{max}	78.9	79.2	79.6	79.7	79.8	79.8	79.9

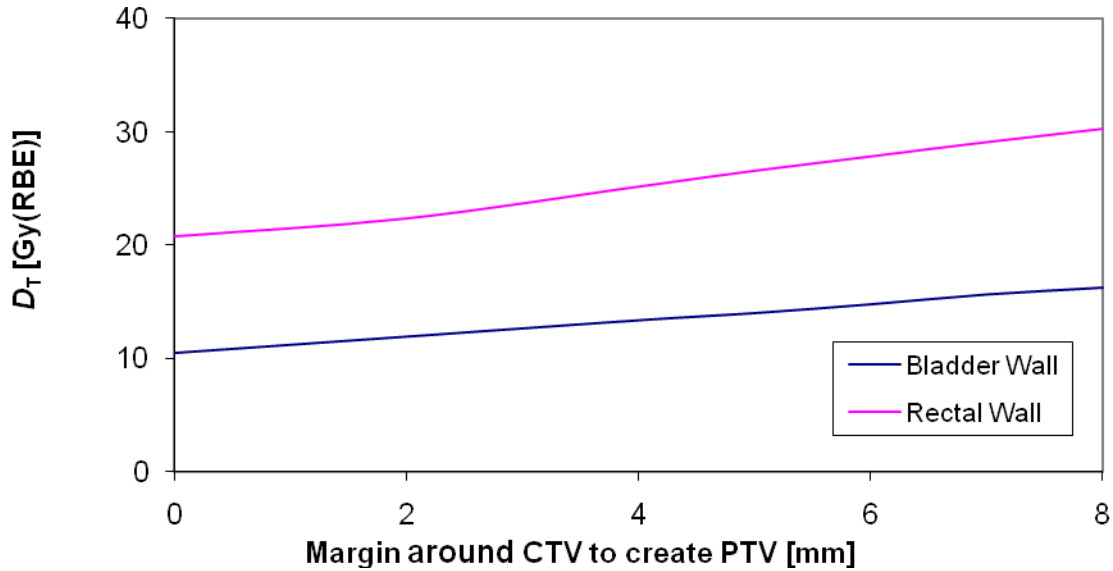


Figure 3.11 – Therapeutic mean dose to the bladder wall and rectal wall as a function of “else” margin size around the CTV to created the PTV for the proton arc therapy treatment plans for specific aim 3. Posterior margins are 2 mm less than those graphed, except for the 0 mm “else” expansion, where the posterior margin is also 0 mm. Plan indices and margin sizes correspond to Tables 2.6 and 2.7. The nominal expansion is 7 mm “else.” As expected, dose increased with margin size.

3.1.3. Dose-Volume Histogram Comparisons

Since DVHs are traditionally plotted for the whole organ (including the contents), we plotted the difference between the traditional whole organ contour and the organ wall contour in Figures 3.12 and 3.13, below. In general, the organ wall curves are slightly higher, indicating a larger percentage of the organ receiving a given dose.

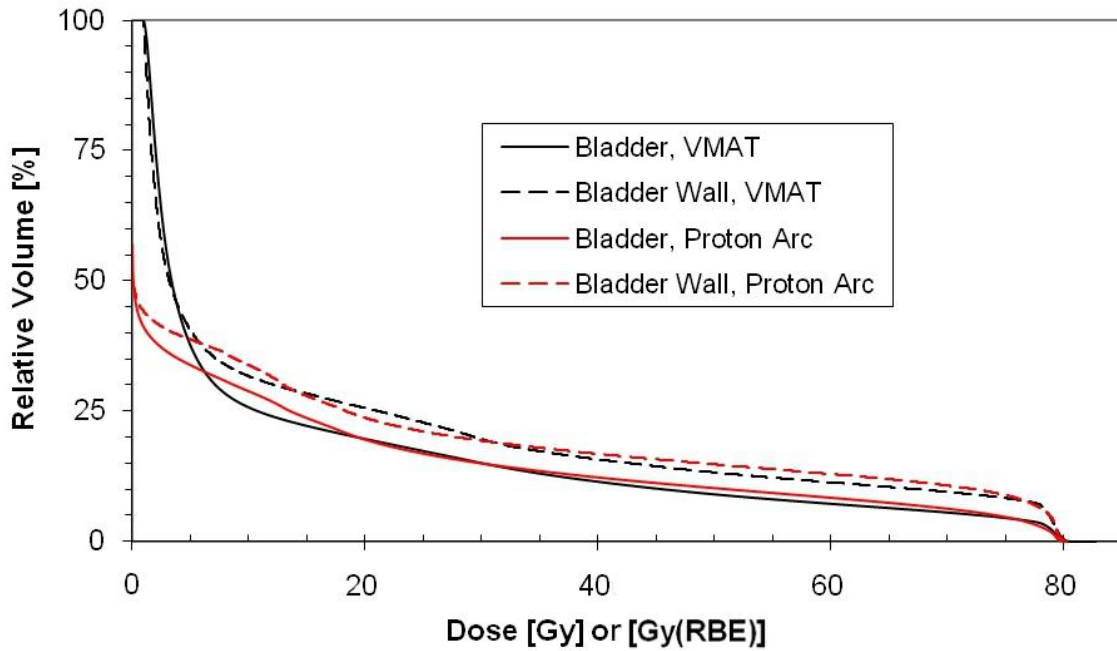


Figure 3.12 - Cumulative dose-volume histogram for the medium patient for VMAT (black; Gy) and uniformly weighted proton arc therapy (red; Gy (RBE)) nominal treatment plans created for specific aim 1 showing the difference between therapeutic absorbed dose to the bladder (and contents) and bladder wall. The bladder wall curves are consistently higher than the bladder curves.

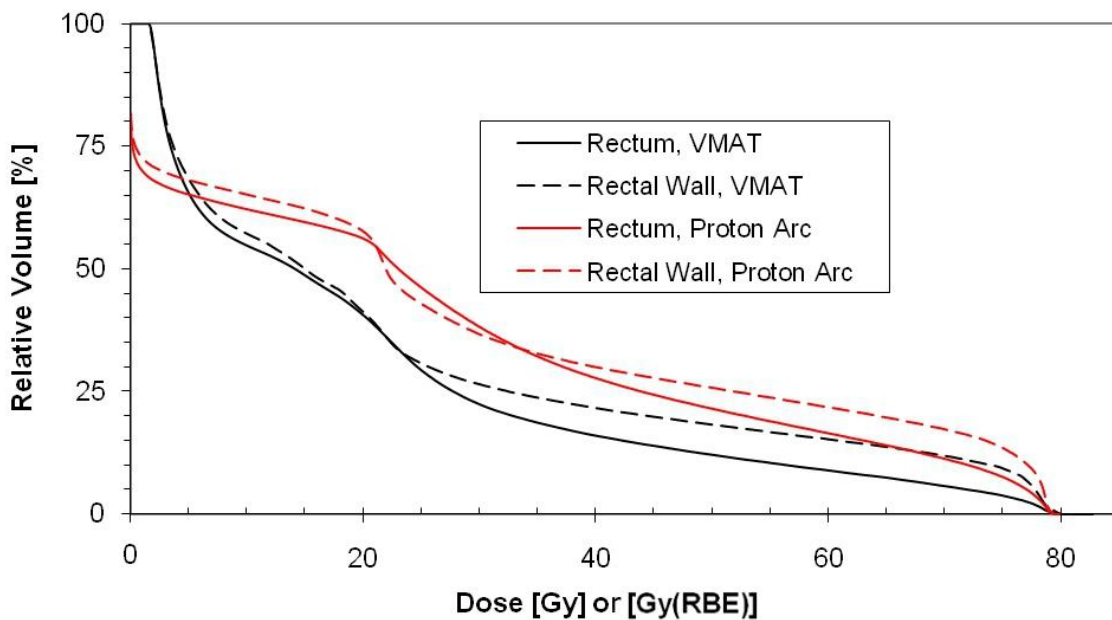


Figure 3.13 - Cumulative dose-volume histogram for the medium patient for the VMAT (black; Gy) and uniformly weighted proton arc therapy (red; Gy (RBE)) nominal treatment plans created for specific aim 1 showing the difference between therapeutic absorbed dose to

the rectum (and contents) and rectal wall. In general, the rectal wall curves are higher than the rectum curves.

Figures 3.14 and 3.15 display the bladder wall and rectal wall DVHs, respectively, for the VMAT and proton arc therapy treatment plans created for specific aim 1. The results from all three patients are plotted together. The only obvious dependence on patient size is that the large patient doses are the highest in all cases. All of the DVH constraints were satisfied for all plans shown in Figures 3.14 and 3.15 and are quantitatively presented in Table 3.6.

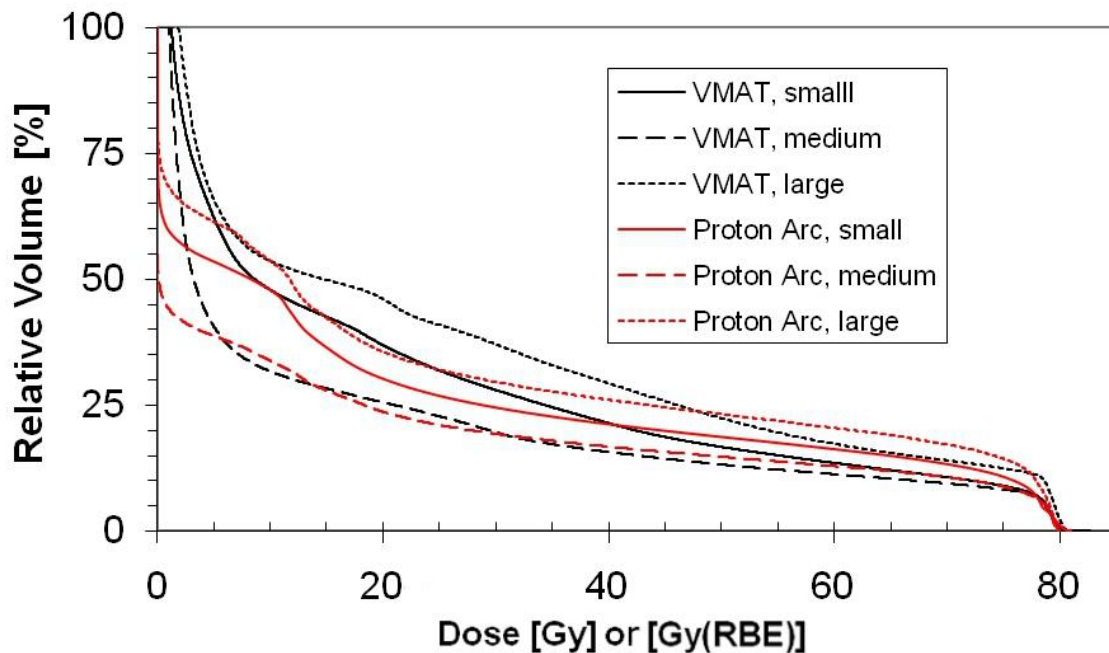


Figure 3.14 - Bladder wall cumulative dose-volume histogram for the small, medium, and large patients' nominal treatment plans for VMAT (black; Gy) and uniformly weighted proton arc therapy (red; Gy (RBE)) for specific aim 1.

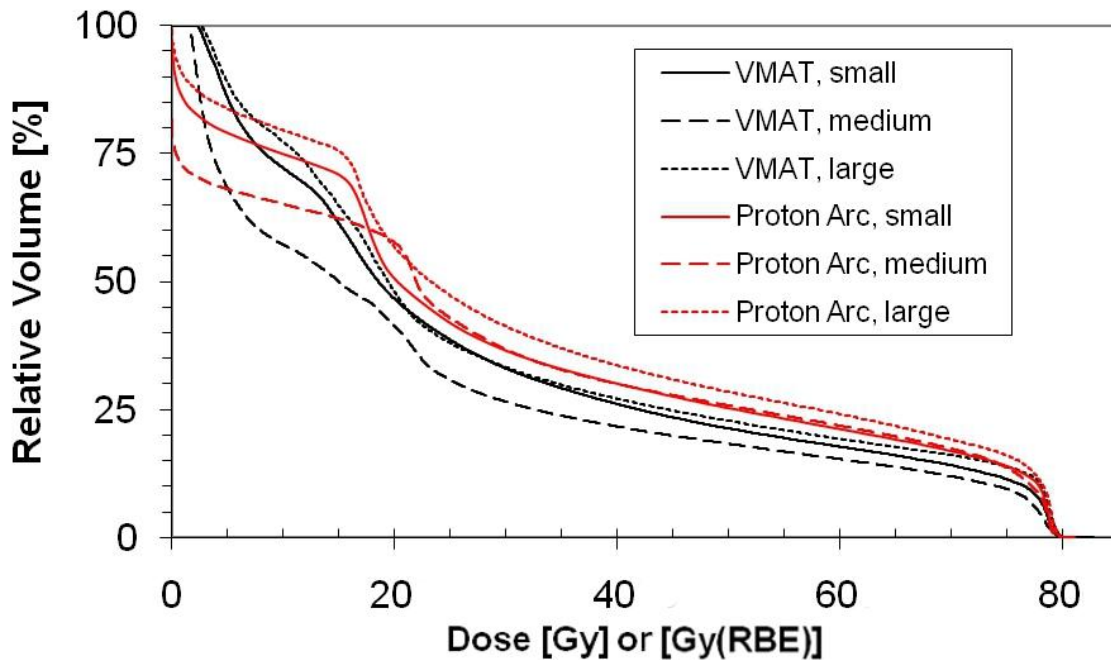


Figure 3.15 - Rectal wall cumulative dose-volume histogram for the small, medium, and large patients' nominal treatment plans for VMAT (black; Gy) and uniformly weighted proton arc therapy (red; Gy (RBE)) for specific aim 1.

Table 3.6 - DVH constraints and results for the bladder and rectum for the small, medium, and large patient treatment plans for specific aim 1 (uniformly weighted proton arc therapy). The results are shown for the bladder and rectum volumes (including contents) for consistency with clinically used DVH constraints. All DVH constraints were met.

Volume	Volume Constraint [%]	Max Dose Constraint [Gy or Gy(RBE)]	VMAT Dose [Gy]			Proton Arc Therapy Dose [Gy(RBE)]		
			Small Patient Plan	Medium Patient Plan	Large Patient Plan	Small Patient Plan	Medium Patient Plan	Large Patient Plan
Bladder	20	70	35.6	19.4	46.2	32.7	19.3	47.7
Rectum	60	40	17.1	6.6	17.3	20.1	14.3	21.0
	50	45	20.9	14.1	20.1	23.9	23.0	24.9
	40	60	25.3	20.2	22.9	29.4	28.8	30.6
	20	70	42.1	32.9	39.4	51.5	53.0	53.1
	15	76	51.4	42.2	50.6	60.6	63.1	62.6
	5	80	74.7	72.0	76.2	77.3	77.0	77.7

For specific aim 2, treatment plans were created to investigate the effect of proton beam weighting on the risk of SMN incidence for proton arc therapy. Figures 3.16 through 3.20 display the DVHs for the bladder wall and rectal wall for the various optimized proton arc

therapy plans compared to the nominal (uniformly weighted) proton arc therapy plan created for specific aim 1. Specifically, Figure 3.16 shows the resulting DVH from the risk-optimized plan where the combined risk of second cancer incidence of the bladder and rectum was minimized. Then, Figures 3.17 and 3.18 correspond to the treatment plans where the risk of second cancer of the bladder only and second rectal cancer only, respectively, were minimized. Finally, the DVHs for the treatment plans for the special case of a patient with a prosthetic hip are shown in Figures 3.19 (prosthetic hip plan 1) and 3.20 (prosthetic hip plan 2). The DVH for the right femoral head is also plotted for the prosthetic hip plans, since it is of particular concern. The quantitative DVH constraints and results for the bladder and rectum are listed in Table 3.7. All DVH constraints for the bladder and rectum were met, except for the rectal constraints shown in red for the bladder-only optimized treatment plan.

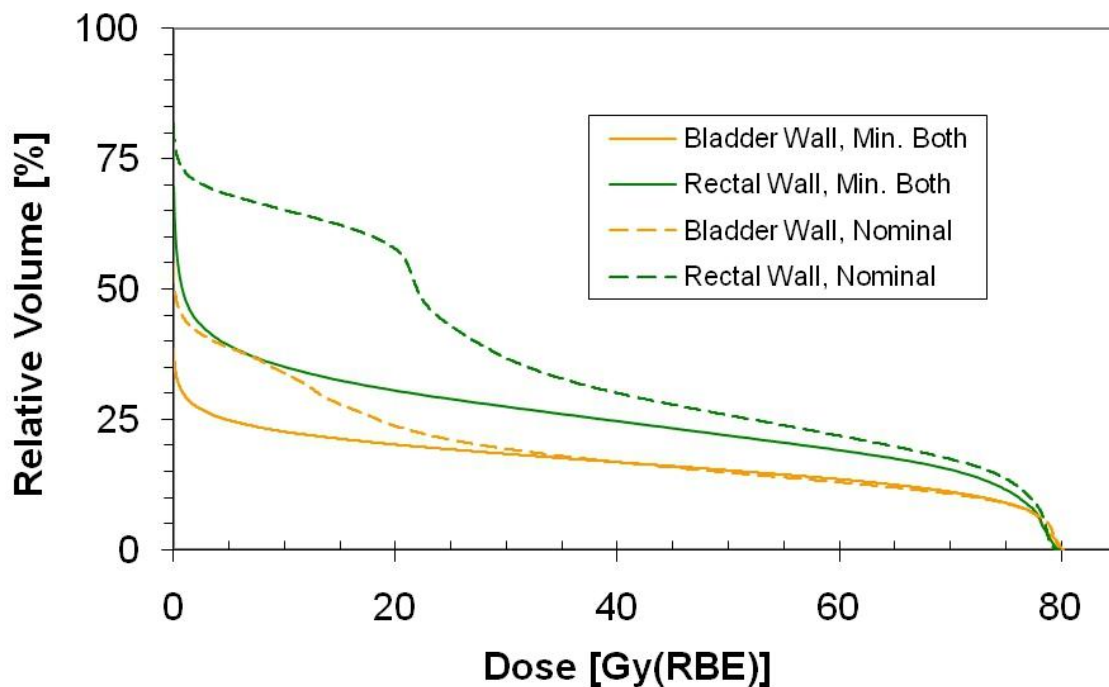


Figure 3.16 - Cumulative dose-volume histogram for the SMN risk-minimized (bladder and rectum) beam weighted treatment plan (solid line) for the bladder wall (orange) and rectal wall (green) for proton arc therapy compared to the nominal equally-weighted treatment plan (dashed line).

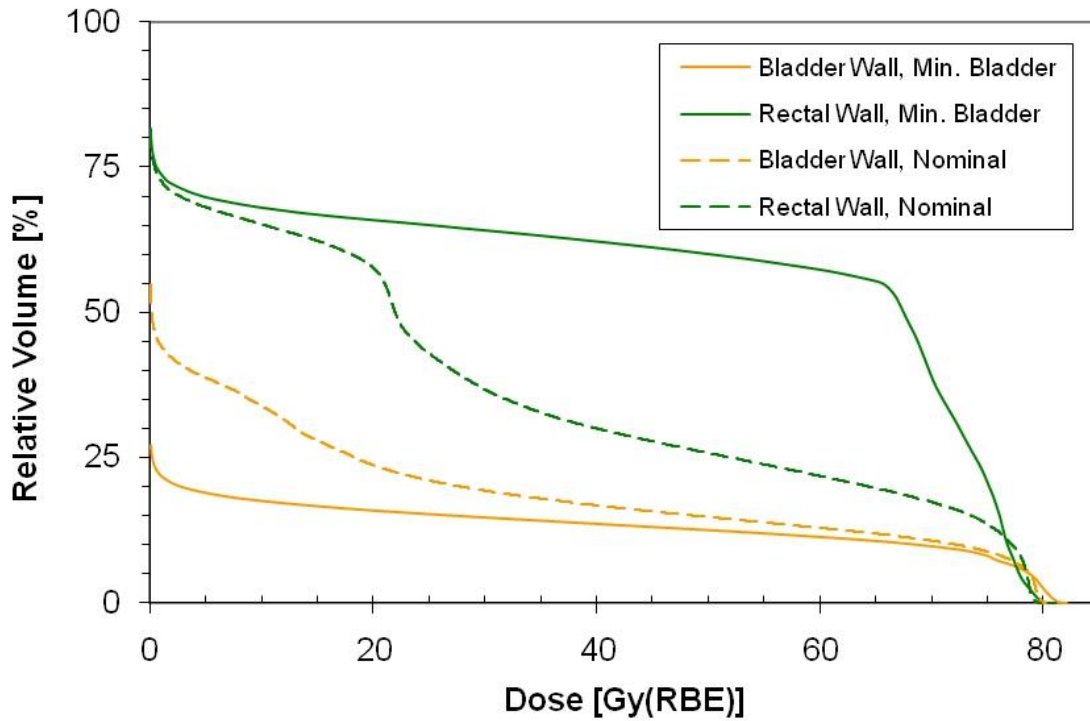


Figure 3.17 - Cumulative dose-volume histogram for the SMN risk-minimized (bladder only) beam weighted treatment plan (solid line) for the bladder wall (orange) and rectal wall (green) for proton arc therapy compared to the nominal equally-weighted treatment plan (dashed line).

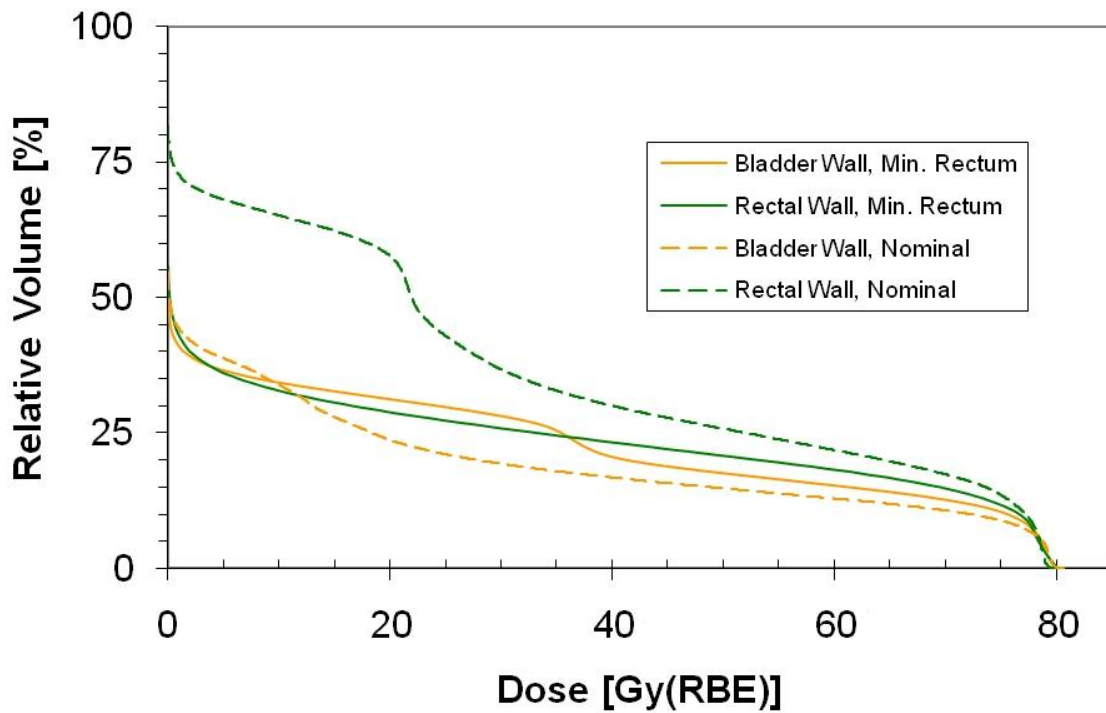


Figure 3.18 - Cumulative dose-volume histogram for the SMN risk-minimized (rectum only) beam weighted treatment plan (solid line) for the bladder wall (orange) and rectal wall (green) for proton arc therapy compared to the nominal equally-weighted treatment plan (dashed line).

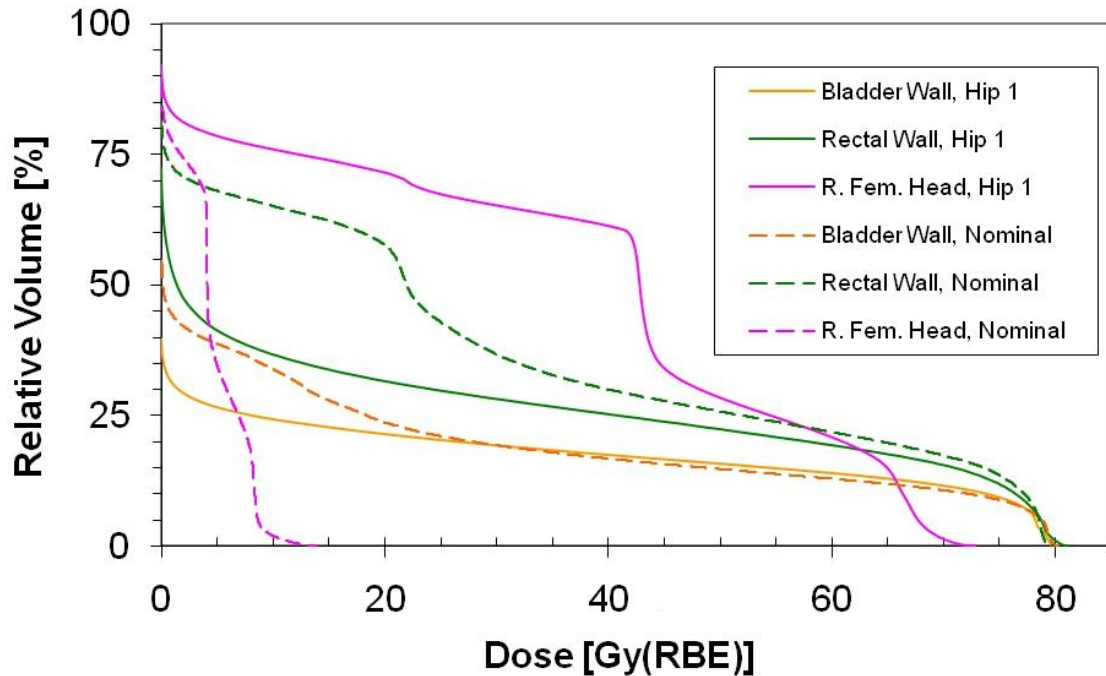


Figure 3.19 - Cumulative dose-volume histogram for the proton arc therapy prosthetic hip plan 1 (solid line) and the nominal uniformly weighted proton arc therapy plan from specific aim 1 (dashed line). The beam weighting was optimized to minimize the combined risk of second cancer of the bladder and rectum.

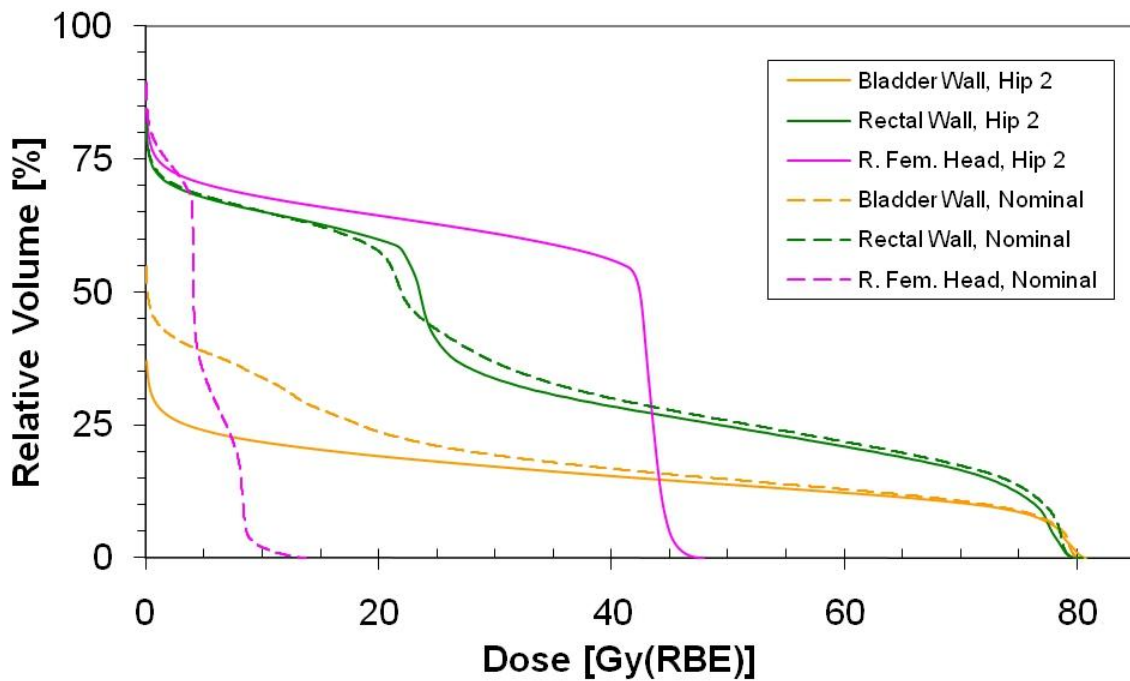


Figure 3.20 - Cumulative dose-volume histogram for the proton arc therapy prosthetic hip plan 2 (solid line) and the nominal uniformly weighted proton arc therapy plan from specific aim 1 (dashed line). The beam weighting was optimized to minimize the combined risk of second cancer of the bladder and rectum.

Table 3.7 - DVH constraints and results for the bladder and rectum for the treatment plans created for specific aim 2 with non-uniform (risk-minimized) beam weighting. The results are shown for the bladder and rectum volumes (including contents) for consistency with traditional DVH constraints. All DVH constraints were met, except the rectal constraints shown in red for the bladder-only optimized plan (50%, 40% and 20% volume constraints).

Volume	Volume Constraint [%]	Max Dose Constraint [Gy(RBE)]	Proton Arc Therapy Dose [Gy(RBE)]				
			Combination Bladder and Rectum Plan	Bladder Only Plan	Rectum Only Plan	Prosthetic Hip Plan 1	Prosthetic Hip Plan 2
Bladder	20	70	5.0	0.2	36	7.8	3.6
Rectum	60	40	0.2	37.3	0.1	6.7	14.4
	50	45	1.1	67.6	0.2	19.2	23.6
	40	60	4.6	70.4	1.4	6.7	25.9
	20	70	41.7	74.5	31.6	43.9	52.2
	15	76	56.9	75.3	49.6	57.7	62.9
	5	80	76.0	76.0	77.2	76.4	76.0

Figures 3.21 through 3.24 show the cumulative DVHs for the treatment plans created for specific aim 3 where the margin size around the CTV was varied. The bladder wall and rectal wall DVHs are shown for the VMAT treatment plans in Figures 3.21 and 3.22, respectively, and the proton arc therapy treatment plans in Figures 3.23 and 3.24, respectively. It can be seen that the DVH curve is higher as the treatment margin increases, indicating a larger volume receiving a given dose. All of the DVH constraints used in the planning process were met for the VMAT and proton arc therapy plans and are listed in Tables 3.8 and 3.9, respectively.

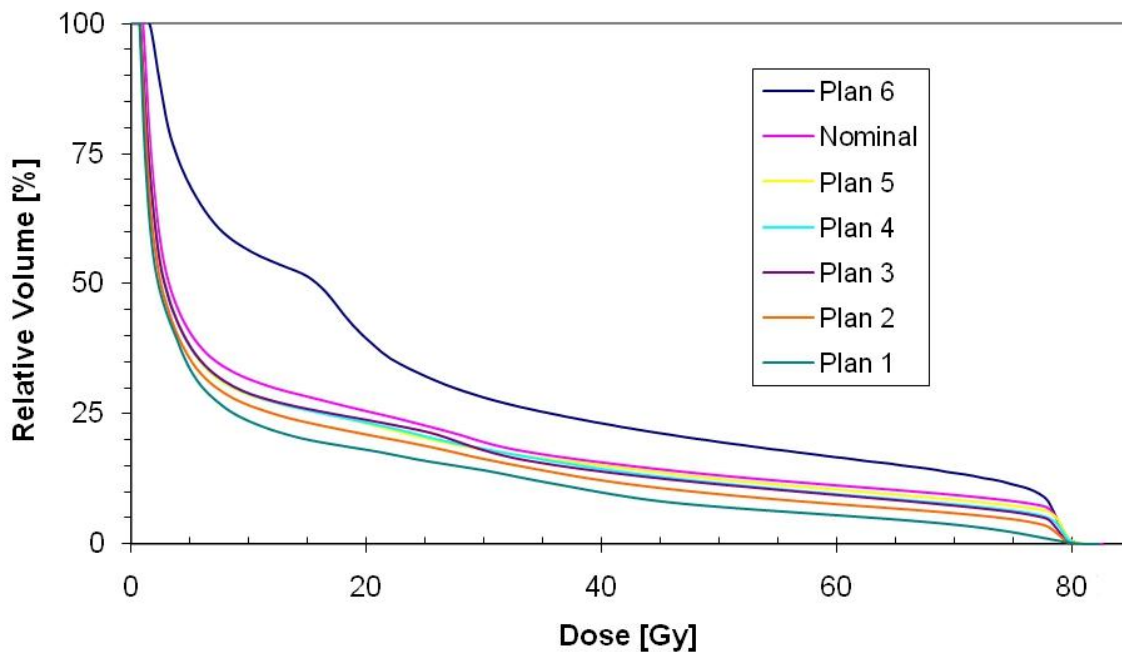


Figure 3.21 - Cumulative dose-volume histogram for the bladder wall for the VMAT treatment plans for specific aim 3. The margin size around the CTV increased with plan index, revealing the positive relationship between volume irradiated and margin size.

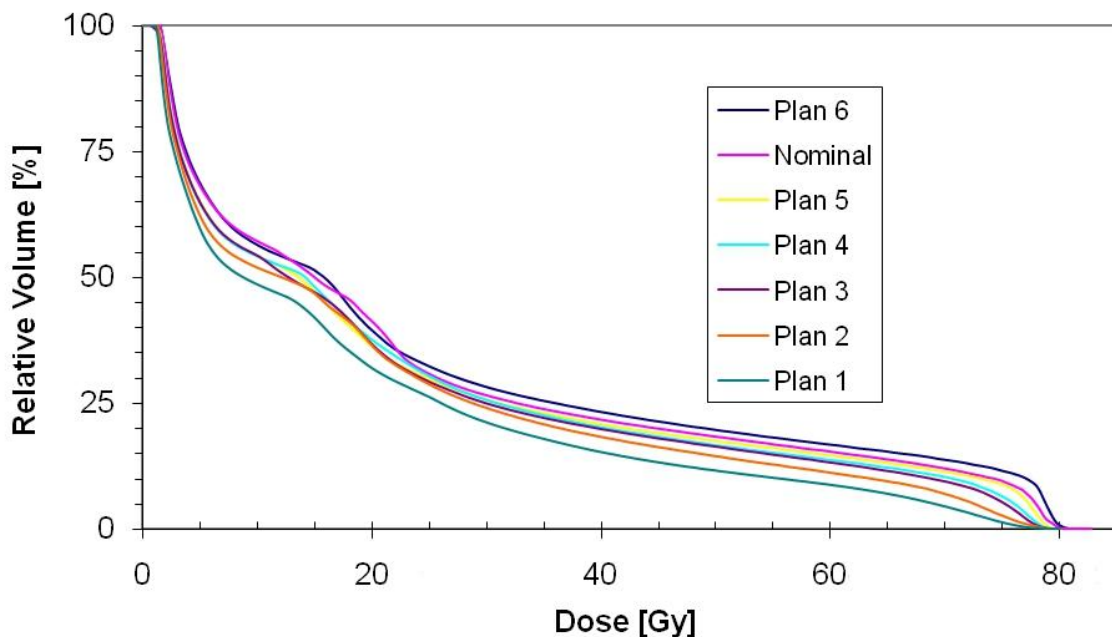


Figure 3.22 - Cumulative dose-volume histogram for the rectal wall for the VMAT treatment plans for specific aim 3. The margin around the CTV increased with plan index, revealing the positive relationship between volume irradiated and margin size.

Table 3.8 - DVH constraints and results for the bladder and rectum for the VMAT treatment plans with varying margin size. The results are shown for the bladder and rectum volumes (including contents) for consistency with traditional DVH constraints. All DVH constraints were met. In general, dose increased with plan index (and margin size).

Volume	Volume Constraint [%]	Max Dose Constraint [Gy]	VMAT Dose [Gy]						
			Plan 1 (Smallest)	Plan 2	Plan 3	Plan 4	Plan 5	Nominal Plan	Plan 6 (Largest)
Bladder	20	70	8.8	11.0	14.3	14.0	13.5	19.4	18.8
Rectum	60	40	4.4	4.8	5.5	5.5	5.6	6.6	6.7
	50	45	7.4	9.3	11.5	11.8	12.1	14.1	14.8
	40	60	16.2	18.6	18.5	19.1	18.6	20.2	21.0
	20	70	29.3	31.3	31.9	32.3	32.8	32.9	38.4
	15	76	34.4	37.3	39.4	40.0	41.7	42.2	49.1
	5	80	55.2	61.4	66.4	67.6	71.1	72.0	75.7

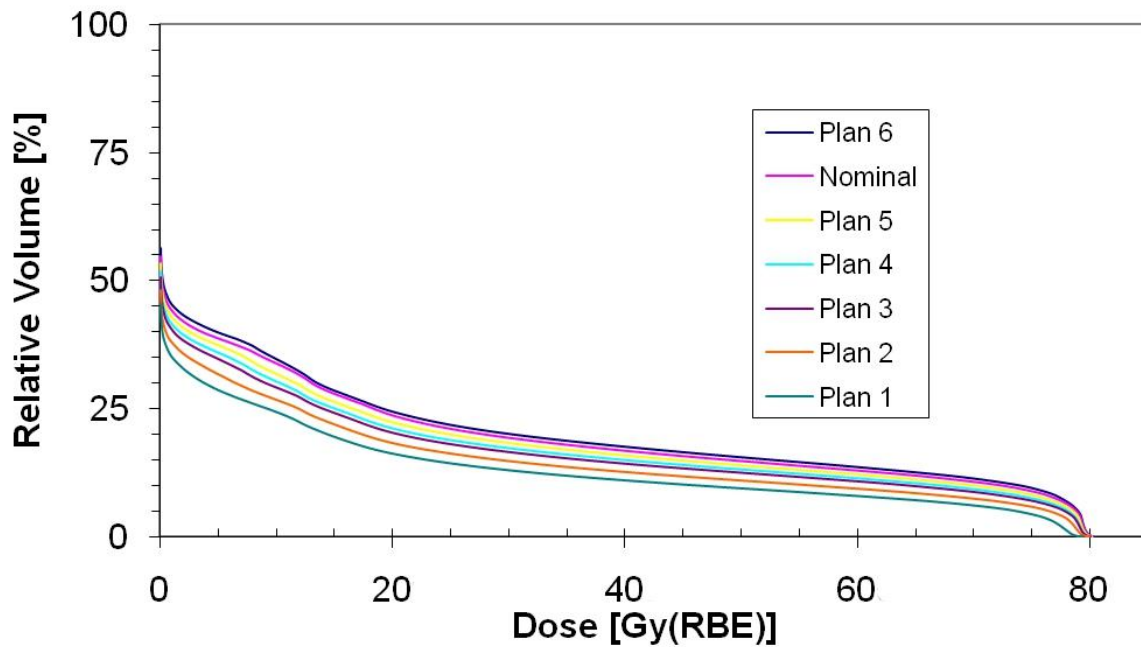


Figure 3.23 - Cumulative dose-volume histogram for the bladder wall for the uniformly weighted proton arc therapy treatment plans for specific aim 3. The margin size around the CTV increased with plan index, revealing the positive relationship between volume irradiated and margin size.

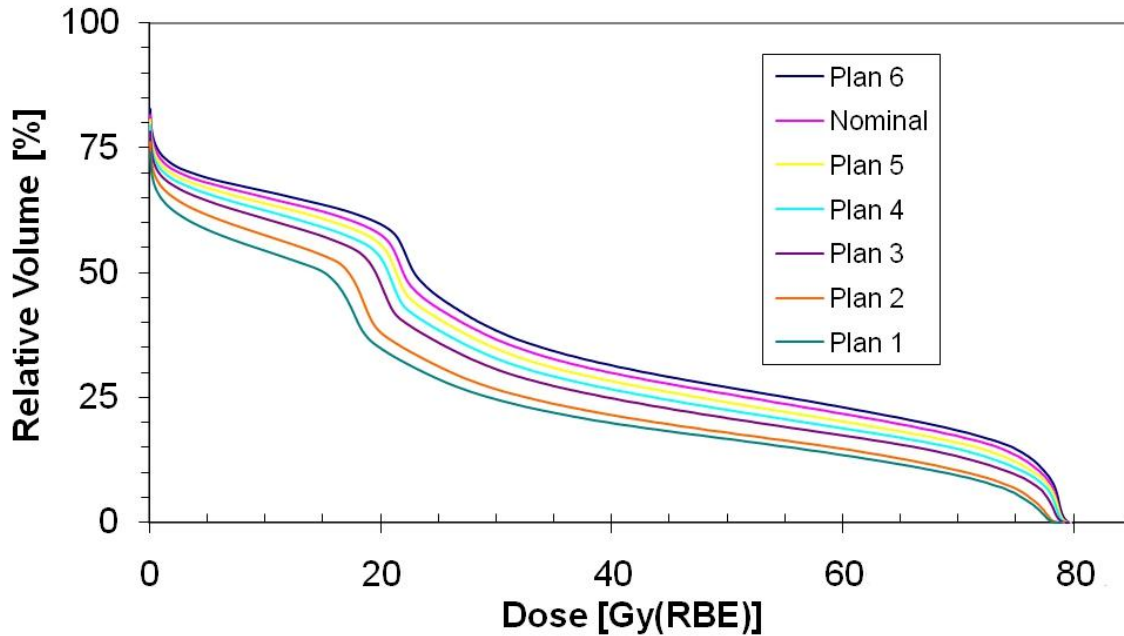


Figure 3.24 - Cumulative dose-volume histogram for the rectal wall for the uniformly weighted proton arc therapy treatment plans for specific aim 3. The margin around the CTV increased with plan index, revealing the positive relationship between volume irradiated and margin size.

Table 3.9 - DVH constraints and results for the bladder and rectum for the proton arc therapy treatment plans with varying margin size. The results are shown for the bladder and rectum volumes (including contents) for consistency with traditional DVH constraints. All DVH constraints were met. In general, dose increased with plan index (and margin size) increases.

Volume	Volume Constraint [%]	Max Dose Constraint [Gy(RBE)]	Proton Arc Therapy Dose [Gy(RBE)]						
			Plan 1 (Smallest)	Plan 2	Plan 3	Plan 4	Plan 5	Nominal Plan	Plan 6 (Largest)
Bladder	20	70	7.3	10.7	13.8	15.4	17.2	19.3	20.8
Rectum	60	40	1.7	3.5	6.9	9.1	11.7	14.3	16.8
	50	45	13.2	16.8	19.7	21.0	22.0	23.0	24.3
	40	60	19.4	21.0	24.0	25.6	27.2	28.8	30.4
	20	70	33.6	35.9	42.1	45.7	49.1	53.0	56.1
	15	76	41.5	44.3	51.9	55.8	59.2	63.1	65.9
	5	80	67.7	69.7	73.9	75.4	76.3	77.0	77.5

3.2 Stray Dose Determination

3.2.1 Volumetric Modulated Arc Therapy Stray Dose

The contribution of stray dose (from leakage and scatter photons) for the VMAT treatment plans was estimated by introducing a correction to out-of-field region (outside the 5% isodose surface calculated by the TPS) where the TPS underestimates stray radiation (Howell *et al*

al., 2010a; Howell *et al.*, 2010b). The nominal correction was defined as a 40% increase applied to the out-of-field dose portion differential DVH for the bladder wall and rectal wall. The effect of this stray dose estimation is shown in Table 3.10. The largest impact of the 40% increase on the mean dose was seen in the bladder wall of the medium patient: a difference of 0.43 Gy. Additionally, the lower and upper bounds of the corrected mean dose were found by increasing the out-of-field dose by 20% and 60%, respectively (Howell *et al.*, 2010a; Howell *et al.*, 2010b). Then, the percent error in the corrected mean dose was found by dividing the difference in the upper bound and lower bound mean doses by two, dividing that by the nominally corrected mean dose, and multiplying by 100. The resulting errors in mean dose ranged from 0.1% to 1.3%, depending on the patient and the organ (see last row in Table 3.10). The nominal, corrected differential DVH was used for the risk calculations, described in section 3.3, and the maximum percent error was used in the uncertainty analysis, described in section 3.3.2.

Table 3.10 - Effect of the stray dose estimation method on the mean dose of the bladder wall and rectal wall for each patient. The maximum difference between the nominal corrected value and the uncorrected value was seen in the bladder wall of the medium patient: a difference of 0.43 Gy. The maximum percent error, 1.3%, was used in the uncertainty analysis described in sections 2.4.5 and 3.3.2.

	Small		Medium		Large	
	Bladder Wall	Rectal Wall	Bladder Wall	Rectal Wall	Bladder Wall	Rectal Wall
Mean Dose No Correction (Gy)	22.08	23.82	16.37	23.82	26.93	29.86
Mean Dose Lower Bound (1.2) (Gy)	22.22	23.96	16.58	23.96	27.08	29.90
Mean Dose Nominal (1.4) (Gy)	22.36	24.10	16.80	24.09	27.23	29.94
Mean Dose Upper Bound (1.6) (Gy)	22.51	24.23	17.01	24.23	27.39	29.98
Error in Mean Dose (Gy)	0.14	0.14	0.21	0.14	0.15	0.04
Percent Error in Mean Dose (%)	0.6	0.6	1.3	0.6	0.6	0.1

3.2.2 Proton Arc Therapy Stray Dose

The stray dose from proton arc therapy was calculated using Monte Carlo simulations for the medium patient and estimated from the literature (Fontenot, 2008; Fontenot *et al.*, 2008) for the small and large patients. The calculated and estimated stray doses are listed below in Table 3.11. The stray rectal dose calculated in this work for the medium patient was slightly higher than the estimated dose from the work of Fontenot *et al.*, most likely due to the posterior component of the arc delivery, which was not accounted for in the estimations from the literature. Another difference in the methodology from the work of Fontenot *et al.* is that their values were obtained using 2 cm diameter receptors at the location of the organ in a phantom, where our work used the mean dose calculated from the organ wall DVH.

Table 3.11 - Stray equivalent doses for the bladder and rectum (and therefore the bladder wall and rectal wall) for the small, medium and large patients for the whole proton arc therapy treatment calculated in MCNPX and estimated from Fontenot *et al.* (2008).

Structure	Small Patient Stray Dose [Sv]	Medium Patient Stray Dose [Sv]		Large Patient Stray Dose [Sv]
	Estimated from literature	Estimated from literature	Our MCNPX calculations	Estimate from literature
Bladder	0.82	0.97	0.96	1.06
Rectum	0.61	0.76	1.13	0.88

3.3 Risk Prediction

The predicted risk of SMN incidence following VMAT and proton arc therapy for prostate cancer at the exposed age of 60 years and the attained age of 70 years is presented below. Table 3.12 lists the predicted *ERR* (sum of bladder and rectum) for the nominal treatment plans created for specific aim 1 (uniformly weighted for proton arc therapy), and Figure 3.25 shows a histogram of this data for the medium patient. Additionally, the *RRRs* (ratios of $ERR_{P\ Arc}$ to ERR_{VMAT}), are reported in Table 3.13 and plotted in Figure 3.26. For all risk models, the mean

ERR of all three patients following proton arc therapy was less than that following VMAT, yielding *RRRs* of less than one.

Table 3.12 – Predicted excess relative risk of SMN incidence of the bladder and rectum for the nominal VMAT and proton arc therapy (‘P Arc’) treatment plans for prostate cancer for the linear-no-threshold, linear-exponential, and the linear-plateau risk models for specific aim 1. The linear-exponential and linear-plateau models had inflection points at 10 Sv and 40 Sv. Risk was calculated for the small, medium, and large patients, as well as the mean of the three. This data is shown in histogram form in Figures 3.25 and 3.26.

Patient	Modality	ERR for given risk model				
		LNT	Lexp 10	Lexp 40	Lplat 10	Lplat 40
Small	VMAT	11.40	1.40	4.63	2.07	4.74
	P Arc	11.59	1.02	3.68	1.74	4.31
Medium	VMAT	9.18	1.32	3.74	1.82	3.86
	P Arc	9.71	0.88	3.35	1.49	3.55
Large	VMAT	13.95	1.34	5.18	2.21	5.37
	P Arc	12.61	1.09	4.60	1.93	4.89
Mean	VMAT	11.51	1.35	4.51	2.03	4.66
	P Arc	11.31	1.00	3.88	1.72	4.25

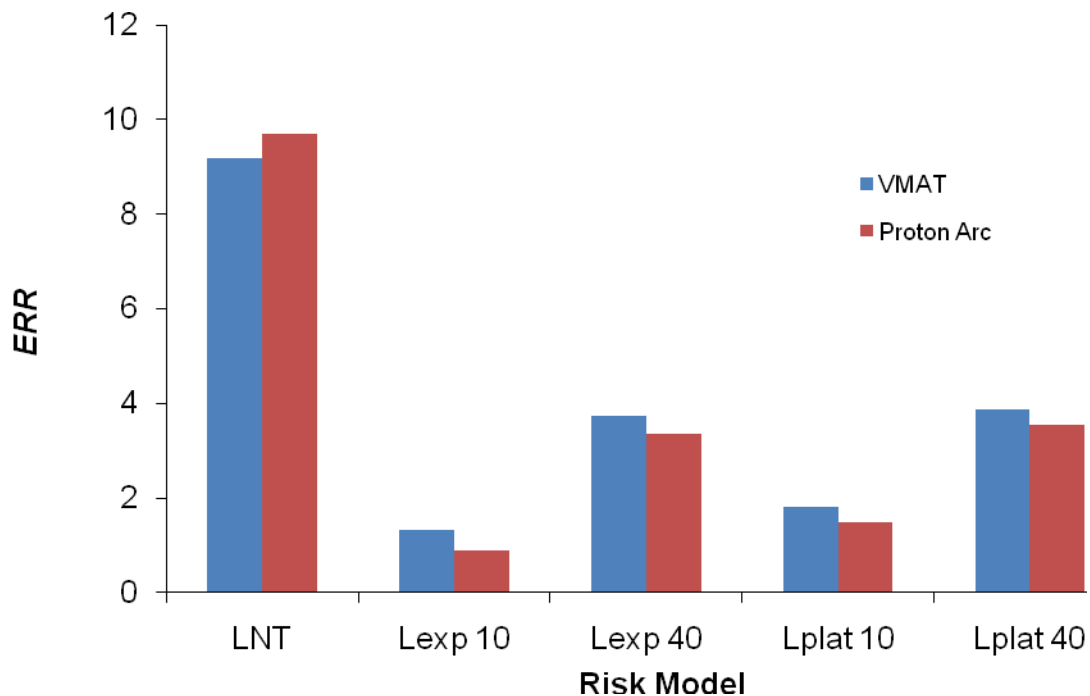


Figure 3.25 - The predicted excess relative risk of SMN incidence in the bladder and rectum for the medium patient following VMAT and uniformly weighted proton arc therapy for the

linear-no-threshold model, linear-exponential model with the inflection point at 10 Sv and 40 Sv, respectively, and the linear-plateau model with the inflection point at 10 Sv and 40 Sv, respectively.

Table 3.13 – The ratio of excess relative risk (*RRR*) following uniformly weighted proton arc therapy relative to the risk following VMAT for specific aim 1. An *RRR* ($ERR_{P\ Arc}/ERR_{VMAT}$) value less than one indicates a lower risk of SMN incidence following proton arc therapy.

Patient	<i>RRR</i> for given risk model				
	LNT	Lexp 10	Lexp 40	Lplat 10	Lplat 40
Small	1.02	0.73	0.79	0.84	0.91
Medium	1.06	0.67	0.90	0.82	0.92
Large	0.90	0.81	0.89	0.87	0.91
Mean	0.99	0.74	0.86	0.84	0.91

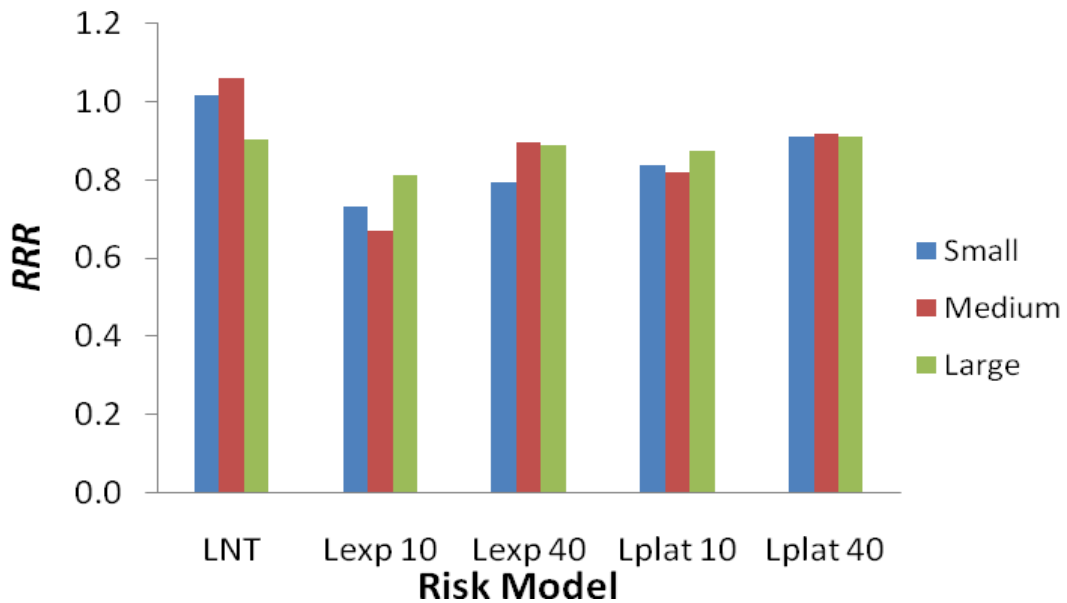


Figure 3.26 – The ratio of excess relative risk of SMN incidence ($ERR_{P\ Arc}/ERR_{VMAT}$) following uniformly weighted proton arc therapy relative to that following VMAT for the small, medium and large patient for the linear-no-threshold model, linear-exponential model with the inflection point at 10 Sv and 40 Sv, respectively, and the linear-plateau model with the inflection point at 10 Sv and 40 Sv, respectively.

For specific aim 2, the risk following proton arc therapy with optimized non-uniform beam weighting was investigated. First, in order for the optimization algorithm to be able to minimize the risk, the risk contributed by each beam angle (or mirrored pair) had to be determined. Table 3.14 and Figure 3.27 show the *ERR* calculated with the LNT model at each beam angle (or

mirrored pair) from therapeutic radiation assuming unit weighting for each. Then, the appropriate relative beam weighting to minimize the risk of SMN incidence of the bladder and rectum, bladder only, and rectum only (Table 3.15) was determined. Additionally, optimal weighting was found to minimize the risk of SMN incidence of the bladder and rectum for the scenario of a patient with a prosthetic hip (Table 3.16). The results of specific aim 2 are summarized and compared to specific aim 1 in Figure 3.28, below.

Table 3.14 - The predicted LNT *ERR* of SMN incidence for the medium patient contributed by each proton beam or beam pair (therapeutic dose only). These reported risks are for each beam (or pair) as if it were 100% of the treatment. The beam angles listed are in degrees and refer to the left (L) and corresponding right (R) mirrored beams, respectively.

Angle L	Angle R	Bladder <i>ERR</i>	Rectum <i>ERR</i>	Total <i>ERR</i>
360		10.30	2.09	12.39
22.5	337.5	9.50	2.14	11.64
45	315	7.32	1.92	9.24
67.5	292.5	5.94	2.30	8.24
90	270	5.37	2.03	7.41
112.5	247.5	5.35	2.95	8.30
135	225	4.70	4.36	9.05
157.5	202.5	4.36	4.67	9.02
180		4.52	4.69	9.20

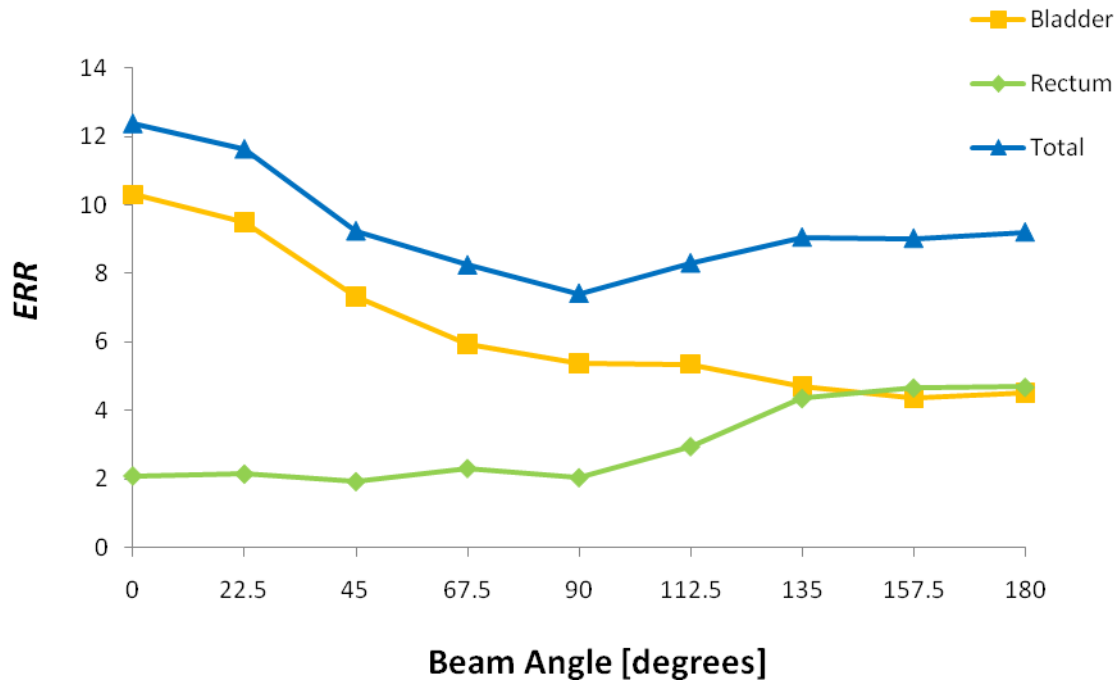


Figure 3.27 - The predicted LNT excess relative risk of SMN incidence for each proton beam or beam pair (therapeutic dose only). These reported risks are for each beam or beam pair normalized as if it were 100% of the treatment. It can be seen that there is a minimum in total risk for the 90 degree and 270 degree beam pair.

Table 3.15 – The non-uniform relative proton beam weights found by the optimization algorithm and the resulting LNT excess relative risk (*ERR*) (risk from stray dose included) for plans optimized to minimize risk of SMN incidence in the bladder and rectum, bladder only, and rectum only for specific aim 2. The third to last row (Sum: ERR_{PARC}) is the total *ERR* for the treatment. The second to last row is the *ERR* following the same (medium) patient’s VMAT treatment plan from specific aim 1 (Table 3.12). The last row (*RRR*) is the ratio of ERR_{PARC} to ERR_{VMAT} .

Angle(s) [Degrees]	Bladder and Rectum		Bladder only		Rectum only	
	Weight [Relative]	Weight*Risk ERR	Weight [Relative]	Weight*Risk ERR	Weight [Relative]	Weight*Risk ERR
360	0	0	0	0	0	0
22.5, 337.5	0	0	0	0	0	0
45, 315	0	0	0	0	1	9.78
67.5, 292.5	0	0	0	0	0	0
90, 270	1	7.97	0	0	0	0
112.5, 247.5	0	0	0	0	0	0
135, 225	0	0	0	0	0	0
157.5, 202.5	0	0	1	9.34	0	0
180	0	0	0	0	0	0
Sum: ERR_{PARC}		7.97		9.34		9.78
ERR_{VMAT}		9.18		9.18		9.18
RRR		0.87		1.02		1.07

Table 3.16 - The non-uniform beam weights found by the optimization algorithm and the resulting LNT risk (*ERR*) (risk from stray dose included) for the two prosthetic hip plans for specific aim 2. The third to last row (Sum: ERR_{PARC}) is the total *ERR* for the treatment. The second to last row is the *ERR* following the same (medium) patient's VMAT treatment plan from specific aim 1 (Table 3.12). The last row (*RRR*) is the ratio of ERR_{PARC} to ERR_{VMAT} .

Angle [Degrees]	Prosthetic Hip Plan 1		Prosthetic Hip Plan 2	
	Weight [Relative]	Weight*Risk ERR	Weight [Relative]	Weight*Risk ERR
360	0	0	0	0
337.5	0	0	0	0
315	0	0	0	0
292.5	0.34	2.91	0	0
270	0.66	5.35	0.66	5.35
247.5	0	0	0	0
225	0	0	0	0
202.5	0	0	0	0
180	0	0	0	0
157.5	0	0	0.34	3.20
135	0	0	0	0
45	0	0	0	0
22.5	0	0	0	0
Sum: ERR_{PARC}		8.26		8.55
ERR_{VMAT}		9.18		9.18
<i>RRR</i>		0.90		0.93

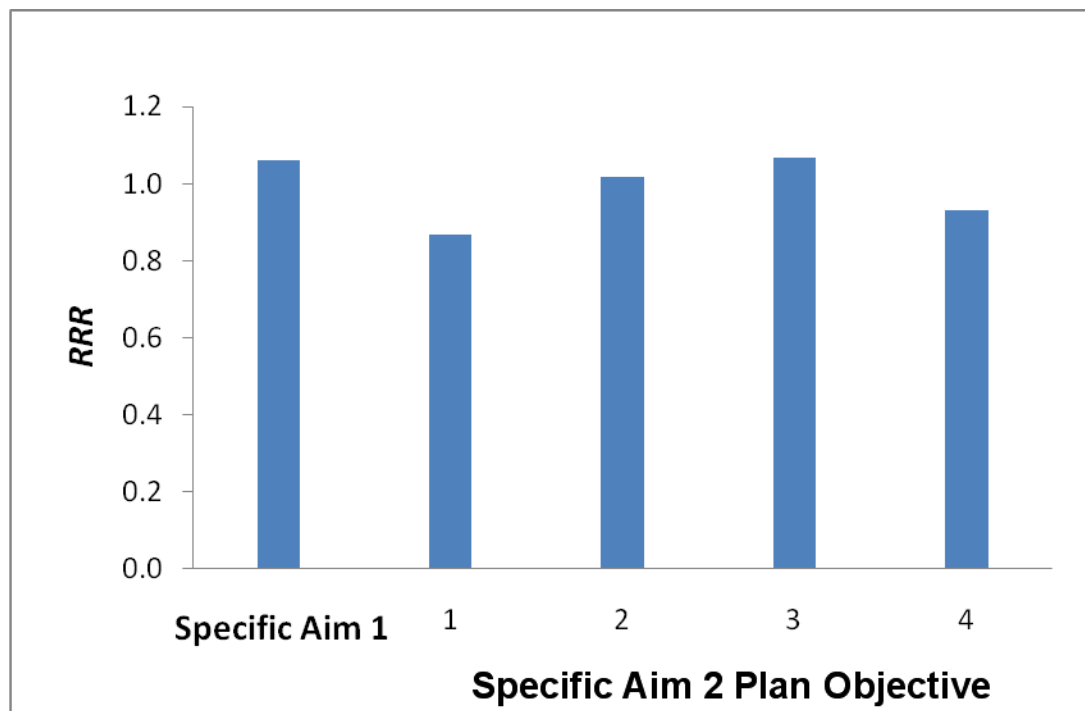


Figure 3.28 – The ratio of excess relative risk (*RRR*) of SMN incidence ($ERR_{P\ Arc}/ERR_{VMAT}$) following proton arc therapy relative to that following VMAT for the medium patient for the linear-no-threshold model. The *RRRs* from the proton arc therapy plans with non-uniform beam weighting optimized for objectives 1, 2, 3 and 4 (Table 2.5) are compared to the *RRR* from uniformly weighted proton arc therapy from specific aim 1

Specific aim 3 was designed to investigate the effect of margin size around the CTV to create the PTV on the predicted risk of SMN incidence following prostate radiotherapies. The predicted risk of SMN incidence in the bladder and rectum following VMAT and uniformly weighted proton arc therapy with varying margins for the medium patient is graphed below in Figures 3.29 through 3.31. First, Figure 3.29 shows the *ERR* of SMN incidence of the bladder, rectum, and the combination of the two organs calculated with the LNT model. It can be seen that the risk of SMN incidence in the bladder is higher than for the rectum and that risk increases as margin size increases for both. Then, the combined *ERR* of SMN incidence in the bladder and rectum for the LNT, linear-exponential, and linear-plateau models for VMAT and proton arc therapy is plotted in Figure 3.30. As expected, the linear-exponential and linear-plateau prediction of *ERR* is less than for LNT. Finally, the *RRR* of SMN (ratio of $ERR_{P\ Arc}$ to ERR_{VMAT}) is plotted in Figure 3.31. The LNT *RRR* is highest, around 1 (range: 1.00 – 1.08), showing little difference between the two modalities and a potential slight advantage for VMAT. The linear-exponential-10 *RRR* yielded the lowest *RRR*, 0.66, showing the largest advantage for proton arc therapy. As seen before in specific aim 1, all alternative risk models indicated an advantage for proton arc therapy with *RRRs* ranging from 0.66 to 0.93. While *ERR* generally increases with increasing margin size (within our bounds of 0 mm to 8 mm), a strong relationship between *RRR* and margin size was not observed.

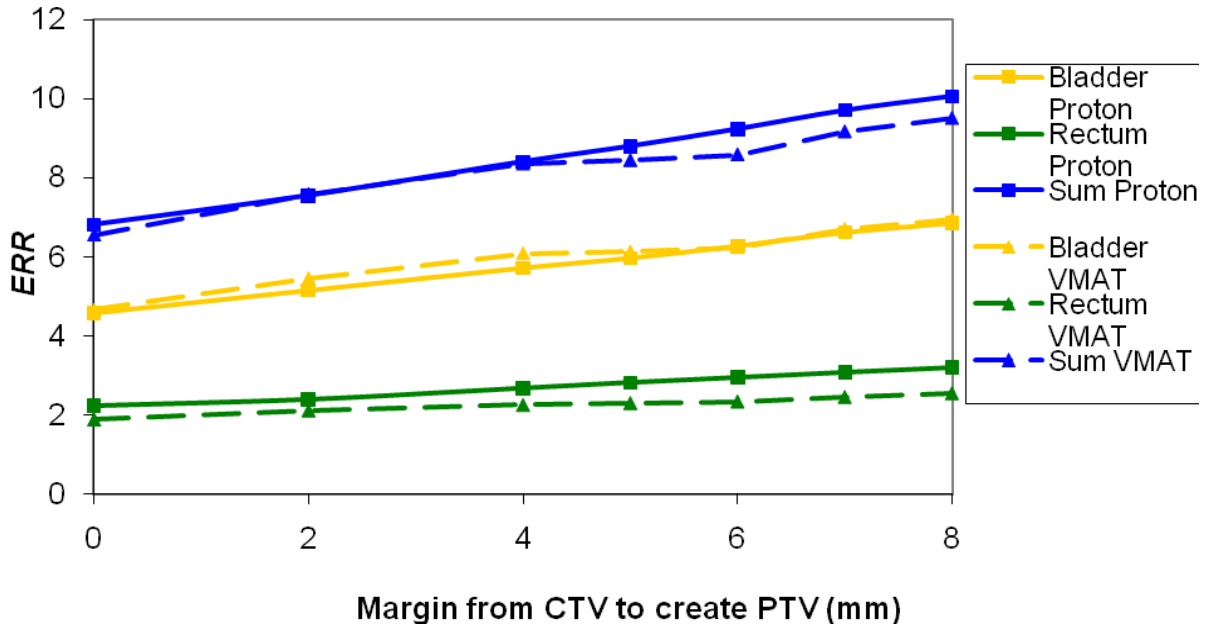


Figure 3.29 – The predicted LNT excess relative risk of SMN incidence of the bladder and rectum and the combination of the two for the medium patient vs. the “else” margin around the CTV to create the PTV for VMAT and uniformly weighted proton arc therapy. The nominal expansion is 7 mm “else.” Posterior margins are 2 mm less than those graphed, except for 0 mm “else” expansion, where the posterior margin is also 0 mm.

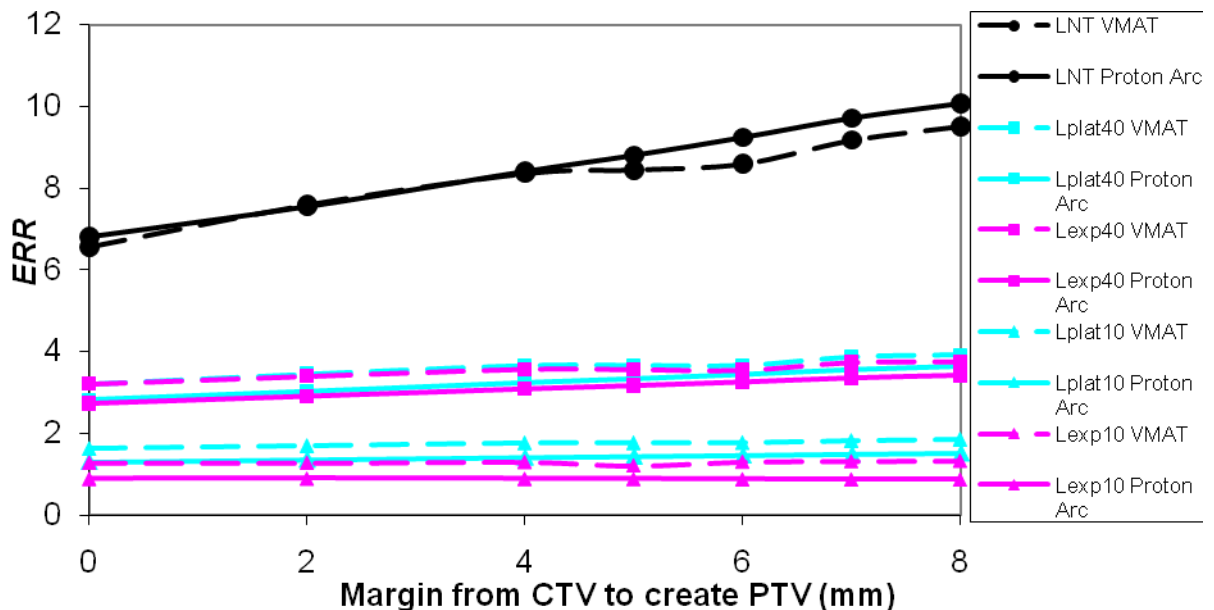


Figure 3.30 – The predicted excess relative risk (*ERR*) of SMN incidence (combined bladder and rectum) for VMAT and uniformly weighted proton arc therapy for the medium patient for the linear-no-threshold model, linear-exponential model, and linear-plateau model vs. the “else” margin around the CTV to create the PTV. The nominal expansion is 7 mm “else.” Posterior

margins are 2 mm less than those graphed, except for 0 mm “else” expansion, where the posterior margin is also 0 mm. The linear-exponential and linear-plateau models have inflection points at 10 Sv and 40 Sv.

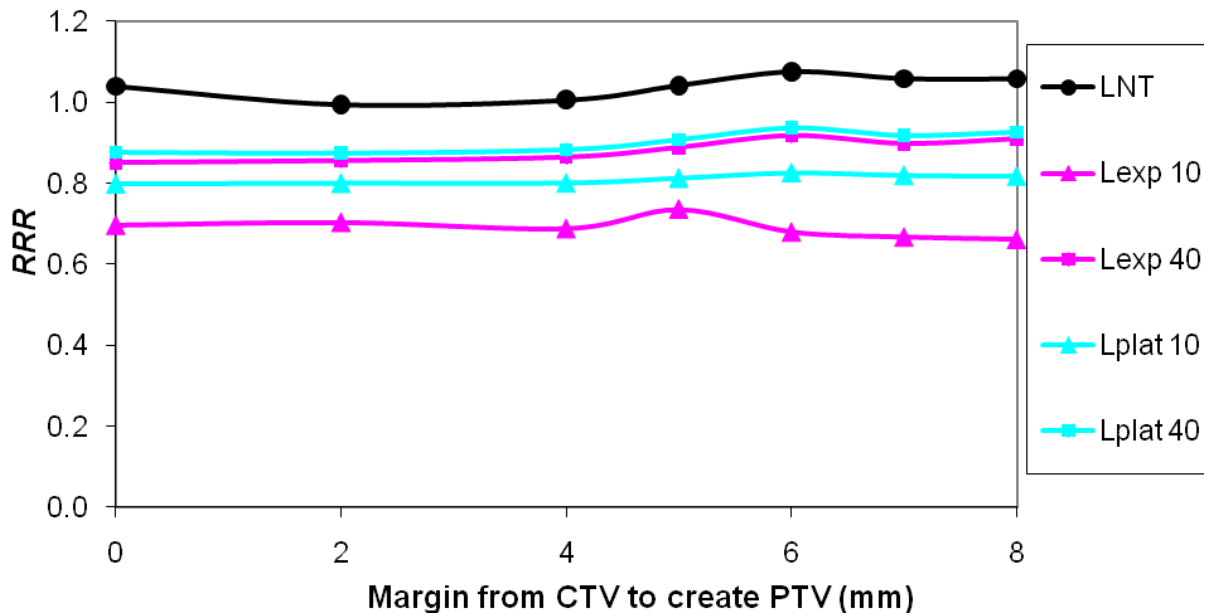


Figure 3.31 – The predicted ratio of excess relative risk (*RRR*) of SMN incidence (combined bladder and rectum) for the medium patient for the linear-no-threshold model, linear-exponential model, and linear-plateau model vs. the “else” margin around the CTV to create the PTV. The nominal expansion is 7 mm “else.” Posterior margins are 2 mm less than those graphed, except for 0 mm “else” expansion, where the posterior margin is also 0 mm. The linear-exponential and linear-plateau models have inflection points at 10 Sv and 40 Sv.

3.3.1 Statistical Analysis

The statistical analysis was performed to test the *RRR* values from specific aim 1 against the value of 1 (small sample size, $n=3$). When the sign test was conducted, the null hypothesis that $P(+)\geq P(-)$ (the probability of $RRR > 1$ being greater than or equal to the probability of $RRR < 1$) was rejected for all alternate risk models, but could not be rejected for the LNT model. Table 3.17 shows the p-values for the sign test for the different risk models, where red indicates a fail ($p > 0.05$; could not reject null hypothesis) and green indicates a pass ($p < 0.05$; rejected null hypothesis).

Table 3.17 - The results of the sign test which compared the *RRR* to 1. Red indicates a fail, where the null hypothesis that the $P(+)\geq P(-)$ cannot be rejected. Green indicates a pass, where the null hypothesis can be rejected, i.e. the *RRR* is significantly less than 1.

Patient	RRR for given risk model				
	LNT	Lexp 10	Lexp 40	Lplat 10	Lplat 40
Small	1.02	0.73	0.79	0.84	0.91
Medium	1.06	0.67	0.90	0.82	0.92
Large	0.90	0.81	0.89	0.87	0.91
Mean	0.99	0.74	0.86	0.84	0.91
sign test p-value	0.28	0.04	0.04	0.04	0.04

The t-test yielded similar results: the null hypothesis that the mean $RRR \geq 1$ was rejected for the alternate risk models, but could not be rejected for the LNT model. Table 3.18 shows the p-values for the t-test for all of the risk models, where red indicates a fail ($p > 0.05$; could not reject null hypothesis) and green indicates a pass ($p < 0.05$; rejected null hypothesis).

Table 3.18 - The results of the t-test which compared the *RRR* to 1. Red indicates a fail, where the null hypothesis that the $RRR \geq 1$ cannot be rejected. Green indicates a pass, where the null hypothesis can be rejected, i.e. the *RRR* is significantly less than 1.

Patient	RRR for given risk model				
	LNT	Lexp 10	Lexp 40	Lplat 10	Lplat 40
Small	1.02	0.73	0.79	0.84	0.91
Medium	1.06	0.67	0.90	0.82	0.92
Large	0.90	0.81	0.89	0.87	0.91
Mean	0.99	0.74	0.86	0.84	0.91
t-test p-value	0.45	0.012	0.03	0.005	0.0005

3.3.2 Uncertainty Analysis

The uncertainty was estimated using propagation of the uncertainties of the components of the risk calculation (equations 2.16a and 2.16b). The uncertainty in the therapeutic absorbed dose from proton therapy was estimated to be 5% from the work of Giebeler *et al.* (2009). Two uncertainties contributed to the total uncertainty in the corrected VMAT dose: the uncertainty in the TPS VMAT dose (2% (Fontenot, 2008)) and the relative uncertainty in the correction method for VMAT (1.3% (section 3.2.1)). Therefore, the quadrature sum of 2% and 1.3% was

used for the uncertainty in the corrected VMAT dose, $\left(\frac{\sigma_{D_1}}{D_1}\right)_v$. The relative uncertainty in the

neutron dose from statistical fluctuations was found with a quadrature sum of the relative uncertainties of the neutron dose from each beam in the region of the bladder and rectum. The

$\left(\frac{\sigma_{\overline{RRR}}}{\overline{RRR}}\right)_{w_R^-}$ and $\left(\frac{\sigma_{\overline{RRR}}}{\overline{RRR}}\right)_{RM}$ values were determined with sensitivity analysis, for which the results are listed in Tables 3.19 and 3.20, respectively. Then, the covariance term was found to account for the effect of correlations in the data on the uncertainty. In this study, it was a negative term, which reduced the overall uncertainty. The absolute value of the covariance term was found to be 3.5% using equation 2.17 and the last term in equation 2.16. The final uncertainty in the mean *RRR* was asymmetric and calculated to be +1.2% and -22.7%. All uncertainty values are listed in Table 3.20 below.

Table 3.19 – The mean LNT *ERRs* for uniformly weighted proton arc therapy and respective *RRRs*. As a sensitivity test, the mean radiation weighting factor for neutrons was varied by factors ranging from 0.5 to 5. The denominator for the mean *RRR* calculation (last row) is the LNT *ERR* for VMAT for each patient (Table 3.12).

w_R Formula	x0.50	x1	x2	x5
w_R Bladder	3.68	7.36	14.72	36.80
w_R Rectum	3.47	6.94	13.88	34.70
Mean <i>ERR</i>	11.07	11.30	11.77	13.18
Mean <i>RRR</i>	0.97	0.99	1.03	1.16

Table 3.20 – Assumed and calculated relative uncertainties for the error propagation and the resulting total uncertainty (equations 2.16a and b). The total uncertainties (positive and negative) are also reported in absolute terms of *RRR* (in parentheses). One σ corresponds to the 68% confidence interval.

Term	Description	Value [%]
$\left(\frac{\sigma_{D_1}}{D_1}\right)_P$	Uncertainty in therapeutic absorbed dose from proton arc therapy (TPS)	5.0
$\left(\frac{\sigma_{D_1}}{D_1}\right)_V$	Uncertainty in dose from VMAT (corrected TPS: see section 3.2.1)	2.4
$\left(\frac{\sigma_{D_2}}{D_2}\right)_P$	Statistical uncertainty in stray absorbed dose from proton arc therapy (Monte Carlo)	< 1.0

$\left(\frac{\sigma_{\overline{RRR}}}{\overline{RRR}}\right)_{w_R}$	Uncertainty contributed from $\overline{w_R}$	4.7
$\left(\frac{\sigma_{\overline{RRR}}}{\overline{RRR}}\right)_{RM}$	Uncertainty contributed from the risk model	26.2
$-2 \frac{\sigma_{ERR_V ERR_P}}{ERR_V ERR_P}$	Covariance term for VMAT and Proton Arc Therapy	-3.5
$+\left(\frac{\sigma_{\overline{RRR}}}{\overline{RRR}}\right)$	Total positive uncertainty in mean RRR	1.2 (0.01)
$-\left(\frac{\sigma_{\overline{RRR}}}{\overline{RRR}}\right)$	Total negative uncertainty in mean RRR	22.7 (0.22)

In addition, the uncertainty was propagated for each patient individually, which can be seen as the error bars in Figure 3.32.

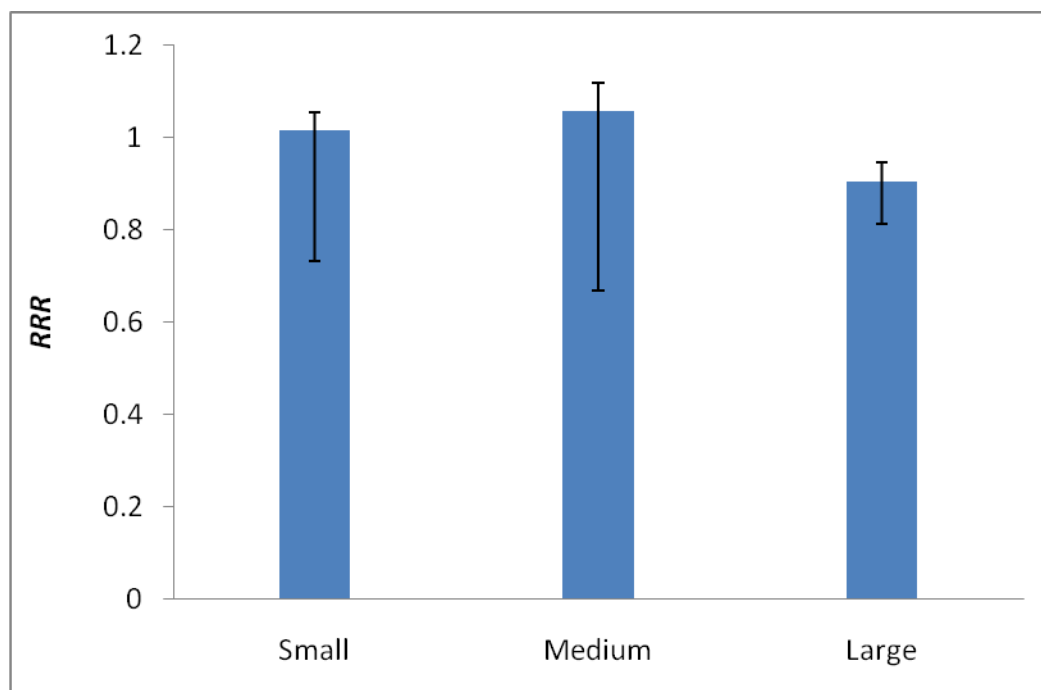


Figure 3.32 – The predicted LNT RRR s for the small, medium and large patients (treatment plans from specific aim 1). The error bars correspond to the uncertainty propagated according to equations 2.18a and 2.18b.

Finally, uncertainty was also propagated for the mean RRR without the term that accounts for uncertainty in $\overline{w_R}$. Then, the mean RRR was plotted vs. $\overline{w_R}$ with error bars that correspond to the uncertainty in all factors except $\overline{w_R}$ (Figure 3.33).

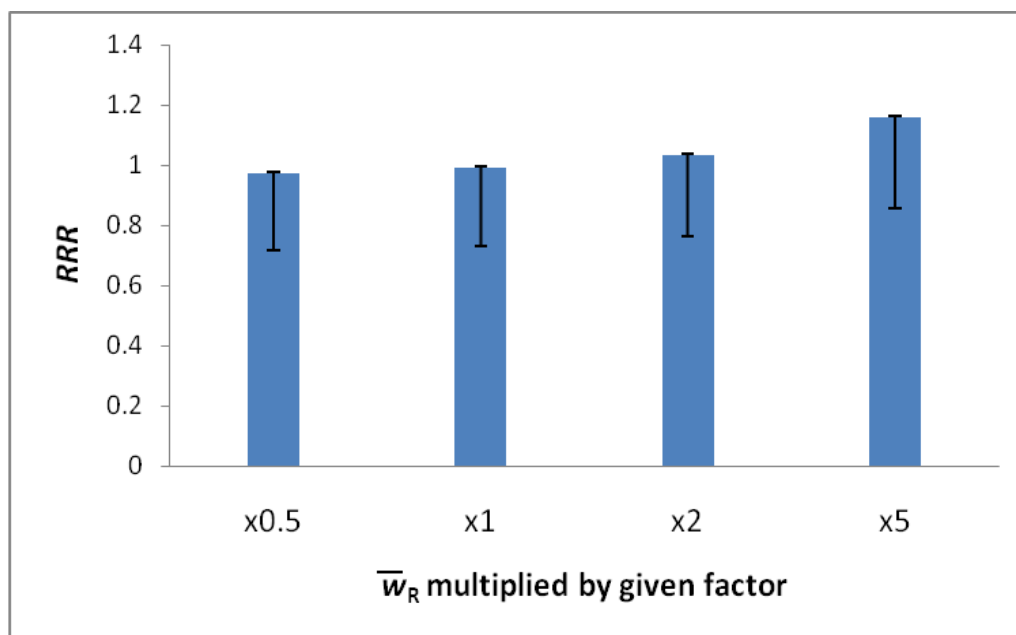


Figure 3.33 – Mean *RRR*s (Table 3.19; treatment plans from specific aim 1) vs. varying \bar{w}_R with error bars that include all uncertainties considered, except those in \bar{w}_R .

Chapter 4

Discussion and Conclusion

This chapter begins with a summary of the outcome of the specific aims (section 4.1) and a comparison with existing literature (section 4.2). Then, the implications and significance (section 4.3), strengths (section 4.4), and limitations (section 4.5) of this work are discussed. Finally, possible future work is mentioned (section 4.6) and the conclusions are stated (section 4.7).

4.1 Outcome of the Specific Aims

4.1.1 Outcome of Specific Aim 1

The goal of specific aim 1 was to predict the *RRR* of SMN incidence of the bladder and rectum following uniformly weighted proton arc therapy relative to that following VMAT using calculated dose distributions and risk models. Specifically, the LNT risk model was used to predict a baseline *RRR*, and the linear-exponential and the linear-plateau risk modes were

applied to estimate the impact on *RRR* from non-linearities in the risk model at high doses. The mean *RRR* for the LNT risk model was 0.99 (+ 0.01 or - 0.22; Table 3.20), which was shown to be not statistically different from 1. The reason for this similarity in LNT risk was that the mean doses to the bladder wall and rectal wall were comparable for both modalities. However, the distribution of the dose was more concentrated for proton arc therapy, which resulted in predicted *RRRs* that were statistically less than 1 for the other risk models. The mean *RRRs* were 0.74, 0.86, 0.84, and 0.91 for the linear-exponential-10 and -40, and linear-plateau-10 and -40 models, respectively. These results are 8% to 25% lower than the *RRR* obtained with the LNT model.

4.1.2 Outcome of Specific Aim 2

The goal of specific aim 2 was to investigate the effect on *RRR* of optimized proton beam weighting. Various host and treatment factors were considered, such as type of second cancer and avoidance of a hip prosthesis on the predicted risk following proton arc therapy. When the sum of LNT risk of SMN incidence in the bladder and rectum was minimized for proton arc therapy, the optimization yielded two lateral arc beams, resulting in an *RRR* of 0.87, compared to the *RRR* of 1.06 for uniformly weighted proton arc therapy. When the LNT risk of SMN incidence in the bladder or rectum alone was minimized, the predicted *RRRs* were 1.02 and 1.07, respectively. Then, the constraint to avoid beams that passed through a prosthetic hip was applied while the risk of SMN incidence in the bladder and rectum combined was minimized, resulting in an *RRR* of 0.93.

The results of this specific aim show that optimized (non-uniform) beam weighting for proton arc therapy can significantly lower the predicted *RRR* of SMN incidence. As expected, the lowest *RRR* was achieved when the combined risk of SMN incidence in the bladder and rectum was minimized for the proton arc therapy plan. Another interesting result from this

specific aim is the optimal beam orientation to minimize risk of SMN incidence for a patient with a contralateral prosthetic hip while sparing the healthy femoral head.

4.1.3 Outcome of Specific Aim 3

The goal of specific aim 3 was to examine the sensitivity of the predicted risk of SMN incidence on the size of the expansion margin around the CTV following both proton arc therapy and VMAT. Using the LNT model, the *ERR* was found to vary between 6.83 and 10.07 for proton arc therapy and 6.55 and 9.52 for VMAT, where risk increased with increasing margin size. The lowest *ERR* of SMN incidence was for the linear-exponential-10 model, which was found to vary between 0.88 and 0.90 for proton arc therapy and 1.28 and 1.32 for VMAT. In general, the *ERR* values calculated with the linear-exponential and linear-plateau risk models were less sensitive to margin size. Moreover, the *RRR* of SMN incidence was virtually independent of margin size for all risk models, with an average of 1.04, 0.69, 0.88, 0.81 and 0.90 for the LNT, linear-exponential-10 and -40, and linear-plateau-10 and -40 models, respectively.

4.2 Comparison with Existing Literature

The study most similar to this work is by Fontenot *et al.* (2009). In their study, the *ERRs* of SMN incidence in the bladder, rectum, and various out-of-field organs were calculated for the same three patients following parallel-opposed beam proton therapy and compared with corresponding *ERRs* following 6 MV IMRT. Additionally, they calculated the *RRR* for the medium patient with the same alternate risk models used in this work. They found the average *RRR* for all three patients to be 0.68 for the LNT model, and the *RRR* for the medium patient to be 0.66, 0.69, 0.69, 0.60, and 0.62 for the LNT, linear-exponential-10 and -40, and linear-plateau-10 and -40 models, respectively. When only the colon and bladder are included in their calculation, the *RRR* for the medium patient becomes 0.65, 0.62, 0.64, 0.57, and 0.59 for the LNT, linear-exponential-10 and -40, and linear-plateau-10 and -40 models, respectively.

The largest numerical difference between *RRR* predictions from the work of Fontenot *et al.* and this work was for the case of the LNT model: 0.66 vs. 1.06, respectively. An obvious source of this difference is that Fontenot *et al.* studied static-beam therapies, where we considered arc therapies. In our study, we found the *ERR* for equally-weighted 360 degree proton arc therapy to be considerably higher than for parallel-opposed beam proton therapy: 11.51 vs. 7.97. This lower value for parallel-opposed beams compares fairly well to the *ERR* reported by Fontenot *et al.* for the bladder and colon of 6.24; however, there are other subtleties that account for the remaining discrepancy. First, Fontenot *et al.* used the whole organ volume (including contents), while we used the organ wall (excluding contents). We showed that this can have a significant impact on the mean organ dose, and therefore the LNT *ERR*. For example, in our study, the mean doses (therapeutic radiation only) to the bladder (and contents) and bladder wall from a parallel-opposed beam treatment were 9.34 Gy (RBE) and 13.40 Gy (RBE), respectively. Second, the mean dose to the target was slightly lower in the study by Fontenot *et al.* When their treatment plan was normalized to the same mean target dose as prescribed in our study, their mean doses to the bladder and bladder wall were 9.19 Gy (RBE) and 13.16 Gy (RBE), respectively, which agree very well with those from our study (listed above). To illustrate how this affects the risk, a table of the LNT *ERR* of SMN incidence in the bladder (and contents), bladder wall, rectum (and contents), and rectal wall from therapeutic dose is shown below (Table 4.1) for the two studies (normalized to the same target dose).

Table 4.1 - The therapeutic dose component of *ERR* for the treatment plans in this study (LR) and the study by Fontenot *et al.* (2009) (JF) calculated with the LNT model for the bladder (and contents), bladder wall, rectum (and contents), and rectal wall. Note the increase in risk when the organ walls were used instead of the whole organ. For the proton plans (last three columns) ‘2 beam’ refers to a parallel-opposed proton beam treatment for prostate (accomplished with weighting for the proton arc plan), where ‘Uniform’ refers to the 360 degree, uniformly weighted proton arc treatment plan. While the ‘2 beam’ proton plans have comparable risk, the ‘Uniform’ proton arc treatment plan has higher risk.

LNT ERR of SMN Following Radiotherapy (Therapeutic Radiation Only)					
Organ	IMRT (JF)	VMAT (LR)	Proton (JF) 2 beam	Proton Arc (LR) 2 beam	Proton Arc (LR) Uniform
Bladder	8.88	5.25	3.68	3.74	4.86
Bladder Wall	10.44	6.55	5.26	5.38	6.24
Rectum	3.32	2.09	2.01	1.76	2.74
Rectal Wall	3.43	2.43	2.19	2.03	2.97

Therefore, when differences in planning technique (arc plans vs. static beam plans, prescription dose) and volume contouring (wall volumes vs. whole organ volumes including contents) are considered, our results agree well with those from Fontenot *et al.*

Schneider *et al.* (2007) also published a study that is relevant to this work. In their study, the whole-body secondary cancer risk of spot-scanned proton radiotherapy relative to 6 MV IMRT was found to be 0.49, 0.50, and 0.51 for the LNT, linear-exponential, and linear-plateau models, respectively. Because of the spot-scanning delivery, dose from external neutrons was minor, in contrast to our work, where it comprises approximately one third of the neutron dose. However, the contribution of external neutron dose to the total *risk* was minimal: approximately 2%. Another difference in their study is that they did not do tissue-specific risk calculations; they estimated risk to a “whole-body” contour. Despite the differences in the methods, our results are remarkably consistent with the results from Schneider *et al.*

This study is not consistent with the work of Dasu *et al.* (2011). They predicted the risk of second cancers in the bladder and rectum following 3DCRT of the prostate for “narrow” margins (4 mm in the posterior direction, 6 mm in other directions) and “wide” margins (10 mm in the posterior direction, 15 mm in other directions) around the CTV. They predicted risk using a model based on the single-dose competition model proposed by UNSCEAR (1993), which is similar to the linear-exponential model in our work. They found that the risk decreased with larger margins, whereas we found that risk either remained approximately constant

(linear-exponential-10) or increased slightly (linear-exponential-40) with margin size (Figure 3.30). However, there are a few major differences in our studies. First, the risk model used by Dasu *et al.* peaks at about 4 Gy, where ours peaked at either 10 or 40 Gy (Gy is equivalent to Sv for photons). Second, the distribution of dose for 3DCRT treatment plans could be significantly different from the distribution of dose for our VMAT and proton arc therapy treatment plans. Finally, the “wide” margins used in their work were considerably larger than the largest margins investigated in our work (10 mm vs. 6 mm in the posterior direction, and 15 mm vs. 8 mm in other directions, respectively). It is possible that these differences account for the discrepancy in the results between the two studies.

4.3 Implications and Significance of this Study

Due to the large population of patients who receive prostate radiotherapy, even a small increase or decrease in risk of cancer due to radiation exposure could have a significant impact on public health. Therefore, risk of SMN incidence following treatment should be considered, along with many factors, in the clinical and policy decision making. The significance of this work is that it characterizes the risk of SMN incidence following two types of radiotherapy for prostate cancer: VMAT and proton arc therapy.

Previous to this work, the risks of SMNs following radiation arc therapies using VMAT and proton arc therapy were unknown. In this work, the *ERR* and *RRR* for the two modalities were characterized for the two modalities for a variety of host and treatment factors: patient size, proton arc therapy beam weighting, mean neutron radiation weighting factor, risk model, and margin size.

Another finding of this work was the ideal proton beam arrangement to minimize the risk of SMN in the bladder and rectum for a patient with a prosthetic hip. It is possible that this finding could be one factor in the choice of beam angles for such patients.

In addition, this study found that two lateral-opposed proton beams is the ideal arrangement to minimize the risk of second cancers of the bladder and rectum following prostate radiotherapy. This result is encouraging in regard to statically delivered proton therapy, because it strengthens the rationale for the beam arrangement in the current standard-of-care used for treating for prostate cancer. However, it is something that should be taken into consideration in the development of proton arc therapy. Therefore, an implication of this finding is that it would be advantageous for a proton arc therapy machine, which has been proposed but not yet built, to have the capability to deliver this type of lateral-opposed treatment, e.g. static or near-static beam delivery capacity.

4.4 Strengths of this Study

This study has several noteworthy strengths. First, to our knowledge, this was the first study to explicitly and algorithmically minimize the risk of second cancer by varying proton beam weights. Others have investigated minimizing risk through choice of treatment modality (Miralbell *et al.*, 2002; Mu *et al.*, 2005; Schneider *et al.*, 2006; Fontenot *et al.*, 2009; Newhauser *et al.*, 2009a; Bednarz *et al.*, 2010) or optimizing treatment plans for uncertainties (Pflugfelder *et al.*, 2008; Unkelbach *et al.*, 2009) or RBE (Wilkens and Oelfke, 2005), but this was the first study to specifically optimize treatment plans to minimize the risk of second cancers. This method could be expanded upon and applied to other treatment sites. In the future, minimizing a patient's risk for developing a second cancer could be one of the many factors in personalized cancer radiotherapy.

Additionally, our study was the first to estimate the risk of SMN incidence following VMAT for prostate cancer. Surprisingly, we found the risk of SMN in the bladder and rectum following VMAT to be lower than following IMRT. This result is of particular interest due to the recent expansion of VMAT and because of the ubiquity of photon-based external beam radiotherapy for prostate cancer.

Another strength of this study was the level of detail of the dose determination and risk estimation. Differential DVHs were exported from the TPS for the bladder and rectum, excluding the contents, and stray dose was estimated or calculated where possible. Then, age-, sex-, and organ-specific parameters were obtained from BEIR VII, used to estimate the LNT risk, and modulated to model cell sterilization with the linear-exponential and linear-plateau risk models.

Finally, the uncertainty analysis was a strength of this work. Other similar works mention the uncertainties associated with risk predictions (Kry *et al.*, 2005a; Schneider *et al.*, 2007; Bednarz *et al.*, 2010) but did not report a full uncertainty propagation. In this work, we extended and adapted the uncertainty analysis of Fontenot *et al.* (2008; 2010) and included uncertainties in the dose (both therapeutic and stray), the neutron radiation weighting factor, and the risk model.

4.5 Limitations of this Study

There are several limitations of this study. First, only the risk of SMNs of the bladder and rectum were considered. This is not a serious limitation, however, because doses to the bladder and rectum account for the vast majority of the risk (Fontenot *et al.*, 2009); the risks of SMN incidence in the bone marrow, skin, and out-of-field organs, which were not included in this study, are of lesser importance.

Moreover, the metric used in this work to express risk of SMN, *ERR*, has limitations of its own. *ERR* is an instantaneous quantity, describing the excess relative risk at a given point in time. In this work, the *ERR* at 10 years post-treatment was chosen as a meaningful surrogate for the lifetime *ERR* for the purposes of estimating *RRR*, giving the typical age of prostate cancer patients. Therefore, this is not a major limitation of this work.

Additionally, only three patients were studied in this work. While a strong dependence on patient-specific differences (patient size, internal anatomy) was not observed in this work, the

sample size was small. Studying a larger patient population would elucidate the dosimetric impact of inter-patient anatomical differences, and might make it possible to see a larger, statistically significant difference in the predicted mean *RRR* value.

Another limitation of this study was that risk-optimized treatment planning was not explicitly available for VMAT. However, the inverse planning method used for all of the VMAT treatment plans was conceptually and functionally similar to the risk-optimized planning method utilized for the proton arc therapy treatment plans for specific aim 2. Both optimization methods minimized the dose to organs of interest: e.g. the bladder and/or rectum. The VMAT inverse planning system accomplished this with a cost function that was based on DVH objectives and constraints for the organs of interest. The risk-minimized proton arc therapy treatment planning method also minimized dose to the bladder and rectum with a cost function, which was based on mean organ dose. Because of these similarities, we believe that the comparison between the modalities was reasonable. For future work, it would be interesting to investigate risk-optimized planning for VMAT.

Furthermore, range compensators were used to create distal conformity for the proton arc treatment plans in this study. If this technique was implemented using passive scattering, different range compensators could not be used for each beam. Either one generic range compensator could be used, or none at all. However, the goal of this study was to investigate the risk of SMN incidence following proton arc therapy in general, not to address all of the design challenges of implementing proton arc therapy on a passively scattered system. Additionally, if scanned beam delivery was used for proton arc therapy, which has its own engineering challenges, range compensators would not be necessary for distal conformity.

The final noteworthy limitation is that variations in the dose distribution (beyond those observed in our sample) were not considered in the uncertainty analysis of *RRR*. The dose distribution for both modalities could be affected by uncertainty in the beam calibration, setup

errors, varying field size, and differences in anatomy. In particular, the dose distribution for proton arc therapy could also be affected by the beam range, SOBPs width, and the air gap.

4.6 Future Work

Treatment-specific measurements to validate the stray dose that was estimated and simulated for this work would lend additional confidence to their accuracy. Due to the difficulty of detecting high-energy neutrons, the stray dose from proton arc therapy would have to be measured with a special detector like an extended Bonner Sphere system (Howell, 2009) or a WENDI-II (Olsher and McLean, 2008). Additionally, stray dose from VMAT has not been explicitly characterized. Even though extensive stray dose measurements have been made for IMRT (Kry *et al.*, 2005b; Howell *et al.*, 2006), verifying that the stray doses between the two modalities are equivalent would be valuable.

This work focused on SMNs of the bladder and rectum. For a more complete representation of the risk of SMN incidence following radiotherapy, the risk calculations could be expanded to include bone marrow, skin, and other out-of-field organs. However, the BEIR VII report does not include specific risk prediction information for skin, and excludes non-melanoma skin cancers. Therefore, another reference would be required for the inclusion of skin, for example, Publication 60 of the ICRP (1991). Also, our patient CT datasets did not span the entire body, so additional whole-body phantoms would be necessary for the Monte Carlo simulations.

Finally, this work could be expanded to other treatment sites and patient populations. A different treatment location yields different doses to organs, thus producing a different risk profile. A different patient population would have a different risk of second cancer based on age at exposure and life expectancy. For example, children treated with radiation have an increased risk of cancer due to increased radiosensitivity (ICRP, 1991) and the potential for a longer life expectancy post treatment. Because of these factors, it would be particularly

meaningful to study and minimize the predicted risk of second cancers following radiotherapy for pediatric patients.

4.7 Conclusions

Proton arc therapy significantly reduces the predicted risk of incidence of radiogenic second malignant neoplasms (SMNs) in the bladder and rectum following prostate radiotherapy compared to VMAT when predicted with the linear-exponential and linear-plateau risk models. On the other hand, no significant difference was seen between the modalities when the risk was predicted with the linear-no-threshold (LNT) model. When the beam weighting for proton arc therapy was optimized to minimize the LNT risk of SMN incidence, a reduction of risk was observed compared to VMAT: *RRR* was reduced from 1.06 to 0.87. Additionally, it was found that while excess relative risk (*ERR*) of SMN incidence increased with PTV margin size for both modalities, the ratio of excess relative risk (*RRR*) between the two modalities was virtually independent of margin size.

Bibliography

- Agosteo S, Birattari C, Caravaggio M, Silari M and Tosi G 1998 Secondary neutron and photon dose in proton therapy *Radiother Oncol* **48** 293-305
- Aspradakis M M, Morrison R H, Richmond N D and Steele A 2003 Experimental verification of convolution/superposition photon dose calculations for radiotherapy treatment planning *Phys Med Biol* **48** 2873-93
- Bedford J L and Warrington A P 2009 Commissioning of volumetric modulated arc therapy (VMAT) *Int J Radiat Oncol Biol Phys* **73** 537-45
- Bednarz B, Athar B and Xu X G 2010 A comparative study on the risk of second primary cancers in out-of-field organs associated with radiotherapy of localized prostate

carcinoma using Monte Carlo-based accelerator and patient models *Med Phys* **37** 1987-94

Bednarz B, Hancox C and Xu X G 2009 Calculated organ doses from selected prostate treatment plans using Monte Carlo simulations and an anatomically realistic computational phantom *Phys Med Biol* **54** 5271-86

Bhatti P, Veiga L H S, Ronckers C c M, Sigurdson A J, Stovall M, Smith S A, Weathers R, Leisenring W, Mertens A C, Hammond S, Friedman D L, Neglia J P, Meadows A T, Donaldson S S, Sklar C A, Robison L L and Inskip P D 2010 Risk of Second Primary Thyroid Cancer after Radiotherapy for a Childhood Cancer in a Large Cohort Study: An Update from the Childhood Cancer Survivor Study *Radiation Research* **174** 741-52

Boice J D, Jr., Engholm G, Kleinerman R A, Blettner M, Stovall M, Lisco H, Moloney W C, Austin D F, Bosch A, Cookfair D L and et al. 1988 Radiation dose and second cancer risk in patients treated for cancer of the cervix *Radiat Res* **116** 3-55

Bortfeld T 2006 IMRT: a review and preview *Phys Med Biol* **51** R363-79

Brahme A, Lind B and Nafstadius P 1987 Radiotherapeutic computed tomography with scanned photon beams *Int J Radiat Oncol Biol Phys* **13** 95-101

Brenner D J, Curtis R E, Hall E J and Ron E 2000 Second malignancies in prostate carcinoma patients after radiotherapy compared with surgery *Cancer* **88** 398-406

Brenner D J and Hall E J 2008 Secondary neutrons in clinical proton radiotherapy: A charged issue *Radiotherapy and Oncology* **86** 165-70

Bues M, Newhauser W D, Titt U and Smith A R 2005 Therapeutic step and shoot proton beam spot-scanning with a multi-leaf collimator: a Monte Carlo study *Radiat Prot Dosimetry* **115** 164-9

- Bzdusek K, Friberger H, Eriksson K, Hardemark B, Robinson D and Kaus M 2009
Development and evaluation of an efficient approach to volumetric arc therapy planning
Med Phys **36** 2328-39
- Caporaso G J, Mackie T R, Sampayan S, Chen Y J, Blackfield D, Harris J, Hawkins S, Holmes
C, Nelson S, Paul A, Poole B, Rhodes M, Sanders D, Sullivan J, Wang L, Watson J,
Reckwerdt P J, Schmidt R, Pearson D, Flynn R W, Matthews D and Purdy J 2008 A
compact linac for intensity modulated proton therapy based on a dielectric wall
accelerator *Phys Med* **24** 98-101
- Carol M 1994 Integrated 3-D conformal multivane intensity modulation delivery system for
radiotherapy. *Proceedings of the 11th International Conference on the Use of
Computers in Radiation Therapy, Madison WI*
- Carol M 1995 Integrated 3D conformal planning/multivane intensity modulating delivery
system for radiotherapy. *In: 3D radiation treatment planning and conformal therapy.
Purdy, Emami, editors. Medical Physics Publishing* 435-45
- Carol M, Grant W H, 3rd, Bleier A R, Kania A A, Targovnik H S, Butler E B and Woo S W
1996 The field-matching problem as it applies to the peacock three dimensional
conformal system for intensity modulation *Int J Radiat Oncol Biol Phys* **34** 183-7
- Chen Y J, Guethlein, G, Caporaso, G, et al. 2009 Compact proton injector and first accelerator
system test for compact proton dielectric wall cancer therapy accelerator *Proc of
PAC09, Vancouver, BC, Canada* **TU6PFP094**
- Chrouser K, Leibovich B, Bergstralh E, Zincke H and Blute M 2005 Bladder cancer risk
following primary and adjuvant external beam radiation for prostate cancer *J Urol* **174**
107-10; discussion 10-1
- Chu W T, Ludewigt, B A, Renner, T R 1993 Instrumentation for treatment of cancer using
proton and light-ion beams *Rev. Sci. Instrum.* **64**

- Chui C S, Chan M F, Yorke E, Spirou S and Ling C C 2001 Delivery of intensity-modulated radiation therapy with a conventional multileaf collimator: comparison of dynamic and segmental methods *Med Phys* **28** 2441-9
- Clasie B, Wroe A, Kooy H, Depauw N, Flanz J, Paganetti H and Rosenfeld A 2010 Assessment of out-of-field absorbed dose and equivalent dose in proton fields *Med Phys* **37** 311-21
- Conover W J 1980 Practicle Nonparametric Statistics: Second Edition *Wiley series in probability and mathematical statistics. John Wiley and Sons, Inc* ISBN: 0-471-02867-3
- Culver D H, Horan T C, Gaynes R P, Martone W J, Jarvis W R, Emori T G, Banerjee S N, Edwards J R, Tolson J S, Henderson T S and et al. 1991 Surgical wound infection rates by wound class, operative procedure, and patient risk index. National Nosocomial Infections Surveillance System *Am J Med* **91** 152S-7S
- Curtis R, Freedman D and Ron E 2006 New malignancies among cancer survivors: SEER cancer registries, 1973-2000. *NIH publication* **05-5302** Bethesda, National Cancer Institute
- D'Amico A V, Whittington R, Malkowicz S B, Schultz D, Blank K, Broderick G A, Tomaszewski J E, Renshaw A A, Kaplan I, Beard C J and Wein A 1998 Biochemical outcome after radical prostatectomy, external beam radiation therapy, or interstitial radiation therapy for clinically localized prostate cancer *JAMA* **280** 969-74
- Dasu A and Toma-Dasu I 2005 Dose-effect models for risk-relationship to cell survival parameters *Acta Oncol* **44** 829-35
- Dasu A, Toma-Dasu I, Franzen L, Widmark A and Nilsson P 2011 Secondary malignancies from prostate cancer radiation treatment: a risk analysis of the influence of target margins and fractionation patterns *Int J Radiat Oncol Biol Phys* **79** 738-46
- Deasy J O, Mackie T R, DeLuca P M 1997 Method and Apparatus for Proton Therapy *United States Patent* **US005668371A**

- Flynn R T, Barbee D L, Mackie T R and Jeraj R 2007 Comparison of intensity modulated x-ray therapy and intensity modulated proton therapy for selective subvolume boosting: a phantom study *Phys Med Biol* **52** 6073-91
- Fontenot J 2008 Proton Therapy Versus Intensity Modulated X-ray Therapy in the Treatment of Prostate Cancer: Estimating Secondary Cancer Risks *Ph.D. Dissertation for The University of Texas Health Science Center at Houston Graduate School of Biomedical Sciences*
- Fontenot J, Newhauser W and Titt U 2005a Design Tools for Proton Therapy Nozzles based on the Double-Scattering Technique *Radiat. Prot. Dosim.* **116** 211-5
- Fontenot J, Taddei P, Zheng Y, Mirkovic D, Jordan T and Newhauser W 2008 Equivalent dose and effective dose from stray radiation during passively scattered proton radiotherapy for prostate cancer *Phys Med Biol* **53** 1677-88
- Fontenot J D, Bloch C, Followill D, Titt U and Newhauser W D 2010 Estimate of the uncertainties in the relative risk of secondary malignant neoplasms following proton therapy and intensity-modulated photon therapy *Phys Med Biol* **55** 6987-98
- Fontenot J D, Lee A K and Newhauser W D 2009 Risk of secondary malignant neoplasms from proton therapy and intensity-modulated x-ray therapy for early-stage prostate cancer *Int J Radiat Oncol Biol Phys* **74** 616-22
- Fontenot J D, Newhauser W D and Titt U 2005b Design tools for proton therapy nozzles based on the double-scattering foil technique *Radiat Prot Dosimetry* **116** 211-5
- Giebeler A 2009 Patient-specific monitor unit determination for patients receiving proton therapy *Master's Thesis for The University of Texas Health Science Center at Houston Graduate School of Biomedical Sciences*
- Goitein M 1978 Compensation for inhomogeneities in charged particle radiotherapy using computed tomography *Int J Radiat Oncol Biol Phys* **4** 499-508

- Gottschalk B, Koehler A, Sisterson J and Wagner M 1991 The case for passive beam spreading
Proton Radiotherapy Workshop Paul Scherrer Institute
- Gragoudas E S 1986 Proton beam therapy of uveal melanomas *Arch Ophthalmol* **104** 349-51
- Hall E J 2006 Intensity-modulated radiation therapy, protons, and the risk of second cancers *Int J Radiat Oncol Biol Phys* **65** 1-7
- Hall E J 2007 The impact of protons on the incidence of second malignancies in radiotherapy
Technol Cancer Res Treat **6** 31-4
- Hall E J and Wu C S 2003 Radiation-induced second cancers: the impact of 3D-CRT and IMRT *Int J Radiat Oncol Biol Phys* **56** 83-8
- Herauld J, Iborra N, Serrano B and Chauvel P 2005 Monte Carlo simulation of a protontherapy platform devoted to ocular melanoma *Med Phys* **32** 910-9
- Howell R M, Burgett, E., Hertel, N. E., Kry S. F., Zhonglu W., Salehpour M. 2009
MEASUREMENT OF HIGH-ENERGY NEUTRON SPECTRA WITH A BONNER
SPHERE EXTENSION SYSTEM *American Nuclear Society*
- Howell R M, Hertel N E, Wang Z, Hutchinson J and Fullerton G D 2006 Calculation of effective dose from measurements of secondary neutron spectra and scattered photon dose from dynamic MLC IMRT for 6 MV, 15 MV, and 18 MV beam energies *Med Phys* **33** 360-8
- Howell R M, Kry S F, Burgett E, Hertel N E and Followill D S 2009 Secondary neutron spectra from modern Varian, Siemens, and Elekta linacs with multileaf collimators *Med Phys* **36** 4027-38
- Howell R M, Scarboro S B, Kry S F and Yaldo D Z 2010a Accuracy of out-of-field dose calculations by a commercial treatment planning system *Phys Med Biol* **55** 6999-7008

Howell R M, Scarboro S B, Taddei P J, Krishnan S, Kry S F and Newhauser W D 2010b

Methodology for determining doses to in-field, out-of-field and partially in-field organs for late effects studies in photon radiotherapy *Phys Med Biol* **55** 7009-23

Huh C H, Bhutani M S, Farfan E B and Bolch W E 2003 Individual variations in mucosa and total wall thickness in the stomach and rectum assessed via endoscopic ultrasound *Physiol Meas* **24** N15-22

ICRP 1991 1990 Recommendations of the International Commission of Radiological Protection *Ann ICRP* **21** 1-201

ICRP 2002 Basic anatomical and physiological data for use in radiological protection: reference values. A report of age- and gender-related differences in the anatomical and physiological characteristics of reference individuals. ICRP Publication 89 *Ann ICRP* **32**

ICRP 2003 Relative biological effectiveness (RBE), quality factor (Q), and radiation weighting factor ($w(R)$). A report of the International Commission on Radiological Protection *Ann ICRP* **33**

ICRU 1999 Report 62 Prescribing, Recording and Reporting Photon Beam Therapy (Supplement to ICRU Report 50) *Journal of the ICRU: International Commission on Radiation Units and Measurements*

ICRU 2007 Report 78 Prescribing, Recording, and Reporting Proton-Beam Therapy *Journal of the ICRU: International Commission on Radiation Units and Measurements* **7**

Inskip P D, Robison L L, Stovall M, Smith S A, Hammond S, Mertens A C, Whitton J A, Diller L, Kenney L, Donaldson S S, Meadows A T and Neglia J P 2009 Radiation dose and breast cancer risk in the childhood cancer survivor study *J Clin Oncol* **27** 3901-7

- Isacsson U, Hagberg H, Johansson K-A, Montelius A, Jung B and Glimelius B 1997 Potential advantages of protons over conventional radiation beams for paraspinal tumours
Radiotherapy and Oncology **45** 63-70
- Jemal A, Siegel R, Xu J and Ward E 2010 Cancer statistics, 2010 *CA Cancer J Clin* **60** 277-300
- Jiang H, Wang B, Xu X G, Suit H D and Paganetti H 2005 Simulation of organ-specific patient effective dose due to secondary neutrons in proton radiation treatment *Phys Med Biol* **50** 4337-53
- Kase K R, Svensson G K, Wolbarst A B and Marks M A 1983 Measurements of dose from secondary radiation outside a treatment field *Int J Radiat Oncol Biol Phys* **9** 1177-83
- Kellerer A M, Ruhm W and Walsh L 2006 Indications of the neutron effect contribution in the solid cancer data of the A-bomb survivors *Health Phys* **90** 554-64
- Kendal W, Eapen L and Nicholas G 2007 Second primary cancers after prostatic irradiation: ensuring an appropriate analysis *Cancer* **109** 164; author reply 5
- Kjaer-Kristoffersen F, Ohlhues L, Medin J and Korreman S 2009 RapidArc volumetric modulated therapy planning for prostate cancer patients *Acta Oncol* **48** 227-32
- Kjellberg R and Kliman B 1973 A system for therapy of pituitary tumors. In. KholerPO, RossGT, eds. *Diagnosis and Treatment of Pituitary Tumors New York: Elsevier* 234-52
- Kjellberg R N, Sweet W H, Preston W M and Koehler A M 1962 The Bragg peak of a proton beam in intracranial therapy of tumors *Trans Am Neurol Assoc* **87** 216-8
- Koehler A M, Schneider R J and Sisterson J M 1975 Range modulators for protons and heavy ions *Nuclear Instruments and Methods* **131** 437-40
- Koehler A M, Schneider R J and Sisterson J M 1977 Flattening of proton dose distributions for large-field radiotherapy *Med Phys* **4** 297-301

- Kry S F, Salehpour M, Followill D S, Stovall M, Kuban D A, White R A and Rosen, II 2005a
The calculated risk of fatal secondary malignancies from intensity-modulated radiation therapy *Int J Radiat Oncol Biol Phys* **62** 1195-203
- Kry S F, Salehpour M, Followill D S, Stovall M, Kuban D A, White R A and Rosen, II 2005b
Out-of-field photon and neutron dose equivalents from step-and-shoot intensity-modulated radiation therapy *Int J Radiat Oncol Biol Phys* **62** 1204-16
- Larsson B, Leksell L and Rexed B 1963 THE USE OF HIGH ENERGY PROTONS FOR CEREBRAL SURGERY IN MAN *Journal Name: Acta Chirurgica Scandinavica (Sweden); Journal Volume: Vol: 125; Other Information: Orig. Receipt Date: 31-DEC-64* Medium: X; Size: Pages: 1-7
- Lawrence J H, Tobias C A, Born J L, Mc C R, Roberts J E, Anger H O, Low-Beer B V and Huggins C B 1958 Pituitary irradiation with high-energy proton beams: a preliminary report *Cancer Res* **18** 121-34
- Lindsay K A, Wheldon E G, Deehan C and Wheldon T E 2001 Radiation carcinogenesis modelling for risk of treatment-related second tumours following radiotherapy *Br J Radiol* **74** 529-36
- Lomax A J 2008 Intensity modulated proton therapy and its sensitivity to treatment uncertainties 2: the potential effects of inter-fraction and inter-field motions *Phys Med Biol* **53** 1043-56
- Longobardi B, De Martin E, Fiorino C, Dell'oca I, Broggi S, Cattaneo G M and Calandrino R 2005 Comparing 3DCRT and inversely optimized IMRT planning for head and neck cancer: equivalence between step-and-shoot and sliding window techniques *Radiother Oncol* **77** 148-56
- Low D A and Mutic S 1997 Abutment region dosimetry for sequential arc IMRT delivery *Phys Med Biol* **42** 1465-70

- Lu H M 2008a A point dose method for in vivo range verification in proton therapy *Phys Med Biol* **53** N415-22
- Lu H M 2008b A potential method for in vivo range verification in proton therapy treatment *Phys Med Biol* **53** 1413-24
- Mackie T, Caporaso G, Sampayan S, Chen Y, Blackfield D, Harris J, Hawkins S, Holmes C, Nelson S, Paul A, Poole B, Rhodes M, Sanders D, Sullivan J, Wang L, Watson J, Reckwerdt P, Schmidt R, Pearson D, Flynn R, Matthews D and Purdy J 2007 TH-C-AUD-09: A Proposal for a Novel Compact Intensity Modulated Proton Therapy System Using a Dielectric Wall Accelerator *Medical Physics* **34** 2628
- Mackie T R 2006 History of tomotherapy *Phys Med Biol* **51** R427-53
- Mackie T R, Balog J, Ruchala K, Shepard D, Aldridge S, Fitchard E, Reckwerdt P, Olivera G, McNutt T and Mehta M 1999 Tomotherapy *Semin Radiat Oncol* **9** 108-17
- Mackie T R, Holmes T, Swerdloff S, Reckwerdt P, Deasy J O, Yang J, Paliwal B and Kinsella T 1993 Tomotherapy: a new concept for the delivery of dynamic conformal radiotherapy *Med Phys* **20** 1709-19
- Manieri C, Carter S S, Romano G, Trucchi A, Valenti M and Tubaro A 1998 The diagnosis of bladder outlet obstruction in men by ultrasound measurement of bladder wall thickness *J Urol* **159** 761-5
- McDonough J and Tinnel B 2007 The University of Pennsylvania/Walter Reed Army Medical Center proton therapy program *Technol Cancer Res Treat* **6** 73-6
- Melancon A D 2010 Range Adaptive Proton Therapy for Prostate Cancer *Ph.D. Dissertation for The University of Texas Health Science Center at Houston Graduate School of Biomedical Sciences*
- Mesoloras G, Sandison G A, Stewart R D, Farr J B and Hsi W C 2006 Neutron scattered dose equivalent to a fetus from proton radiotherapy of the mother *Med Phys* **33** 2479-90

- Mettlin C J, Menck H R, Winchester D P and Murphy G P 1997 A comparison of breast, colorectal, lung, and prostate cancers reported to the National Cancer Data Base and the Surveillance, Epidemiology, and End Results Program *Cancer* **79** 2052-61
- Miralbell R, Lomax A, Cella L and Schneider U 2002 Potential reduction of the incidence of radiation-induced second cancers by using proton beams in the treatment of pediatric tumors *Int J Radiat Oncol Biol Phys* **54** 824-9
- Moon K, Stukenborg G J, Keim J and Theodorescu D 2006 Cancer incidence after localized therapy for prostate cancer *Cancer* **107** 991-8
- Moyers M, Benton E, Ghebremedhin A and Coutrakon G 2008a Leakage and scatter radiation from a double scattering based proton beamline *Medical Physics* **35** 128-44
- Moyers M F, Benton E R, Ghebremedhin A and Coutrakon G 2008b Leakage and scatter radiation from a double scattering based proton beamline *Med Phys* **35** 128-44
- Moyers M F and Miller D W 2003 Range, range modulation, and field radius requirements for proton therapy of prostate cancer *Technol Cancer Res Treat* **2** 445-7
- Moyers M F, Miller D W, Bush D A and Slater J D 2001 Methodologies and tools for proton beam design for lung tumors *Int J Radiat Oncol Biol Phys* **49** 1429-38
- Mu X, Bjork-Eriksson T, Nill S, Oelfke U, Johansson K A, Gagliardi G, Johansson L, Karlsson M and Zackrisson D B 2005 Does electron and proton therapy reduce the risk of radiation induced cancer after spinal irradiation for childhood medulloblastoma? A comparative treatment planning study *Acta Oncol* **44** 554-62
- Munzenrider J E 1999 Proton therapy for uveal melanomas and other eye lesions *Strahlenther Onkol* **175 Suppl 2** 68-73
- Munzenrider J E, Gragoudas E, Verhey L, Goitein M, Koehler A and Suit H D 1980 Radiotherapy of Ocular Melanomas - Precision High-Dose External Beam Proton Therapy *International Journal of Radiation Oncology Biology Physics* **6** 1410-1

- Munzenrider J E and Liebsch N J 1999 Proton therapy for tumors of the skull base *Strahlenther Onkol* **175 Suppl 2** 57-63
- NCRP 1993 (National Council on Radiation Protection and Measurements) Report No. 116 -
Limitation of Exposure to Ionizing Radiation (Bethesda, MD)
- NCRP 2005 National Council on Radiation Protection and Measurements Report No. 151
Structural Shielding Design and Evaluation for Megavoltage X- and Gamma-Ray
Radiotherapy Facilities
- Neugut A I, Ahsan H, Robinson E and Ennis R D 1997 Bladder carcinoma and other second malignancies after radiotherapy for prostate carcinoma *Cancer* **79** 1600-4
- Newhauser W, Fontenot J, Koch N, Dong L, Lee A, Zheng Y, Waters L and Mohan R 2007a
Monte Carlo simulations of the dosimetric impact of radiopaque fiducial markers for
proton radiotherapy of the prostate *Phys Med Biol* **52** 2937-52
- Newhauser W, Fontenot J, Zheng Y, Polf J, Titt U, Koch N, Zhang X and Mohan R 2007b
Monte Carlo simulations for configuring and testing an analytical proton dose-
calculation algorithm *Phys Med Biol* **52** 4569-84
- Newhauser W D, Fontenot J D, Mahajan A, Kornguth D, Stovall M, Zheng Y, Taddei P J,
Mirkovic D, Mohan R, Cox J D and Woo S 2009a The risk of developing a second
cancer after receiving craniospinal proton irradiation *Phys Med Biol* **54** 2277-91
- Newhauser W D, Fontenot J D, Taddei P J, Mirkovic D, Giebeler A, Zhang R, Mahajan A,
Kornguth D, Stovall M, Yepes P, Woo S and Mohan R 2009b Contemporary Proton
Therapy Systems Adequately Protect Patients from Exposure to Stray Radiation *AIP
Conf Proc* **1099** 450-5
- Newhauser W D, Giebeler A, Langen K M, Mirkovic D and Mohan R 2008 Can megavoltage
computed tomography reduce proton range uncertainties in treatment plans for patients
with large metal implants? *Phys Med Biol* **53** 2327-44

- Nihei K, Ogino T, Onozawa M, Murayama S, Fuji H, Murakami M and Hishikawa Y 2010
Multi-Institutional Phase II Study of Proton Beam Therapy for Organ-Confined Prostate
Cancer Focusing on the Incidence of Late Rectal Toxicities *Int J Radiat Oncol Biol
Phys*
- NRC 2006 BEIR-VII Biological Effects of Ionizing Radiation VII Report. Health risks from
exposure to low levels of ionizing radiation. *National Research Council of the National
Academies. Washington D. C.*
- Oelfke U and Bortfeld T 2000 Intensity modulated radiotherapy with charged particle beams:
studies of inverse treatment planning for rotation therapy *Med Phys* **27** 1246-57
- Olsher R H and McLean T D 2008 High-energy response of the PRESCILA and WENDI-II
neutron rem meters *Radiat Prot Dosimetry* **130** 510-3
- Otto K 2008 Volumetric modulated arc therapy: IMRT in a single gantry arc *Med Phys* **35** 310-
7
- Paganetti H, Jiang H, Lee S Y and Kooy H M 2004 Accurate Monte Carlo simulations for
nozzle design, commissioning and quality assurance for a proton radiation therapy
facility *Med Phys* **31** 2107-18
- Palma D, Vollans E, James K, Nakano S, Moiseenko V, Shaffer R, McKenzie M, Morris J and
Otto K 2008 Volumetric modulated arc therapy for delivery of prostate radiotherapy:
comparison with intensity-modulated radiotherapy and three-dimensional conformal
radiotherapy *Int J Radiat Oncol Biol Phys* **72** 996-1001
- Pelowitz D B 2007 MCNPX User's Manual Version 2.6.0 *LA-CP-07*
- Pflugfelder D, Wilkens J J and Oelfke U 2008 Worst case optimization: a method to account
for uncertainties in the optimization of intensity modulated proton therapy *Phys Med
Biol* **53** 1689-700

- Pickles T and Phillips N 2002 The risk of second malignancy in men with prostate cancer treated with or without radiation in British Columbia, 1984-2000 *Radiother Oncol* **65** 145-51
- Polf J C and Newhauser W D 2005 Calculations of neutron dose equivalent exposures from range-modulated proton therapy beams *Phys Med Biol* **50** 3859-73
- Polf J C, Newhauser W D and Titt U 2005 Patient neutron dose equivalent exposures outside of the proton therapy treatment field *Radiat Prot Dosimetry* **115** 154-8
- Preston D L, Ron E, Tokuoka S, Funamoto S, Nishi N, Soda M, Mabuchi K and Kodama K 2007 Solid cancer incidence in atomic bomb survivors: 1958-1998 *Radiat Res* **168** 1-64
- Quinn M and Babb P 2002 Patterns and trends in prostate cancer incidence, survival, prevalence and mortality. Part I: international comparisons *BJU Int* **90** 162-73
- Ramsey C, Seibert R, Mahan S L, Desai D and Chase D 2006 Out-of-field dosimetry measurements for a helical tomotherapy system *J Appl Clin Med Phys* **7** 1-11
- Ron E, Lubin J H, Shore R E, Mabuchi K, Modan B, Pottern L M, Schneider A B, Tucker M A and Boice J D, Jr. 1995 Thyroid cancer after exposure to external radiation: a pooled analysis of seven studies *Radiat Res* **141** 259-77
- Ronckers C M, Sigurdson A J, Stovall M, Smith S A, Mertens A C, Liu Y, Hammond S, Land C E, Neglia J P, Donaldson S S, Meadows A T, Sklar C A, Robison L L and Inskip P D 2006 Thyroid cancer in childhood cancer survivors: a detailed evaluation of radiation dose response and its modifiers *Radiat Res* **166** 618-28
- Rosner B 2006 Fundamentals of Biostatistics: Sixth Edition *Thomson Brooks/Cole* **ISBN-13: 978-0-534-41820-5**
- Ruben J D, Davis S, Evans C, Jones P, Gagliardi F, Haynes M and Hunter A 2008 The effect of intensity-modulated radiotherapy on radiation-induced second malignancies *Int J Radiat Oncol Biol Phys* **70** 1530-6

- Sachs R K and Brenner D J 2005 Solid tumor risks after high doses of ionizing radiation *Proc Natl Acad Sci U S A* **102** 13040-5
- Sandison G A, Papiez E, Bloch C and Morphis J 1997 Phantom assessment of lung dose from proton arc therapy *Int J Radiat Oncol Biol Phys* **38** 891-7
- Schaffner B 2008 Proton dose calculation based on in-air fluence measurements *Phys Med Biol* **53** 1545-62
- Schneider U, Agosteo S, Pedroni E and Besserer J 2002 Secondary neutron dose during proton therapy using spot scanning *Int J Radiat Oncol Biol Phys* **53** 244-51
- Schneider U, Lomax A, Besserer J, Pemler P, Lombriser N and Kaser-Hotz B 2007 The impact of dose escalation on secondary cancer risk after radiotherapy of prostate cancer *Int J Radiat Oncol Biol Phys* **68** 892-7
- Schneider U, Lomax A, Pemler P, Besserer J, Ross D, Lombriser N and Kaser-Hotz B 2006 The impact of IMRT and proton radiotherapy on secondary cancer incidence *Strahlenther Onkol* **182** 647-52
- Schneider U, Zwahlen D, Ross D and Kaser-Hotz B 2005 Estimation of radiation-induced cancer from three-dimensional dose distributions: Concept of organ equivalent dose *Int J Radiat Oncol Biol Phys* **61** 1510-5
- SEER 2007 Surveillance Epidemiology and End Results
- Sengbusch E, Perez-Andujar A, DeLuca P M, Jr. and Mackie T R 2009 Maximum proton kinetic energy and patient-generated neutron fluence considerations in proton beam arc delivery radiation therapy *Med Phys* **36** 364-72
- Sigurdson A J, Ronckers C M, Mertens A C, Stovall M, Smith S A, Liu Y, Berkow R L, Hammond S, Neglia J P, Meadows A T, Sklar C A, Robison L L and Inskip P D 2005 Primary thyroid cancer after a first tumour in childhood (the Childhood Cancer Survivor Study): a nested case-control study *Lancet* **365** 2014-23

- Sisterson J 2005 Ion beam therapy in 2004 *Nuclear Instruments and Methods in Physics Research Section B: Beam Interactions with Materials and Atoms* **241** 713-6
- Slater J D, Rossi C J, Jr., Yonemoto L T, Bush D A, Jabola B R, Levy R P, Grove R I, Preston W and Slater J M 2004 Proton therapy for prostate cancer: the initial Loma Linda University experience *Int J Radiat Oncol Biol Phys* **59** 348-52
- Slopsema R L and Kooy H M 2006 Incorporation of the aperture thickness in proton pencil-beam dose calculations *Phys Med Biol* **51** 5441-53
- Sterzing F, Schubert K, Sroka-Perez G, Kalz J, Debus J and Herfarth K 2008 Helical tomotherapy. Experiences of the first 150 patients in Heidelberg *Strahlenther Onkol* **184** 8-14
- Stovall M, Blackwell C R, Cundiff J, Novack D H, Palta J R, Wagner L K, Webster E W and Shalek R J 1995 Fetal dose from radiotherapy with photon beams: report of AAPM Radiation Therapy Committee Task Group No. 36 *Med Phys* **22** 63-82
- Stovall M, Weathers R, Kasper C, Smith S A, Travis L, Ron E and Kleinerman R 2006 Dose reconstruction for therapeutic and diagnostic radiation exposures: use in epidemiological studies *Radiat Res* **166** 141-57
- Suit H D, Goitein M, Munzenrider J, Verhey L, Davis K R, Koehler A, Linggood R and Ojemann R G 1982 Definitive radiation therapy for chordoma and chondrosarcoma of base of skull and cervical spine *J Neurosurg* **56** 377-85
- Taddei P, Mirkovic D, Fontenot J, Giebeler A, Zheng Y, Titt U, Woo S and Newhauser W 2009a Reducing stray radiation dose for a pediatric patient receiving proton craniospinal irradiation *Nucl Technol* **168** 108-12
- Taddei P J, Chell E, Hansen S, Gertner M and Newhauser W D 2010a Assessment of targeting accuracy of a low-energy stereotactic radiosurgery treatment for age-related macular degeneration *Phys Med Biol* **55** 7037-54

- Taddei P J, Fontenot J D, Zheng Y, Mirkovic D, Lee A K, Titt U and Newhauser W D 2008
Reducing stray radiation dose to patients receiving passively scattered proton
radiotherapy for prostate cancer *Phys Med Biol* **53** 2131-47
- Taddei P J, Howell R M, Krishnan S, Scarboro S B, Mirkovic D and Newhauser W D 2010b
Risk of second malignant neoplasm following proton versus intensity-modulated photon
radiotherapies for hepatocellular carcinoma *Phys Med Biol* **55** 7055-65
- Taddei P J, Mahajan A, Mirkovic D, Zhang R, Giebeler A, Kornguth D, Harvey M, Woo S and
Newhauser W D 2010c Predicted risks of second malignant neoplasm incidence and
mortality due to secondary neutrons in a girl and boy receiving proton craniospinal
irradiation *Phys Med Biol* **55** 7067-80
- Taddei P J, Mirkovic D, Fontenot J D, Giebeler A, Zheng Y, Kornguth D, Mohan R and
Newhauser W D 2009b Stray radiation dose and second cancer risk for a pediatric
patient receiving craniospinal irradiation with proton beams *Phys Med Biol* **54** 2259-75
- Tayama R, Fujita Y, Tadokoro M, Fujimaki H, Sakae T and Terunuma T 2006a Measurement
of neutron dose distribution for a passive scattering nozzle at the Proton Medical
Research Center (PMRC) *Nuclear Instruments and Methods in Physics Research
Section A: Accelerators, Spectrometers, Detectors and Associated Equipment* **564** 532-6
- Tayama R, Fujita Y, Tadokoro M, Fujimaki H, Sakae T and Terunuma T 2006b Measurement
of neutron dose distribution for a passive scattering nozzle at the Proton Medical
Research Center (PMRC) *Nuclear Instruments & Methods in Physics Research Section
a-Accelerators Spectrometers Detectors and Associated Equipment* **564** 532-6
- Taylor J R 1982 An Introduction to Error Analysis: The Study of Uncertainties in Physical
Measurements *University Science Books* ISBN: 0-935702-10-5

- Thompson D E, Mabuchi K, Ron E, Soda M, Tokunaga M, Ochikubo S, Sugimoto S, Ikeda T, Terasaki M, Izumi S and et al. 1994 Cancer incidence in atomic bomb survivors. Part II: Solid tumors, 1958-1987 *Radiat Res* **137** S17-67
- Thompson I, Thrasher, J.B., et al. 2007 Prostate Cancer. Guideline for the Management of Clinically Localized Prostate Cancer: 2007 Update *American Urological Association*
- Titt U, Mirkovic D, Sawakuchi G O, Perles L A, Newhauser W D, Taddei P J and Mohan R 2010 Adjustment of the lateral and longitudinal size of scanned proton beam spots using a pre-absorber to optimize penumbræ and delivery efficiency *Phys Med Biol* **55** 7097-106
- Travis L B, Hill D, Dores G M, Gospodarowicz M, van Leeuwen F E, Holowaty E, Glimelius B, Andersson M, Pukkala E, Lynch C F, Pee D, Smith S A, Van't Veer M B, Joensuu T, Storm H, Stovall M, Boice J D, Jr., Gilbert E and Gail M H 2005 Cumulative absolute breast cancer risk for young women treated for Hodgkin lymphoma *J Natl Cancer Inst* **97** 1428-37
- Travis L B, Hill D A, Dores G M, Gospodarowicz M, van Leeuwen F E, Holowaty E, Glimelius B, Andersson M, Wiklund T, Lynch C F, Van't Veer M B, Glimelius I, Storm H, Pukkala E, Stovall M, Curtis R, Boice J D, Jr. and Gilbert E 2003 Breast cancer following radiotherapy and chemotherapy among young women with Hodgkin disease *JAMA* **290** 465-75
- Trofimov A, Nguyen P L, Coen J J, Doppke K P, Schneider R J, Adams J A, Bortfeld T R, Zietman A L, Delaney T F and Shipley W U 2007 Radiotherapy treatment of early-stage prostate cancer with IMRT and protons: a treatment planning comparison *Int J Radiat Oncol Biol Phys* **69** 444-53

- Unkelbach J, Bortfeld T, Martin B C and Soukup M 2009 Reducing the sensitivity of IMPT treatment plans to setup errors and range uncertainties via probabilistic treatment planning *Med Phys* **36** 149-63
- UNSCEAR 1993 Sources and effects of ionising radiation. 1993 Report of the General Assembly. New York: United Nations
- Urie M, Goitein M, Holley W R and Chen G T 1986 Degradation of the Bragg peak due to inhomogeneities *Phys Med Biol* **31** 1-15
- Urie M, Goitein M and Wagner M 1984 Compensating for heterogeneities in proton radiation therapy *Phys Med Biol* **29** 553-66
- Van Esch A, Tillikainen L, Pyykkonen J, Tenhunen M, Helminen H, Siljamaki S, Alakuijala J, Paiusco M, Lori M and Huyskens D P 2006 Testing of the analytical anisotropic algorithm for photon dose calculation *Med Phys* **33** 4130-48
- Virnig B A, Warren J L, Cooper G S, Klabunde C N, Schussler N and Freeman J 2002 Studying radiation therapy using SEER-Medicare-linked data *Med Care* **40** IV-49-54
- Wagner M S 1982 Automated range compensation for proton therapy *Med Phys* **9** 749-52
- Wang B and Xu X G 2008 Measurements of non-target organ doses using MOSFET dosimeters for selected IMRT and 3D CRT radiation treatment procedures *Radiat Prot Dosimetry* **128** 336-42
- Wang X, Sahoo N, Zhu R X, Zullo J R and Gillin M T 2010 Measurement of neutron dose equivalent and its dependence on beam configuration for a passive scattering proton delivery system *Int J Radiat Oncol Biol Phys* **76** 1563-70
- Waters L S, McKinney G W, Durkee J W, Fensin M L, Hendricks J S, James M R, Johns R C and Pelowitz D B 2007 The MCNPX Monte Carlo Radiation Transport Code *AIP Conference Proceedings* **896** 81-90

- Wijesooriya K, Bartee C, Siebers J V, Vedam S S and Keall P J 2005 Determination of maximum leaf velocity and acceleration of a dynamic multileaf collimator: implications for 4D radiotherapy *Med Phys* **32** 932-41
- Wilkens J J and Oelfke U 2005 Optimization of radiobiological effects in intensity modulated proton therapy *Med Phys* **32** 455-65
- Wilson R R 1946 Radiological use of fast protons *Radiology* **47** 487-91
- Wingate C, Archambeau J, Koehler A and Bennett G 1977 Proton penetration and control in nonhomogeneous phantoms *Med Phys* **4** 198-201
- Wolff D, Stieler F, Welzel G, Lorenz F, Abo-Madyan Y, Mai S, Herskind C, Polednik M, Steil V, Wenz F and Lohr F 2009 Volumetric modulated arc therapy (VMAT) vs. serial tomotherapy, step-and-shoot IMRT and 3D-conformal RT for treatment of prostate cancer *Radiother Oncol* **93** 226-33
- Wroe A, Clasié B, Kooy H, Flanz J, Schulte R and Rosenfeld A 2009 Out-of-field dose equivalents delivered by passively scattered therapeutic proton beams for clinically relevant field configurations *Int J Radiat Oncol Biol Phys* **73** 306-13
- Wroe A, Rosenfeld A and Schulte R 2007 Out-of-field dose equivalents delivered by proton therapy of prostate cancer *Med Phys* **34** 3449-56
- Xia P, Fu K K, Wong G W, Akazawa C and Verhey L J 2000 Comparison of treatment plans involving intensity-modulated radiotherapy for nasopharyngeal carcinoma *Int J Radiat Oncol Biol Phys* **48** 329-37
- Xu X G, Bednarz B and Paganetti H 2008 A review of dosimetry studies on external-beam radiation treatment with respect to second cancer induction *Phys Med Biol* **53** R193-241
- Yan X, Titt U, Koehler A M and Newhauser W D 2002 Measurement of neutron dose equivalent to proton therapy patients outside of the proton radiation field *Nuclear*

*Instruments and Methods in Physics Research Section A: Accelerators, Spectrometers,
Detectors and Associated Equipment* **476** 429-34

- Yang J N, Mackie T R, Reckwerdt P, Deasy J O and Thomadsen B R 1997 An investigation of tomotherapy beam delivery *Med Phys* **24** 425-36
- Yepes P, Randeniya S, Taddei P J and Newhauser W D 2009 Monte Carlo fast dose calculator for proton radiotherapy: application to a voxelized geometry representing a patient with prostate cancer *Phys Med Biol* **54** N21-8
- Yonai S, Kase Y, Matsufuji N, Kanai T, Nishio T, Namba M and Yamashita W 2010 Measurement of absorbed dose, quality factor, and dose equivalent in water phantom outside of the irradiation field in passive carbon-ion and proton radiotherapies *Med Phys* **37** 4046-55
- Yoo S, Wu Q J, Lee W R and Yin F F 2010 Radiotherapy treatment plans with RapidArc for prostate cancer involving seminal vesicles and lymph nodes *Int J Radiat Oncol Biol Phys* **76** 935-42
- Yu C X 1995 Intensity-modulated arc therapy with dynamic multileaf collimation: an alternative to tomotherapy *Phys Med Biol* **40** 1435-49
- Zacharatou Jarlskog C, Lee C, Bolch W E, Xu X G and Paganetti H 2008 Assessment of organ-specific neutron equivalent doses in proton therapy using computational whole-body age-dependent voxel phantoms *Phys Med Biol* **53** 693-717
- Zelefsky M J, Fuks Z, Happersett L, Lee H J, Ling C C, Burman C M, Hunt M, Wolfe T, Venkatraman E S, Jackson A, Skwarchuk M and Leibel S A 2000 Clinical experience with intensity modulated radiation therapy (IMRT) in prostate cancer *Radiother Oncol* **55** 241-9

- Zhang P, Happersett L, Hunt M, Jackson A, Zelefsky M and Mageras G 2009 Volumetric Modulated Arc Therapy: Planning and Evaluation for Prostate Cancer Cases *Int J Radiat Oncol Biol Phys*
- Zhang R, Perez-Andujar A, Fontenot J D, Taddei P J and Newhauser W D 2010 An analytic model of neutron ambient dose equivalent and equivalent dose for proton radiotherapy *Phys Med Biol* **55** 6975-85
- Zhang X, Dong L, Lee A K, Cox J D, Kuban D A, Zhu R X, Wang X, Li Y, Newhauser W D, Gillin M and Mohan R 2007 Effect of anatomic motion on proton therapy dose distributions in prostate cancer treatment *Int J Radiat Oncol Biol Phys* **67** 620-9
- Zheng Y, Fontenot J, Taddei P, Mirkovic D and Newhauser W 2008a Monte Carlo simulations of neutron spectral fluence, radiation weighting factor and ambient dose equivalent for a passively scattered proton therapy unit *Phys Med Biol* **53** 187-201
- Zheng Y, Fontenot J, Taddei P, Mirkovic D and Newhauser W 2008b Monte Carlo simulations of neutron spectral fluence, radiation weighting factor and ambient dose equivalent for a passively scattered proton therapy unit *Phys Med Biol* **53** 187-201
- Zheng Y, Newhauser W, Fontenot J, Taddei P and Mohan R 2007a Monte Carlo study of neutron dose equivalent during passive scattering proton therapy *Phys Med Biol* **52** 4481-96
- Zheng Y, Newhauser W D, Fontenot J D, Koch N C and Mohan R 2007b Monte Carlo simulations of stray neutron radiation exposures in proton therapy *Journal of Nuclear Materials* **361** 289-97

Laura Ann Rechner was born with her maiden name last name, Broaded, in San Diego, California on December 26, 1984, the daughter of Eleanor Marie Broaded and Charles Montgomery “Monte” Broaded. She spent most of her childhood years in Pittsburgh, Pennsylvania, with a short time in Sydney, Australia. After completing high school at North Central High School, Indianapolis, Indiana, she entered Butler University, Indianapolis, Indiana where she received the degree of Bachelor of Science with a major in Physics and minor in Mathematics in May, 2007. In August of 2008, she moved to Houston with her husband, Drew Rechner, to enter the Medical Physics program at The University of Texas Health Science Center at Houston Graduate School of Biomedical Sciences, M. D. Anderson Cancer Center.

Permanent address:

1126 West 77th Street South Drive

Indianapolis, Indiana 46260